Light Primordial Black Holes as a Dark Matter candidate

Valentin Thoß

München 2026

Light Primordial Black Holes as a Dark Matter candidate

Valentin Thoß

Dissertation
an der Fakultät für Physik
der Ludwig–Maximilians–Universität
München

vorgelegt von
Valentin Thoß
geboren in München

München, den 07.01.2026

Erstgutachter: Prof. Dr. Andreas Burkert
Zweitgutachter: Prof. Dr. Volker Springel
Tag der mündlichen Prüfung: 24.02.2026

Contents

Zusammenfassung

Primordiale schwarze Löcher (PBHs), welche sich in den ersten Sekundenbruchteilen nach dem Urknall bilden könnten, sind ein wichtiger Kandidat, um die Natur der dunklen Materie zu erklären. Bisher wurde angenommen, dass diese dafür eine Masse von $M_{\mathrm{PBH}} \gtrsim 10^{17}\,\mathrm{g}$ haben müssen, da man sonst ihre Verdampfung durch Hawkingstrahlung beobachten würde. Dass schwarze Löcher nach den semiklassischen Berechnungen von Stephen Hawking vollständig verdampfen können, wurde jedoch zuletzt auf Grundlage des Memory-Burden-Effekts infrage gestellt. Dieser besagt, kurz gefasst, dass die große Entropie eines schwarzen Lochs eine Rückreaktion bedingt, welche die Verdampfung spätestens dann aufhält, wenn es die Hälfte seiner anfänglichen Masse verloren hat. Dies hat enorme Bedeutung für leichte PBHs, da es deren Lebensdauer erheblich verlängert.

In dieser Dissertation beschäftigen wir uns mit der Frage, ob leichte PBHs aufgrund des Memory-Burden-Effekts wieder als Kandidat für die dunkle Materie infrage kommen. Dazu berechnen wir ihre (extra-)galaktische Gammastrahlung sowie ihren Effekt auf die kosmische Hintergrundstrahlung und die primordiale Nukleosynthese, unter Berücksichtigung des Memory-Burden-Effekts. Durch den Abgleich mit Beobachtungsdaten leiten wir die maximale Anzahldichte der PBHs ab. Unsere Resultate eröffnen einen neuen Massenbereich, in dem leichte PBHs die gesamte dunkle Materie ausmachen können. Abhängig von der Stärke des Memory-Burden-Effekts und der Dauer, bis dieser seine volle Wirkung entfaltet, erstreckt sich der Massenbereich bis hinunter zu einer Masse von $M_{\mathrm{PBH}} \sim 1\,\mathrm{g}$.

Auf Grundlage unserer Resultate untersuchen wir im Anschluss Möglichkeiten, um PBHs in dem neuen Massenbereich anhand ihres gravitativen Signals zu detektieren, wenn diese das Sonnensystem durchqueren. Der Vorbeiflug eines PBH an einem Gravitationswellendetektor würde die Bewegung der Testmassen beeinflussen und ein potenziell detektierbares Signal induzieren. Wir berechnen die Stärke und Frequenzabhängigkeit dieses Signals und vergleichen es mit der Sensitivität verschiedener Gravitationswellenexperimente. Der geplante Detektor DECIGO wäre in der Lage, PBHs mit Massen von $M_{\mathrm{PBH}} \in [10^7, 10^{11}]\,\mathrm{g}$ zu detektieren, wenn diese die dunkle Materie ausmachen.

In einer ergänzenden Arbeit studieren wir mithilfe von N-Körper-Simulationen die Störungen, welche PBHs in den Bahnen der Planeten im Sonnensystem hervorrufen können. Wir zeigen, dass die Stärke der Störungen durch den Beitrag des schwarzen Lochs, das am nächsten an dem Planeten vorbeizieht, bestimmt wird. Für den präzise gemessenen Abstand zwischen der Erde und dem Mars sind die erzeugten Störungen geringer als die aktuellen Messungenauigkeiten. Eine Reduktion der Messfehler um eine Größenordnung könnte die Detektion von dunkler Materie in der Form von PBHs mit einer Masse von $M_{\mathrm{PBH}} \in [10^{19}, 10^{21}]\,\mathrm{g}$ ermöglichen. In diesem Massenbereich sind PBHs bisher schwer zugänglich, was die Bedeutung dieser Detektionsmethode hervorhebt.

Der in dieser Arbeit aufgezeigte neue Massenbereich für leichte PBHs als Kandidat für die dunkle Materie unterstreicht die Notwendigkeit, neue Methoden zur Suche nach der dunklen Materie zu entwickeln. Diese Arbeit inspiriert auch weitere Forschung zur fundamentalen Natur schwarzer Löcher, um ein besseres Verständnis ihres Verdampfungsprozesses zu erlangen. Dies wird dabei helfen, Fragen zur Natur der dunklen Materie und zu den Bedingungen im frühen Universum zu beantworten.

Abstract

Primordial black holes (PBHs), forming within the first fraction of a second after the Big Bang, are a key candidate to explain the nature of dark matter. It was previously thought that, to make up the dark matter, their mass would have to be larger than $M_{\rm PBH} \gtrsim 10^{17}$, to avoid detectable Hawking radiation. However, the assumption that black holes can fully evaporate according to the semiclassical calculations by Stephen Hawking has recently been challenged on the basis of the so-called 'memory burden' effect. It states that the large entropy of a black hole imposes a backreaction which stalls the evaporation at the latest when the black hole has lost half of its initial mass. This has enormous implications for light PBHs by significantly extending their lifetime.

In this thesis, we address the question of whether light PBHs can be a viable dark matter candidate due to the memory burden effect. We compute constraints from Hawking evaporation based on their (extra)galactic γ-ray emission, and effects on the cosmic microwave background and Big Bang Nucleosynthesis, taking the memory burden effect into account. Our results reveal a new mass window for light PBHs to make up the entire dark matter. Depending on the strength of the memory burden effect, and how quickly it becomes effective, PBHs as light as $M_{\rm PBH} \sim 1\,\mathrm{g}$ can be a viable dark matter candidate.

Motivated by our results, we investigate the possibility of detecting light PBHs in the newly opened mass window. For this purpose, we study their gravitational signal as they traverse the Solar System. Close encounters of PBHs with gravitational wave detectors would perturb the detector test masses and induce a potentially detectable signal. We compute the amplitude and frequency dependence of this signal and compare it to the sensitivity of several gravitational wave experiments. The detector DECIGO would be able to detect PBHs with mass $M_{\rm PBH} \in [10^7, 10^{11}]\,\mathrm{g}$, if they make up the entire dark matter.

In a complementary work, we study the perturbations induced by PBHs on the orbits of planets in the Solar System by performing N-body simulations. We find that the perturbation strength is dominated by the closest encounter. Using the well-measured Earth–Mars distance as an observational probe, we show that the magnitude of the perturbations is below the current measurement uncertainties. An improvement of the ranging accuracy by one order of magnitude could enable the detection of dark matter in the form of PBHs with masses $M_{\rm PBH} \in [10^{19}, 10^{21}]\,\mathrm{g}$. This is inside a currently open mass window for PBHs, highlighting the value of this detection method.

The new mass window for PBHs, discovered in this work, highlights the necessity to develop new methods to search for dark matter in a previously neglected parameter space. It also inspires further research into the fundamental nature of black holes to get a better understanding of their evaporation process. This will help to answer questions about the nature of dark matter and the conditions of the very early universe.

Chapter 1

Preface

Imagine that there are invisible objects in the Solar System, similar in size to a hydrogen atom, but each of them as massive as a mountain range. Having a speed of several hundred kilometres per second, they traverse the inner Solar System in a couple of weeks without emitting detectable radiation. Only through the force of gravity do they interact very weakly with the planets in the Solar System.

What sounds like science fiction could indeed be a realistic scenario and, at the same time, open the door to solving one of the greatest problems in modern physics: the nature of dark matter that dominates the cosmos. The mysterious objects that we are talking about are primordial black holes (PBHs), formed in the first instants after the Big Bang. A period of rapid inflation could have seeded the universe with extremely rare but significant density fluctuations on cosmologically small scales that inevitably collapsed into black holes, long before the onset of structure formation (Escrivà, 2022; Escrivà et al., 2024).

The fact that such fascinating objects could form with almost any mass in the very early universe was already realized more than 50 years ago (Hawking, 1971; Carr and Hawking, 1974). It was soon recognized (Chapline, 1975) that PBHs are not merely curious objects but also a viable candidate to constitute the dark matter, whose gravitational effects we observe in the entire cosmos, but whose physical nature remains a mystery (Cirelli et al., 2024). They thereby offer an alternative to the paradigm of particle dark matter. Efforts to detect candidates for these particles have not been successful so far, motivating the investigation of alternative explanations for the nature of dark matter.

In the last decade, scientific interest in PBHs has markedly increased as they have been invoked as an explanation for a number of astrophysical observations (see Carr et al. (2024) for a review). This is in part due to the beginning of the era of gravitational wave astronomy (Abbott et al., 2016), which opened a new window to directly observe the inspiral and merger of black holes. Notably, some of the gravitational wave events observed by LIGO are challenging to explain with stellar remnants, indicating a possible primordial origin (Carr et al., 2024). Another source of interest in PBHs comes from the observations of overly-massive galaxies and supermassive black holes at high redshift by the James Webb Space Telescope (JWST), both of which could be explained by the existence of PBHs (Liu and Bromm, 2022; Zhang et al., 2025; Maiolino et al., 2025).

While these observational hints are intriguing, there are also various independent constraints on the fraction of dark matter that can be in the form of PBHs (see Carr et al. (2021a) for a review). These come from a wide range of different astronomical observations, including gravitational lensing, gravitational waves, ultra-faint dwarf galaxies, and others. Taken at face value, these constraints rule out a large fraction of the available parameter space for PBHs as dark matter. An exception to this is the so-called 'asteroid mass window', with PBH masses in the range $M_{\rm PBH} \in [10^{17}, 10^{23}]\,\mathrm{g}$, where so far no firm constraints have been placed[1]. This motivates a more thorough investigation of this parameter space to address the question of whether dark matter can be in the form of asteroid mass PBHs and how we can probe this scenario, which is one of the key questions investigated in this thesis.

The study of PBHs has led to the theoretical prediction of the existence of Hawking radiation, an important milestone for our understanding of black holes (Hawking, 1974, 1975). While this radiation is negligible over cosmological timescales for stellar-mass or supermassive black holes, it can play a significant role for PBHs of masses $M_{\rm PBH} \lesssim 10^{17}\,\mathrm{g}$, with PBHs of initial masses $M_{\rm PBH} < 5 \times 10^{14}\,\mathrm{g}$ predicted to have fully evaporated by the present day. The evaporation of PBHs has been used to place strong constraints on their dark matter fraction and sets the lower mass limit of $M_{\rm PBH} \sim 10^{17}\,\mathrm{g}$ of the asteroid mass window.

Recently, the view that black holes can fully evaporate according to the semiclassical (SC) calculations by Hawking (1974) has been challenged. Dvali (2018) demonstrated that the large microstate entropy of a black hole stabilizes it against decay. This so-called 'memory burden' effect drastically alters the prediction about the fate of light PBHs, questioning previous results that were derived based on SC Hawking radiation. Of particular importance is the potential consequence for the role of light PBHs as dark matter candidates. If their evaporation is significantly suppressed, then they could be stable over the age of the universe and serve as a candidate for dark matter. However, the range of PBH masses and parameters of the memory burden effect for which this is the case has not been studied before. Furthermore, if light PBHs are able to make up the dark matter, this raises additional questions about methods to detect them. In summary, the two main questions that we want to address in this thesis are:

- What implications does the memory burden effect have for light PBHs, and under what conditions can they make up the dark matter?
- How can we probe PBHs as a dark matter candidate in the newly opened mass window and the asteroid mass window?

To address these questions, Chapter 3 of this thesis is devoted to a detailed computation of the parameter space, for which light PBHs can make up the entire dark matter due to the memory burden effect. We extend this analysis in Chapter 4, by probing the existence of evaporated PBHs in the early universe. In Chapter 5, we extend the previous model to account for the transition from the SC to the memory burden phase and discuss the implications for light PBHs. Having demonstrated that a new mass window for light PBHs as a dark matter candidate emerges, we study a dynamical detection method based on perturbations of gravitational wave detectors. In Chapter 6, we show that this provides the possibility to

[1] Actual asteroids span an enormous mass range, exceeding both the upper and lower mass limit of this window, so the term 'asteroid mass window' should not be interpreted literally. Within the scope of this thesis, it simply refers to the quoted open mass range.

detect light PBHs in part of the newly opened mass window. Another probe of light PBHs, based on their effect on the orbits of planets in the Solar System, is discussed in Chapter 7, opening a future possibility to detect PBHs in the asteroid mass window.

Before we discuss our methods and results, Chapter 2 provides an introduction to the physics of dark matter and PBHs. We briefly discuss the evidence for dark matter and potential candidates. Focussing on PBHs, we discuss their formation as well as observational constraints, providing the necessary context for the remainder of this thesis.

Chapter 2

Introduction to Primordial Black Holes

This chapter serves as an introduction to the field of PBHs. Because this thesis focuses on their role as a dark matter candidate, we begin with a brief review of the dark matter paradigm in Section 2.1. We discuss the evidence for dark matter and proposed candidates that could explain its fundamental nature, which includes PBHs. In Section 2.2, we review the basic concepts of PBH formation, and Section 2.3 discusses observational signatures and constraints. While we put special emphasis on aspects that are of key relevance for this thesis, we also attempt to provide a broad overview of important concepts that will help the reader in interpreting the context of our results. References to several recent reviews of the topic are given, which can be referred to for further reading.

2.1 Dark matter paradigm

2.1.1 Evidence for dark matter

This is a brief review of the most important evidence for the existence of dark matter. We begin with a historical overview, based largely on the review by Bertone and Hooper (2018).

In 1933, Fritz Zwicky published his famous paper that investigated the dynamics of the Coma Cluster by measuring the velocity of eight constituent galaxies (Zwicky, 1933). By applying the virial theorem, he estimated the mass of the cluster, finding a value that was much larger than the one inferred from the luminosity of its stars. He wrote:

> *„Falls sich dies bewahrheiten sollte, würde sich also das überraschende Resultat ergeben, dass dunkle Materie in sehr viel grösserer Dichte vorhanden ist als leuchtende Materie.“*
>
> Translation: *‘If this holds true, it would imply the surprising result that dark matter is present in much greater density than luminous matter.’*

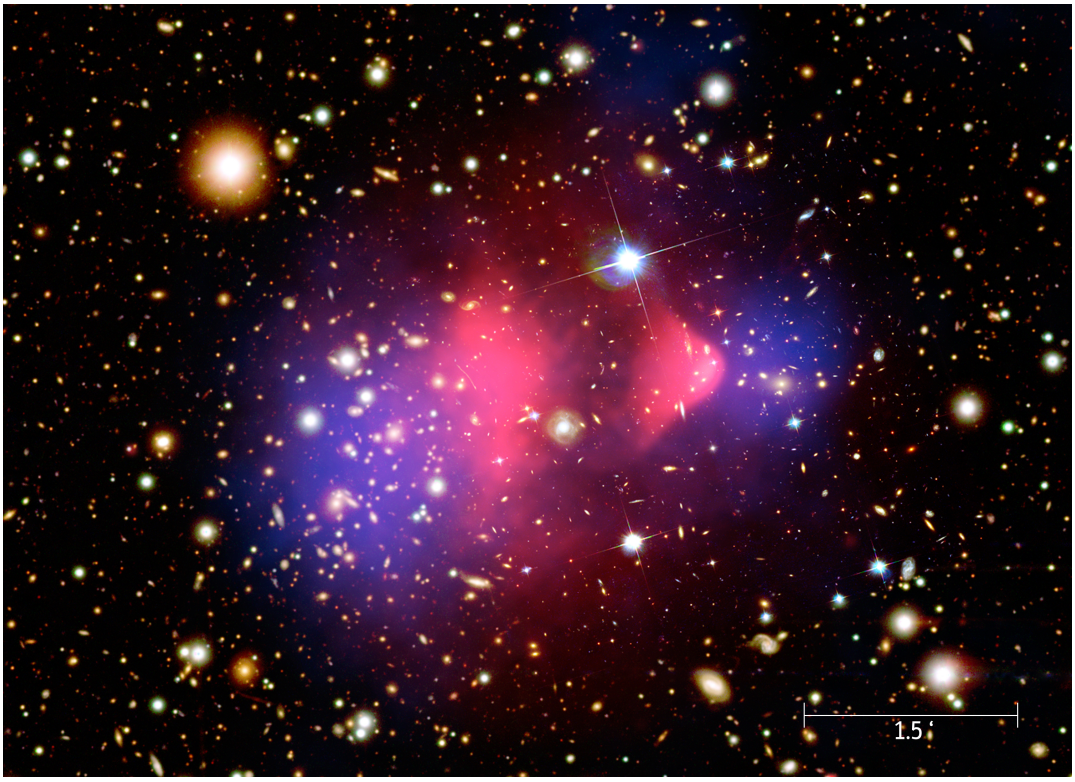

Figure 2.1: Image of the bullet cluster obtained by the Hubble Space Telescope, overlaid with data on the X-ray emission from the Chandra X-ray Observatory in purple. The blue colour highlights the mass distribution inferred from weak lensing. The spatial offset between the gas component, traced by the X-ray flux, and the matter distribution, inferred through lensing, is a striking visual evidence for the presence of a large fraction of non-baryonic matter (see the text for further details). Image source: NASA

At the time, the term 'dunkle Materie' (dark matter) did not imply the presence of unknown forms of matter but rather referred to faint stars, asteroids, 'nebulous matter', and gas that would be too dim to be visible (Zwicky, 1937; Bertone and Hooper, 2018). It was not until decades later that it was determined that baryonic matter[1] cannot account for phenomena associated with dark matter, as we discuss below.

There was no consensus on the reality of dark matter and the interpretation of the results of Zwicky and others until around the 1970s. At this time, strong evidence accumulated that the outer regions of galaxies were rotating much faster than expected based on their luminous content. Because gravity dictates that $v_{\rm rot}(r) \sim \sqrt{GM(r)/r}$, where $M(r)$ is the mass enclosed within a radius r and G is the gravitational constant, the faster-than-expected rotation speed implies a larger mass. Enabled by the development of sensitive spectrographs, Rubin and Ford (1970) and following studies established the flatness of the rotation curves beyond the stellar disk, which implies that the enclosed mass grows as $M(r) \sim r$, incompatible with the observed density of stars. This led to the conclusion that galaxies contained much more mass than present in stars (Einasto et al., 1974; Ostriker et al., 1974).

[1]This refers to 'ordinary' matter made up by baryons, mostly protons and neutrons. In the late universe, standard model particles that are non-baryonic, e.g. photons, electrons, and neutrinos, contribute negligibly to the overall mass budget.

In the following decades, a large number of other dynamical probes have provided striking evidence for the presence of dark matter. These include strong and weak gravitational lensing, where the bending of light rays due to gravity can be used to infer the amount and the distribution of matter. The X-ray emission of galaxy clusters is a probe of the gas temperature in these environments, which, under the assumption of virial equilibrium, can be used to probe the depth of the gravitational potential of those clusters and thus determine their mass.

A particularly striking visual evidence for the existence of dark matter that combines these two probes is the so-called 'bullet cluster' (Clowe et al., 2004, 2006), shown in Figure 2.1. The picture shows two galaxy clusters after their collision, imaged with the Hubble Space Telescope. Overlaid in purple colour is the X-ray emission, tracing the hot gas component, measured by the Chandra X-ray Observatory. The matter distribution, inferred through weak gravitational lensing, is shown in blue colour. The gas shows clear signs of the recent collision in the form of a shock front and is, crucially, offset from the overall matter distribution. This offset can be explained if most of the matter is weakly-interacting and can pass through each other without notable dissipation, with its dynamics determined by gravity. This is exactly what would be expected if dark matter dominates the mass of the galaxy cluster.

Independent arguments for the presence of dark matter that also demonstrated its non-baryonic nature emerged from the field of cosmology, in particular from the study of the cosmic microwave background (CMB), discovered by Penzias and Wilson (1965). Observations of the CMB revealed a nearly homogeneous distribution of baryonic matter at the time of recombination, with fluctuations relative to the background density ρ_b on the order of $\delta\rho/\rho_b \sim 10^{-5}$. These small overdensities cannot grow quickly enough to account for the formation of structure in the universe. Gunn et al. (1978) and Peebles (1982) first noted that if a large fraction of the matter in the universe is made up by a neutral, weakly-interacting particle, it could start condensing and forming structure well before ordinary matter. This was the first hint of the key relevance of dark matter in the process of structure formation. Later, precise measurements of the anisotropies of the CMB by WMAP (Hinshaw et al., 2013) and Planck (Planck Collaboration et al., 2020b), that are sensitive to the ratio of dark matter to baryonic matter, revealed that baryons make up only around 20% of the matter content of the universe.

Further observational evidence for the existence of dark matter comes from the formation of the first elements in the early universe, Big Bang nucleosynthesis (BBN) (Alpher et al., 1948). The abundance of light elements is a sensitive probe of the baryon-to-photon ratio and was used by Reeves et al. (1973) to determine that only a small fraction of the universe could be in the form of baryons. Modern studies agree with the 20% fractional abundance inferred from the CMB spectrum and provide independent and strong evidence that most of the matter in the universe is non-baryonic.

2.1.2 Properties of dark matter

Over the last decades, a variety of observations, from the kpc-scales of dwarf galaxies to galaxy clusters with sizes of several Mpc, have revealed important properties of dark matter:

- Dark matter is mostly **cold**, which refers to its low velocity at the onset of structure formation, around matter-radiation equality. A warm dark matter candidate would

still be semi-relativistic at this time, suppressing the formation of structure on small scales. Observations are overall consistent with cold dark matter, allowing only a small fraction to be warm. This limits the mass of a fermionic dark matter candidate to $m \gtrsim 5\,\mathrm{keV}$ (Cirelli et al., 2024), strongly excluding (among other reasons) the standard model neutrinos.

- Dark matter is **collisionless**, which is equivalent to the observation that it shows no significant interaction with itself and baryonic matter except through gravity. This also means that it does not dissipate energy on an observable level, which is the reason why it does not condense into disks or stars, as baryonic matter does.

- Dark matter is **stable** over at least the age of the universe. Observations strongly limit the rate of decay of dark matter from BBN until the present epoch (Cirelli et al., 2024).

Large, high-resolution computer simulations, such as the Millennium run (Springel et al., 2005), have been incredibly valuable for our understanding of dark matter. They were able to make detailed predictions for the large-scale structure of a universe composed of cold dark matter (CDM). The good agreement with observations helped to support the ΛCDM model, where Λ indicates the cosmological constant, responsible for the accelerated expansion of the universe at late times. These simulations also provide a rich source of information about the global properties of dark matter, including its distribution in the universe, density profiles, kinematics, and its role in the formation of structure. Simulations show that dark matter resides in roughly spherical halos that extend far beyond the stellar component of galaxies. These halos have a rich substructure in the form of smaller halos that frequently merge or are disrupted through tidal forces (Cirelli et al., 2024).

2.1.3 Dark matter candidates

The prevailing hypothesis is that dark matter is made up of a neutral elementary particle. This cannot be part of the standard model as the only plausible candidates, the neutrinos, have been ruled out due to their low cosmic abundance and too high velocity (see below). However, this leaves a plethora of proposed particles beyond the standard model, whose mass can range over many orders of magnitude. Efforts to detect dark matter generally consist of attempts of direct detection in experiments, indirect detection of decay or annihilation signals, or the production of dark matter particles at colliders. The following summary is based in part on the review by Cirelli et al. (2024), which we refer to for further reading.

One of the most prominent candidates is the 'WIMP' (weakly interacting massive particle), produced via thermal freeze-out. In this scenario, the particle decouples from the thermal bath in the early universe and self-annihilates until a relic density is left that scales as $\Omega_{\mathrm{DM}} \sim 10^{-27}\,\mathrm{cm}^3\,\mathrm{s}^{-1}/\langle\sigma \mathrm{v}\rangle$ (Kolb and Turner, 1990; Cirelli et al., 2024). Intriguingly, a particle with TeV-scale mass, interacting through the weak force, automatically produces the right dark matter abundance, which is often dubbed as the 'WIMP miracle' (Jungman et al., 1996). A huge effort to search for these types of particles has been undertaken, most importantly through direct detection experiments on Earth, usually involving scattering on heavy nuclei, including Xenon, Argon, Germanium, and other elements. Through longer exposure and more sensitive experiments, increasingly strong constraints on the scattering cross section of dark

matter above the GeV-scale have been obtained. Despite extensive search efforts, there has been no confident detection of a WIMP-like particle (Cirelli et al., 2024). Further constraints on the properties of WIMPs come from searches for electromagnetic signals from their decay or self-annihilation.

The absence of any observational evidence for the existence of a WIMP-like particle has led to increasing interest in light particles, sometimes called 'WISPs' (weakly interacting sub-eV particle). Due to the Pauli exclusion principle, these would have to be bosonic if their mass is below the Gunn-Tremaine bound of $m \approx 0.1\,\mathrm{keV}$ (Tremaine and Gunn, 1979). Below the eV-scale, dark matter has a wave-like behaviour as its de Broglie wavelength exceeds the Bohr radius. A lower limit on the possible mass comes from the requirement that the wavelength must not exceed the size of the smallest dwarf galaxies, giving $m \gtrsim 10^{-21}\,\mathrm{eV}$ (Cirelli et al. (2024), see also Burkert (2020)). DM candidates near this limit have been discussed under the term 'fuzzy dark matter'. A prominent WISP candidate is the axion, first discussed in 1977 as a solution to the strong CP problem (Weinberg, 1978; Wilczek, 1978). Its coupling to photons and electrons has been probed by Earth-bound experiments and astrophysical probes, with many ongoing detection efforts (Cirelli et al., 2024).

One of the first proposed candidates for dark matter, the standard model neutrino, was later ruled out by simulations of structure formation (White et al., 1983) for being too warm. In addition, standard model neutrinos are not abundant enough to make up the dark matter, and their mass is below the Gunn-Tremaine bound. However, so-called 'sterile' or 'right-handed' neutrinos have been considered as a theoretically well-motivated dark matter candidate. While they would not have any direct standard model coupling with baryons, interacting only gravitationally, they could mix weakly with ordinary neutrinos, leading to a potentially observable decay signal in the X-ray regime (Drewes, 2013).

In principle, a hypothetical dark matter particle could be as massive as the Planck mass $M_{\mathrm{pl}} = \sqrt{\hbar c/G}$. Beyond this scale, it would be a composite object, made up from other elementary constituents. These constituents cannot be baryonic based on the constraints from BBN and CMB, as we mentioned before. However, if a small fraction of the ordinary matter and radiation collapse into black holes in the early universe, well before BBN, then these would effectively only interact gravitationally with the remaining universe, avoiding cosmological bounds. These objects are primordial black holes, the subject of this thesis, and they are a macroscopic[2] dark matter candidate. Their maximum possible mass as a dark matter candidate is set by ultra-faint dwarf galaxies, the smallest objects which we observe to be composed of dark matter. Requiring that PBHs do not exceed the mass of the cores of these galaxies gives a maximum mass of the order of $M_{\mathrm{PBH}} \lesssim 10^5\,\mathrm{M}_\odot$. Together with the bounds of $m \gtrsim 10^{-21}\,\mathrm{eV}$ for 'fuzzy dark matter', these are strong upper and lower mass limits for any dominant constituent of dark matter.

The first discussion of PBHs was a work by Zel'dovich and Novikov (1967), which essentially argued that if a region of the early universe collapsed to form a black hole, then its accretion would be extremely large, with the black hole growing as fast as the universe. A relativistic calculation by Carr and Hawking (1974) later showed that the accretion is actually rather mild, reinvigorating the interest in such a hypothesis. Chapline (1975) first pointed out that

[2]The term 'macroscopic' is a bit awkward in the context of light PBHs, which we study in this thesis. A PBH with a mass of $M_{\mathrm{PBH}} = 1\,\mathrm{g}$ might be macroscopic in terms of its mass, but its size, $r_S \approx 10^{-30}\,\mathrm{m}$, is extremely small.

PBHs could constitute a significant fraction of the mass budget of the present-day universe and make up the dark matter, the evidence for whose existence was accumulating at that time (see Section 2.1.1). Today, more than 50 years after their first discussion, PBHs are receiving growing interest (Carr and Green, 2025), partly as an alternative candidate for dark matter. In addition to potentially solving this longstanding problem, PBHs are also interesting candidates for the seeds of supermassive black holes that reside at the centre of galaxies (Düchting, 2004), especially in the context of recent observations by JWST (Maiolino et al., 2025). In this thesis, we will focus on their role as a dark matter candidate and put special focus on those with mass $M_{\mathrm{PBH}} \lesssim 10^{-10}\,\mathrm{M}_\odot$. In the remainder of this chapter, we will review the physics of primordial black hole formation (Section 2.2) and observational constraints (Section 2.3) on the fraction of dark matter which they could make up.

Before we close our discussion on the possible explanations of dark matter, we want to point out that all the available evidence for dark matter and its properties is purely gravitational. No electromagnetic signal of its existence has been detected so far. This opens the possibility that dark matter is neither a particle nor a macroscopic object, but rather that our theory of gravity is incomplete. This was first suggested by Milgrom (1983), and these theories are often referred to as 'MOND' (modified Newtonian dynamics). The observable effects of dark matter are relevant only in regimes where the acceleration is extremely low, $a \sim v_{\mathrm{rot}}/r^2 \sim 10^{-10}\,\mathrm{m\,s^{-2}}$ in the case of galactic rotation curves, and even lower for galaxy clusters.[3] The underlying idea of MOND and related theories is that the force of gravity or Newton's second law ($F = ma$) is modified at low accelerations to fit the observations. While this could explain, for instance, galactic rotation curves, these theories often face challenges to explain the entire variety of evidence for dark matter in a simple framework, which includes the formation of structure and observations of the CMB. In addition, the discovery of galaxies with little dark matter content and the observation of the bullet cluster are difficult to reconcile with MOND-like theories (Clowe et al. (2006), see also the discussion in Cirelli et al. (2024)).

2.2 Formation of primordial black holes

Observations of the CMB reveal a nearly homogeneous universe at the time of recombination, with only small fluctuations in the density $\delta\rho/\rho_b \sim 10^{-5}$ (Planck Collaboration et al., 2020b,c). Gravity forces these initial perturbations to grow over time, eventually giving rise to the large-scale structure of the universe, as predicted by the ΛCDM model. Measurements of the CMB reveal nearly scale-invariant primordial fluctuations of the universe down to comoving length scales of around 1 Mpc (Planck Collaboration et al., 2020a,c). However, the formation of PBHs is sensitive to scales that are much shorter, as we will show. It is therefore conceivable that the fluctuations on these scales are enhanced relative to CMB levels by some mechanism, giving rise to $\delta\rho/\rho_b \sim 1$. Once such a local overdensity enters the horizon, it inevitably collapses into a black hole. Its mass is roughly given by the energy inside the horizon $R_H = 2ct_0$ at the time of formation t_0,

$$M_{\mathrm{PBH}} = \gamma \frac{4\pi}{3} \rho R_H^3 = \frac{\gamma c^3 t_0}{G} \approx 2 \times 10^5\,\mathrm{M}_\odot \frac{\gamma t_0}{1\,\mathrm{s}}\,, \tag{2.1}$$

[3] Accelerations due to gravity scale as $a \sim v/r^2 \sim \sqrt{GM/r^5} \sim 1/r$, if $M \sim r^3$, which means that the accelerations on larger scales tend to be lower.

where γ is a factor of order unity, c is the speed of light, and we have used $\rho = 3H^2/(8\pi G)$ and $H = 1/(2t_0)$. A primordial black hole, once formed, is physically the same object as any astrophysical black hole. Equivalently to black holes from stellar collapse or supermassive black holes, it has a horizon that is described by its Schwarzschild radius if it is non-spinning and uncharged,

$$r_S = \frac{2GM_{\rm PBH}}{c^2}\,. \tag{2.2}$$

Equation 2.1 highlights that even the most massive PBHs would form in the very early universe, during the epoch of radiation domination and well before BBN. For PBHs of asteroidal masses, on which we focus in this work, formation happens earlier than $t_0 \sim 10^{-15}\,\mathrm{s}$ after the Big Bang.

Observed black holes span a mass range from $M_{\rm BH} \gtrsim \mathrm{M}_\odot$ up to $M_{\rm BH} \sim 10^{10}\,\mathrm{M}_\odot$ (Kelly and Merloni, 2012; Sicilia et al., 2022a,b), while PBHs can be much lighter. In fact, the formation of PBHs from inflationary seeded perturbations (discussed below) can produce PBHs as light as $M_{\rm PBH} \sim 1\,\mathrm{g}$ and as heavy as $M_{\rm PBH} \sim 10^{12}\,\mathrm{M}_\odot$ (if the constraint from μ-distortions is circumvented by non-Gaussianities, see Section 2.3.5). The lower limit comes from the Hubble rate at the end of the inflation, constrained by Planck Collaboration et al. (2020c) to $H \lesssim 5 \times 10^{38}\,\mathrm{s}^{-1}$ at 95% confidence, which gives the stated bound from Equation 2.1. The upper limit is set by observations of the primordial power spectrum by CMB experiments such as Planck, which give $\delta\rho/\rho_B \approx 10^{-5}$ on comoving scales larger than 1 Mpc (Planck Collaboration et al., 2020a). The scale of the overdensity that forms a PBH of mass $M_{\rm PBH}$ is given by R_H, which we can relate to the PBH mass,

$$R_H = 2ct_0 = \frac{2GM_{\rm PBH}}{\gamma c^2} = r_S/\gamma\,, \tag{2.3}$$

and r_S is the Schwarzschild radius of the black hole. Converted to comoving units, using cosmological parameters from Planck Collaboration et al. (2020b) ($h = 0.68$, $\Omega_{\rm m} = 0.31$ and $\Omega_\Lambda = 0.69$), this implies

$$R_H \approx 3 \times 10^{-7}\mathrm{cMpc}\,\left(\frac{M_{\rm PBH}}{1\,\mathrm{M}_\odot}\right)^{1/2}\gamma^{-1/2}\,, \tag{2.4}$$

demonstrating that the scale of the inhomogeneities that form PBHs are well below those measured through the CMB, as long as $M_{\rm PBH} \lesssim 10^{12}\,\mathrm{M}_\odot$. Note that both the upper and lower limit we just discussed concern the mass of PBHs at formation. It could decrease or increase throughout cosmic time due to Hawking evaporation, accretion, and mergers. Independent observational constraints on the abundance of PBHs come from astrophysical probes after their formation, ranging from BBN up to the present day. They are discussed separately in Section 2.3.

There are many physical mechanisms that can produce the necessary perturbations that enable the formation of PBHs (see Escrivà et al. (2024) for a review). In the most commonly invoked scenario, they are seeded during the epoch of inflation. This rapid phase of expansion following the Big Bang can explain the origin of the fluctuations observed in the CMB as well as the flatness and isotropy of the universe. In the simplest case, the process of inflation is driven by a scalar field ϕ, subject to a potential $V(\phi)$. Canonical models of inflation predict nearly scale-invariant primordial fluctuations in accordance with CMB observations. However, other models of inflation provide significantly enhanced inhomogeneities at much smaller, so far unconstrained, scales. In the case of a single scalar field ϕ, this can be realized, e.g. by

an inflection in the potential $V(\phi)$. There are many other inflation models that produce the necessary conditions for the formation of PBHs. In addition, phase transitions in the early universe can also trigger the formation of PBHs, e.g. through the collisions of bubbles or the collapse of domain walls. Discussing all formation scenarios that have been proposed in the literature is beyond the scope of this thesis, and we refer the reader to the overview given by Carr et al. (2021a); Escrivà et al. (2024) and the references listed therein. For our purposes, it suffices to understand that some process seeds an inhomogeneity shortly after the Big Bang, which, after horizon re-entry, collapses into a black hole.

Connecting the primordial fluctuations, e.g. seeded by inflation, to the final distribution of PBHs requires two important steps. First, one needs to understand the dynamical evolution of a given inhomogeneity, its collapse into a black hole, and the subsequent accretion. Building on these results for individual black holes, a statistical description of the density field in the early universe is needed to predict the overall abundance of PBHs and their distribution of initial masses. Both aspects are the subject of ongoing research, and we will briefly describe the results from previous studies in the following.

The dynamical evolution of a spherically symmetric local overdensity during radiation domination and its potential collapse into a black hole is described by the fully relativistic Misner-Sharp equations (Misner and Sharp, 1964). Many studies, the first one conducted by Nadezhin et al. (1978), have investigated the necessary conditions to form black holes in the early universe and the dependency of the final black hole mass on the initial density profile of the perturbation $\delta\rho(r)$ and the equation-of-state parameter $\omega = p/\rho c^2$. We briefly discuss the results from these studies here, based on the discussions by Niemeyer and Jedamzik (1998), Yokoyama (1998), Gow et al. (2021), and the review by Escrivà (2022), which we refer to for references and further reading.

A key result of the analysis of gravitational collapse in the early universe is that the final black hole mass follows a scaling-law,

$$M_{\mathrm{PBH}} = \mathcal{K} M_H (\delta - \delta_c)^{\alpha}\,, \tag{2.5}$$

exactly valid as long as $\delta - \delta_c \lesssim 10^{-2}$. Here, M_H is the mass inside the horizon at the time of formation, given by Equation 2.1, δ denotes the amplitude of the perturbation and δ_c is the threshold for collapse to occur, i.e. $\delta > \delta_c$. Any perturbation with $\delta < \delta_c$ disperses as gravity does not overcome the local pressure in this case. The threshold of collapse δ_c and the pre-factor $\mathcal{K}$ are dependent on the specific shape of the perturbation and ω. However, α is dependent only on the equation of state, demonstrating that gravitational collapse is a critical phenomenon with a universal scaling law. For a relativistic fluid with $\omega = 1/3$ it has been found that $\alpha \approx 0.356$. As stated before, this scaling is only exact as long as $\delta - \delta_c \lesssim 10^{-2}$. It should be noted that the precise definition of δ for a given density profile is based on the so-called 'compaction function', but for our purposes it suffices to say that δ is proportional to the mass excess $\delta \sim \frac{M(R) - M_b(R)}{M_b(R)}$ on the scale of the fluctuation R with $M_b(R) = \frac{4\pi}{3}\rho_b R^3$. For a wide range of shapes of the initial perturbation, it is found that $\mathcal{K} \sim 1 - 10$ and $\delta_c \sim 0.4 - 0.7$, confirming that $M_{\mathrm{PBH}} \sim M_H$ and $\gamma \sim 1$ for modest overdensities. One key implication of Equation 2.5 is that even an enhancement of the primordial power spectrum on a singular scale[4] $P_{\mathcal{R}} \sim \delta_D(k - k_{\mathrm{PBH}})$ will produce a broad range of PBH masses due to the scaling law, as we will show below.

[4] $\delta_D(x)$ indicates the Dirac Delta distribution, not to be confused with the relative overdensity δ

Let us define the initial PBH abundance as the fraction of energy density that collapses into PBHs at the time of formation (Carr et al., 2021a),

$$\beta_{\mathrm{PBH}} = \frac{\rho_{\mathrm{PBH}}(t_0)}{\rho(t_0)} \,. \tag{2.6}$$

Because PBHs behave like matter, $\rho_{\mathrm{PBH}}(a) \sim a^{-3}$, where a is the cosmological scale factor. On the other hand, radiation scales as $\rho_{\mathrm{rad}} \sim a^{-4}$, which dominates the energy density of the universe at PBH formation, $\rho(t_0) \approx \rho_{\mathrm{rad}}(t_0)$. Therefore, the fractional abundance of PBHs $\rho_{\mathrm{PBH}}(t)/\rho(t)$ increases up to matter-radiation equality ($\Omega_{\mathrm{m}}(a_{\mathrm{eq}}) = \Omega_{\mathrm{rad}}(a_{\mathrm{eq}})$) by a factor a_{eq}/a_0, where a_0 denotes the scale factor of PBH formation. After matter-radiation equality, neglecting the effect of dark energy, the fractional abundance of PBHs stays constant, allowing us to relate β_{PBH} to the present-day density of PBHs,

$$\Omega_{\mathrm{PBH}} \approx \beta_{\mathrm{PBH}} \frac{a_{\mathrm{eq}}}{a_0} = \beta_{\mathrm{PBH}} \left(\frac{t_{\mathrm{eq}}}{t_0}\right)^{1/2} \approx 10^8 \beta_{\mathrm{PBH}} \left(\frac{M_{\mathrm{PBH}}}{1\,\mathrm{M}_\odot}\right)^{1/2} \gamma^{1/2} \,. \tag{2.7}$$

A more accurate estimate, taking the time-dependent expansion of the universe into account, yields $\Omega_{\mathrm{PBH}} = 4 \times 10^8 \beta_{\mathrm{PBH}} (M_{\mathrm{PBH}}/\mathrm{M}_\odot)$. This highlights that only a small initial abundance β_{PBH} is required to obtain $\Omega_{\mathrm{PBH}} = \Omega_{\mathrm{DM}} \approx 0.26$, e.g. $\beta_{\mathrm{PBH}} \approx 6 \times 10^{-16}$ for $M_{\mathrm{PBH}} = 10^{20}\,\mathrm{g}$ in the centre of the asteroid mass window. This is simply a result of the dilution of radiation relative to matter during the expansion of the universe.

Note that a change in the cosmological parameters will affect the relation between β_{PBH} and Ω_{PBH}. A more detailed calculation shows that $\beta_{\mathrm{PBH}} \sim \Omega_{\mathrm{PBH}} h^2 \gamma^{-1/2} g_{\star,0}^{1/4}$ (Carr et al., 2021a), where h is related to the Hubble constant through $H_0 = h \times 100\,\mathrm{km\,s^{-1}Mpc^{-1}}$ and $g_{\star,0}$ are the effective degrees of freedom at PBH formation. In the literature, a rescaled PBH abundance,

$$\beta'_{\mathrm{PBH}} = \beta_{\mathrm{PBH}} \left(\frac{h}{0.68}\right)^{-2} \left(\frac{g_{\star,0}}{106.75}\right)^{-1/4} \gamma^{1/2} \,, \tag{2.8}$$

is often used, which absorbs the dependence on cosmological values. For the purposes of this thesis we assume $\gamma = 1$, $h = 0.68$ and $g_{\star,0}$ such that $\beta'_{\mathrm{PBH}} = \beta_{\mathrm{PBH}}$.

In order to predict the initial abundance of PBHs from a given primordial power spectrum, we have to take into account the density field in the early universe. We assume that the distribution of overdensities follows a Gaussian,

$$p(\delta) = \frac{1}{\sqrt{2\pi}\sigma} \exp\left(-\frac{\delta^2}{2\sigma^2}\right) \,, \tag{2.9}$$

where the variance σ is related to the primordial power spectrum,

$$\sigma = \int_0^\infty \mathrm{d}k \, \frac{\mathcal{P}_\delta(k)}{k} \,. \tag{2.10}$$

As PBHs form once the density contrast δ exceeds the collapse threshold δ_c, we can compute their abundance by integrating the distribution of initial masses, weighted by the probability of the respective overdensity δ,

$$\beta_{\mathrm{PBH}} = \frac{\rho_{\mathrm{PBH}}(t_0)}{\rho(t_0)} = 2 \int_{\delta_c}^\infty \mathrm{d}\delta \, \frac{M_{\mathrm{PBH}}(\delta)}{M_H} p(\delta) \,. \tag{2.11}$$

This corresponds to the well-known Press-Schechter formalism (Press and Schechter, 1974) (including the usual factor 2 correction), that is also used to predict the halo mass function in cosmological studies. If we assume, for the moment, that all PBHs have the same mass $M_{\rm PBH} = M_H$ then we obtain

$$\beta_{\rm PBH} = \mathrm{erfc}\left(\frac{\delta_c}{\sqrt{2}\sigma}\right), \tag{2.12}$$

where $\mathrm{erfc}(x)$ is the complementary error function. This result highlights the extreme sensitivity of the PBH abundance to the amplitude of the power spectrum, incorporated into σ. To achieve $\Omega_{\rm PBH} = \Omega_{\rm DM}$ for $\delta_c = 0.5$ requires $\sigma = 0.084$ for $M_{\rm PBH} = \mathrm{M}_\odot$ ($\beta_{\rm PBH} \approx 3 \times 10^{-9}$) and $\sigma = 0.047$ for $M_{\rm PBH} = 1\,\mathrm{g}$ ($\beta_{\rm PBH} = 6 \times 10^{-26}$). The two amplitudes differ only by a factor of two despite a difference in β_{PBH} of 17 orders of magnitude.

As we have discussed before, even an enhancement of the primordial power spectrum on a singular scale produces PBHs with a range of masses due to the relation between the overdensity δ and the black hole mass $M_{\rm PBH}$, given by Equation 2.5. If we insert this relation into Equation 2.11, we get

$$\begin{aligned}\beta_{\rm PBH} &= 2\int_{\delta_c}^{\infty} \mathrm{d}\delta\, \mathcal{K}(\delta-\delta_c)^\gamma \frac{1}{\sqrt{2\pi}\sigma}\exp\left(-\frac{\delta^2}{2\sigma^2}\right) \\ &= \frac{2^{-(1+\gamma)/2}\mathcal{K}\delta_c\sigma^{\gamma-1}}{\sqrt{\pi}}\Gamma(1+\gamma)U\left(1+\frac{\gamma}{2},\frac{3}{2},\frac{\delta_c^2}{2\sigma^2}\right)\exp\left(-\frac{\delta_c^2}{2\sigma^2}\right),\end{aligned} \tag{2.13}$$

where $\Gamma(x)$ is the gamma function and $U(a,b,x)$ is the Tricomi confluent hypergeometric function. For $\mathcal{K} = 1$, the required values of σ for PBHs to make up the dark matter are very similar to the previous case ($\sigma = 0.088$ for $M_{\rm PBH} = \mathrm{M}_\odot$ and $\sigma = 0.048$ for $M_{\rm PBH} = 1\,\mathrm{g}$), due to the exponential sensitivity of $\beta_{\rm PBH}$ on δ_c. We can use the scaling law from Equation 2.5 to express the integral in Equation 2.13 in terms of the PBH mass

$$\beta_{\rm PBH} = 2\int_0^\infty \mathrm{d}M_{\rm PBH}\,\frac{2}{\gamma M_H}\left(\frac{M_{\rm PBH}}{\mathcal{K}M_H}\right)^{1/\gamma}\frac{1}{\sqrt{2\pi}\sigma}\exp\left(-\frac{1}{2\sigma^2}\left(\left(\frac{M_{\rm PBH}}{\mathcal{K}M_H}\right)^{1/\gamma}+\delta_c\right)^2\right) \tag{2.14}$$

Because the initial PBH mass function is given by $\frac{\mathrm{d}\rho_{\rm PBH}}{\mathrm{d}M_{\rm PBH}} \sim \frac{\mathrm{d}\beta_{\rm PBH}}{\mathrm{d}M_{\rm PBH}}$, we can read off the mass distribution from the integrand,

$$\frac{\mathrm{d}\rho_{\rm PBH}}{\mathrm{d}M_{\rm PBH}} \sim M_{\rm PBH}^{1/\gamma}\exp\left(-\frac{\delta_c}{\sigma^2}\left(\frac{M_{\rm PBH}}{\mathcal{K}M_H}\right)^{1/\gamma}\right), \tag{2.15}$$

where we have omitted constants and neglected a term $\sim M_{\rm PBH}^{2/\gamma}$ in the exponent with insignificant contribution. This shows that a sharp peak in the primordial power spectrum yields a mass distribution of PBHs with a power law tail $\sim M_{\rm PBH}^{1/\gamma} \approx M_{\rm PBH}^{2.8}$ extending to $M_{\rm PBH}/\mathcal{K}M_H \sim (\sigma^2/\delta_c)^\gamma \sim 0.1 - 0.2$ for the previously stated values of δ_c and σ that provide all the dark matter in the form of PBHs. Given that $\mathcal{K} \sim 1 - 10$ for typical profiles of the overdensity, this means that the mass function is exponentially suppressed for $M_{\rm PBH} \gtrsim M_H$.

The previous derivation of the PBH abundance and mass distribution demonstrates some qualitative features of PBH production, but we left out several key aspects for simplicity that are relevant to make more detailed predictions. So far, the physical scale of PBH formation has only implicitly entered through M_H. In general, σ needs to be replaced by a scale-dependent

quantity $\sigma(R)$ to describe the power on a given physical scale. It is obtained by smoothing the primordial power spectrum with a suitable window function $\tilde{W}(kR)$,

$$\sigma(R) = \int_0^\infty \mathrm{d}k \, \frac{\mathcal{P}_\delta(k)}{k} \tilde{W}^2(k, R) \,, \tag{2.16}$$

for which one typically uses a top-hat in real space, corresponding to

$$\tilde{W}(k, R) = 3 \frac{\sin(kR) - kR\cos(kR)}{(kR)^3} \tag{2.17}$$

in Fourier space. By inserting $\sigma(R)$ into Equation 2.11 one can compute $\beta_{\mathrm{PBH}}(R)$, and by relating R to M_{PBH} (see Equation 2.1) obtain the PBH mass distribution. In addition, the Press-Schechter formalism, developed to describe the formation of dark matter haloes, is not the most accurate approach to describe the formation of PBHs. A more sophisticated way to model the abundance of PBHs relies on counting the number of peaks in the density field of the early universe that suffice $\delta > \delta_c$, a technique first described by Bardeen et al. (1986). This is different from Press-Schechter, which only requires the smoothed overdensity on a scale R to be above the threshold δ_c. There are different formalisms of peaks theory that compute the number of distinct peaks that are above the critical threshold for collapse. It is beyond the scope of this thesis to review the detailed concepts of peak theory, and we refer the reader to Germani and Musco (2019), Young and Musso (2020), and Germani and Sheth (2023) for recent work on the topic. We want to note that studies using peaks theory still recover the power-law dependence $\sim M_{\mathrm{PBH}}^{1/\gamma}$ in the low-mass tail of the mass function (see Equation 2.15). In general, the specific shape of the mass function depends on the shape of the primordial power spectrum, with a broader peak leading to a correspondingly wider distribution of PBH masses.

As discussed before, the threshold δ_c for collapse is a monotonic function of the equation-of-state parameter ω in the early universe. A smaller value of ω implies a reduced pressure resisting the collapse and thus a lower δ_c and in turn an enhanced PBH production. During the epoch of radiation domination, the equation-of-state parameter is given by $\omega = 1/3$ for a relativistic fluid. However, within the standard model, the value of ω undergoes several temporary drops in the early universe. These reductions in pressure happen as particle species become non-relativistic and decouple from the thermal bath, leading to a brief reduction in ω. The strongest drop of ω occurs during the Quantum Chromodynamics transition at $T \sim 200\,\mathrm{MeV}$, when the quark-gluon plasma turns into a hadronic gas of pions and baryons, leading to a temporary reduction on the order of $\Delta\omega \sim 0.1$ (Carr et al., 2021b). This significantly enhances the production of solar-mass PBHs. Similarly, the electroweak transition increases the abundance of PBHs with a mass of $M_{\mathrm{PBH}} \sim \mathrm{M}_\oplus$ and electron-positron annihilation increases the number of PBHs with $M_{\mathrm{PBH}} \sim 10^6\,\mathrm{M}_\odot$. In summary, the thermal history of the early universe favours the production of PBHs of distinct masses, leading to a potentially multi-modal mass distribution given a broad enough enhancement of the initial power spectrum (Carr et al., 2021b).

Let us summarise the key points of PBH formation:

- PBH formation requires an enhancement of the amplitude of primordial overdensities beyond the level observed on large scales in the CMB.

- These overdensities could be seeded by a feature in the inflationary potential or a phase transition in the early universe.
- Gravitational collapse is a critical phenomenon, leading to a scaling law between the black hole mass and the magnitude of the overdensity.
- PBHs generally form with an extended mass function, whose precise shape depends on the primordial power spectrum.

2.3 Constraints on primordial black holes

The existence of PBHs can be probed by a plethora of different methods and observational datasets, each typically sensitive to a certain mass scale. Over the past decades, a large number of constraints on the abundance of PBHs have been derived. These are typically expressed in terms of the allowed dark matter fraction of PBHs, $f_{\rm PBH} = \Omega_{\rm PBH}/\Omega_{\rm DM}$, with $f_{\rm PBH} = 1$ implying that 100% of the dark matter can be in the form of PBHs. Figure 2.2 shows a compilation of observational constraints on the fraction of dark matter that can be in the form of PBHs of a given mass, taken from the review of Carr et al. (2021a). The previously mentioned asteroid mass window from $M_{\rm PBH} = 10^{17}\,\mathrm{g}$ to $M_{\rm PBH} = 10^{23}\,\mathrm{g}$ stands out as being unconstrained and situated in-between the bounds from Hawking evaporation and gravitational lensing, shown in red and purple colour. We will discuss the different sources of constraints shortly. Before we proceed, it should be noted that any bound on the PBH abundance is subject to the uncertainty of both the underlying model as well as the observational data that is being used to derive it. Indeed, in this thesis, we demonstrate that the constraints based on Hawking evaporation can change substantially in the light of the memory burden effect, discussed in Chapter 3. Therefore, some caution should be applied when interpreting the limits on PBHs.

Another important aspect for the discussion of PBH constraints is the assumed mass distribution. As is standard in most of the literature, the results in Figure 2.2 are displayed as a function of the PBH mass, assuming a monochromatic mass function. Our discussion in Section 2.2 shows that such a mass distribution has no physical meaning and is rather used to simplify the interpretation of results and facilitate comparisons. Any concrete mass function is dependent on the specific primordial power spectrum and is thus strongly model-dependent. Constraints for a given mass distribution $\frac{\mathrm{d}\rho}{\mathrm{d}M}$ can be derived from those for a monochromatic mass function according to the procedure presented in Carr et al. (2017), as long as each PBH mass contributes independently to the observable.[5] In this case, one has

$$\int \mathrm{d}M \, \frac{\mathrm{d}\rho}{\mathrm{d}M} f_{\rm mc}(M)^{-1} \leq 1 \tag{2.18}$$

with $f_{\rm mc}(M)$ denoting the allowed dark matter fraction for a monochromatic mass function with mass M.

[5] For example, in the context of the constraints derived in Chapter 3, this is strictly true for the (extra)galactic γ-ray background but not the case for the CMB anisotropies.

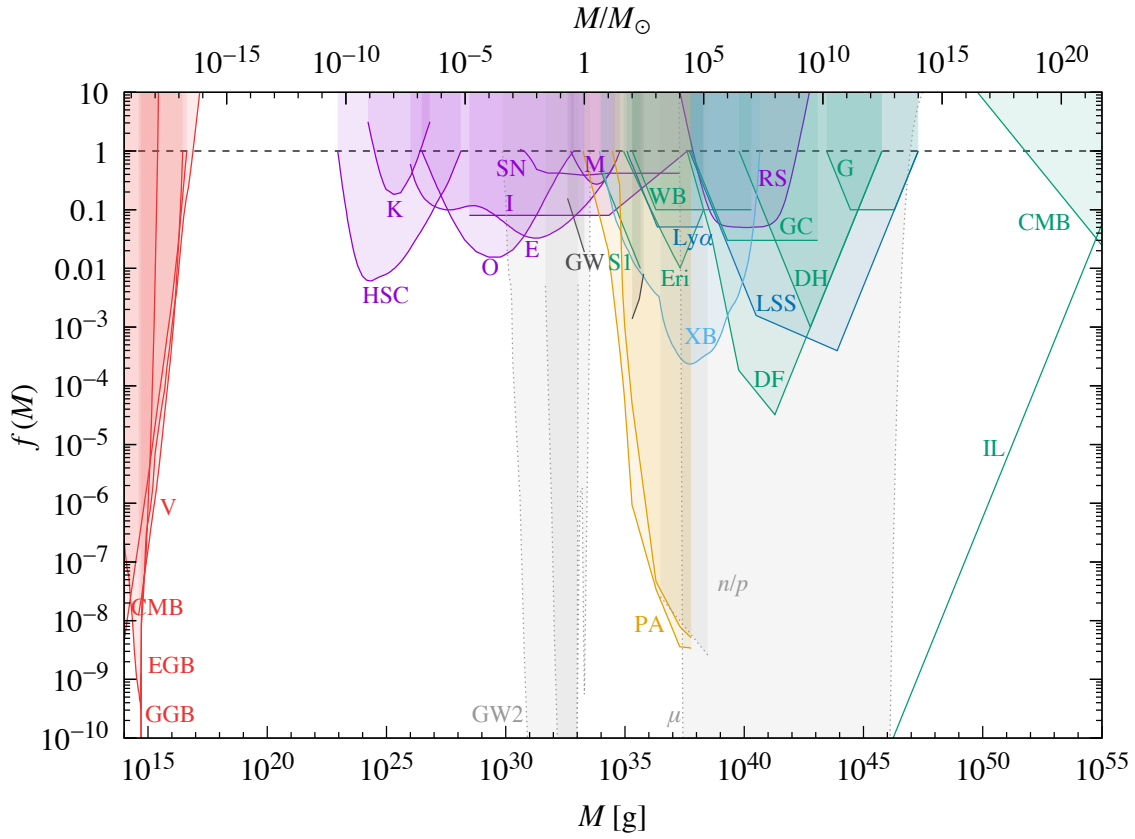

Figure 2.2: Compilation of constraints on the dark matter fraction of PBHs, $f(M)$, as a function of the PBH mass M, assuming a monochromatic mass function. This figure has been taken from the review of Carr et al. (2021a) with permission. The constraints in this figure are based on Hawking evaporation (red), gravitational lensing (purple), gravitational waves (grey), accretion (light blue), CMB distortions (orange), dynamical effects (green) and the large-scale structure (dark blue). The grey regions indicate constraints based on the formation of PBHs. The references of the individual constraints indicated by the abbreviations can be found in Carr et al. (2021a).

Computations of constraints for several mass distributions with a single peak have been carried out by Carr et al. (2017) (updated in Carr et al. (2021a)). Generally, extended mass functions tend to broaden the range of PBH masses that are constrained while slightly relaxing the strongest limit on f_{PBH}. Overall, mass distributions with a single peak do not significantly improve the prospects of PBHs as a dark matter candidate, even closing the asteroid mass window if they are very broad (Gorton and Green, 2024). The situation can be different for multimodal distributions that would emerge as a result of the thermal history of the early universe (see Carr et al. (2021b) and Section 2.2).

In the following, we will provide a brief description of the most important classes of PBH constraints, sorted by the governing observational signature. We do not attempt to review all the available literature but rather summarise key results and highlight some important recent work that is not yet included in any of the existing reviews. For a more detailed and exhaustive discussion, we refer to the reviews by Carr et al. (2021a) and Escrivà et al. (2024).

2.3.1 Hawking evaporation

The theoretical prediction of Hawking radiation is historically linked to the study of PBHs and has been used to derive some of the strongest constraints on the PBH abundance. Chapter 3 and 4 of this thesis are devoted to the computation of constraints on evaporating PBHs in light of the memory burden effect. The latter emerges when one goes beyond the SC calculations carried out by Stephen Hawking, which assume a fixed metric, i.e. no backreaction of the radiation on the black hole. As a consequence of the memory burden effect, existing constraints in the literature are strongly modified, as we show in this thesis. To provide context, we will neglect the memory burden effect at this stage and give a brief summary of the key aspects of Hawking radiation and discuss the implications for PBHs. The memory burden effect and its phenomenology will be discussed in Chapter 3.

In 1972, Jacob Bekenstein first proposed that black holes must have an entropy in order to preserve the second law of thermodynamics Bekenstein (1972, 1973, 1974). He argued that the entropy of a black hole is proportional to its surface area $S_{\rm BH} \sim r_S^2 \sim M_{\rm BH}^2$ and that its surface gravity $\kappa_{\rm BH}$ plays the role of a temperature $T_{\rm BH} \sim \kappa_{\rm BH} \sim 1/M_{\rm BH}$. James M. Bardeen, Brandon Carter, and Stephen Hawking formulated the laws of black hole thermodynamics (Bardeen et al., 1973), confirming that the area and surface gravity of a black hole behave analogously to entropy and temperature in classical thermodynamics. Hawking (1974) demonstrated that the black hole temperature is not merely a thermodynamic analogy but has a physical manifestation, by showing that black holes emit a quasi-thermal spectrum of elementary particles with a temperature

$$k_B T_{\rm BH} = \frac{\hbar c^3}{8\pi G M_{\rm BH}}\,, \tag{2.19}$$

where $\hbar$ is the reduced Planck constant and k_B the Boltzmann constant. In a later work, Hawking also derived the expression of the particle spectrum and the black hole entropy (Hawking, 1975), the latter given by

$$S_{\rm BH} = \frac{4\pi k_B G M_{\rm BH}^2}{\hbar c}\,. \tag{2.20}$$

The details of the particle spectrum from Hawking radiation and its computation are discussed in Chapter 3. Without extensive calculations, we can obtain the scaling of the mass loss rate by assuming that the black hole behaves like a perfect thermodynamic blackbody, implying

$$\dot{M}_{\rm BH} = -P_{\rm rad}/c^2 \sim -r_S^2 T_{\rm BH}^4 \sim -1/M_{\rm BH}^2\,, \tag{2.21}$$

where we used the Stefan-Boltzmann law, $T_{\rm BH} \sim 1/M_{\rm BH}$, and the validity of the SC description throughout the entire evaporation process. This has two important implications. First, the lifetime of a black hole undergoing Hawking evaporation scales strongly with the black hole mass, as $\tau_{\rm BH} \sim M_{\rm BH}/|\dot{M}_{\rm BH}| \sim M_{\rm BH}^3$. Second, the evaporation rate increases as the mass shrinks and the emitted quanta become more energetic, suggesting a final 'black hole explosion' - the title of Hawking's original paper. A more detailed, quantitative analysis shows that black holes with as mass of $M_{\rm BH} \approx 5 \times 10^{14}\,$g would evaporate within the age of the universe (MacGibbon et al., 2008). For comparison, a solar-mass black hole would have a lifetime of the order of 10^{57} Hubble times.[6] The memory burden effect fundamentally changes this picture

[6] A stellar-mass black hole cannot lose mass due to Hawking radiation at the present epoch, as its accretion rate is orders of magnitude larger.

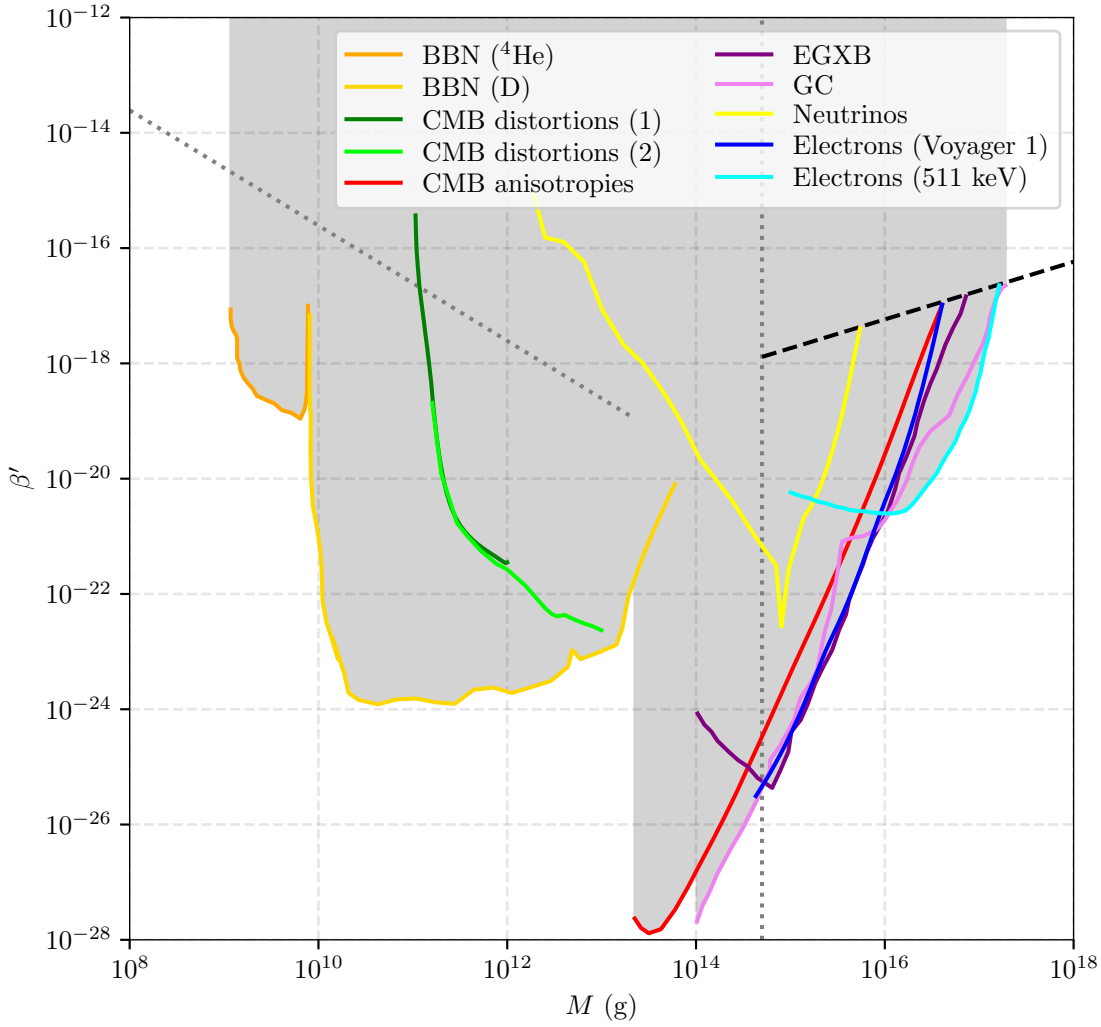

Figure 2.3: Compilation of constraints on the initial abundance of PBHs, $\beta(M)$, due to Hawking evaporation, taken from the review of Auffinger (2023) with permission. The grey shaded region is excluded with the individual coloured lines corresponding to different constraints, explained in the text. $f_{\rm PBH} = 1$ is indicated by a dashed black line. The grey vertical dotted line indicates the mass of $M_{\rm PBH} = 5 \times 10^{14}\,{\rm g}$, where PBHs would evaporate at the present epoch. Another dotted grey line extending from $M = 10^8\,{\rm g}$ to $M \sim 10^{13}\,{\rm g}$ shows the threshold $\beta_{\rm PBH}(M)$ above which PBHs temporarily dominate the energy density of the universe, leading to an early phase of matter-domination.

as we discuss in Chapters 3, 4, and 5. In particular, it extends the lifetime of black holes by many orders of magnitude with important implications for PBHs and breaks the self-similarity of the evaporation process.

It should be emphasized that a black hole emits all fundamental particles. However, the emission of particles with $mc^2 \gtrsim k_B T_{\rm BH}$ is exponentially suppressed. This means that a black hole with $k_B T_{\rm BH} \ll 0.5\,{\rm MeV} \approx m_e c^2$ effectively only emits photons, neutrinos, and gravitons, whereas all particles of the standard model are emitted above the electroweak scale, $k_B T_{\rm BH} \gg k_B T_{\rm EW} \approx 200\,{\rm GeV}$.

The emission of particles by PBHs can be used to derive various constraints, which are displayed in Figure 2.3, taken from the review of Auffinger (2023). We discuss relevant constraints in more detail in Chapter 3 and only provide a brief overview here. Because PBHs which fully evaporate before the present day cannot make up the dark matter, it is common to display constraints from evaporation in terms of the initial PBH abundance $\beta_{\rm PBH}$, introduced in Equation 2.6. This can be converted into an initial dark matter fraction at formation based on Equation 2.7. PBHs with $M_{\rm PBH} < 10^8\,{\rm g}$ evaporate sufficiently early to be unconstrained by any current cosmological probe. Indeed, PBHs could even dominate the energy density of the universe at early times, leading to an early phase of matter domination. This would be the case if their abundance lies above the grey dotted line in Figure 2.3. The earliest direct probe of PBHs comes from Big Bang Nucleosynthesis (BBN), the formation of the first light elements taking place a few minutes after the Big Bang. The standard BBN model is very successful in predicting the abundance of light elements, leaving little room for any form of energy input from evaporating PBHs. Energy injection at a time $t \gtrsim 7 \times 10^6\,{\rm s}$ after the Big Bang, but before recombination at $t \sim 380,000\,{\rm yr}$ can lead to distortions of the thermal spectrum of the CMB, giving the constraints shown in green colour, that is subdominant to the one from BBN but might improve significantly with the future CMB experiment PIXIE (Kogut et al., 2025). After recombination, the ionisation of neutral hydrogen by evaporating PBHs would soften the well-measured anisotropies in the CMB through Compton scattering of photons, giving a very strong constraint on the initial PBH abundance. The integrated extragalactic flux of photons and neutrinos from recombination to the present day can be used to derive the limits shown as 'EXGB' and 'Neutrinos' in Figure 2.3. Finally, the present-day emission from evaporating PBHs in the Milky Way halo can be used to place constraints that limit $f_{\rm PBH} < 1$ up to a mass of $M_{\rm PBH} \approx 10^{17}\,{\rm g}$. They are shown for the case of photons from the Galactic centre (GC) as well as electrons/positrons in Figure 2.3. A detailed review of all existing constraints of evaporating PBHs is presented in Auffinger (2023) and Carr et al. (2021a).

In Chapter 3 and 4 of this thesis, we compute constraints from PBH evaporation, accounting for the memory burden effect. We find that existing constraints can change drastically and thus want to stress that the results shown in Figure 2.3 need to be interpreted with caution.

2.3.2 Gravitational lensing

The compactness of PBHs makes them ideal sources of microlensing, where they amplify the light of a background star as they pass in front of it. If the light source and the PBH, acting as the lens, can be treated as a point mass, then the normalized amplification is given by (Paczynski, 1986)

$$A(u) = \frac{u^2+1}{u\sqrt{u^2+4}}\,, \tag{2.22}$$

with u being the angular separation from the source in units of the angular radius of the Einstein ring, given by

$$\theta_E = \sqrt{\frac{4GM_{\rm PBH}}{c^2}\frac{d_S - d_L}{d_S d_L}}\,, \tag{2.23}$$

in radians. In other words, a PBH must pass within an angle $\theta < \theta_E$ of a background star to lead to a noticeable lensing event. The (non)-observation of microlensing events can be turned into a constraint on their dark matter fraction by comparison to the predicted event rate, based on models of the dark matter distribution and velocity. This also means that bounds

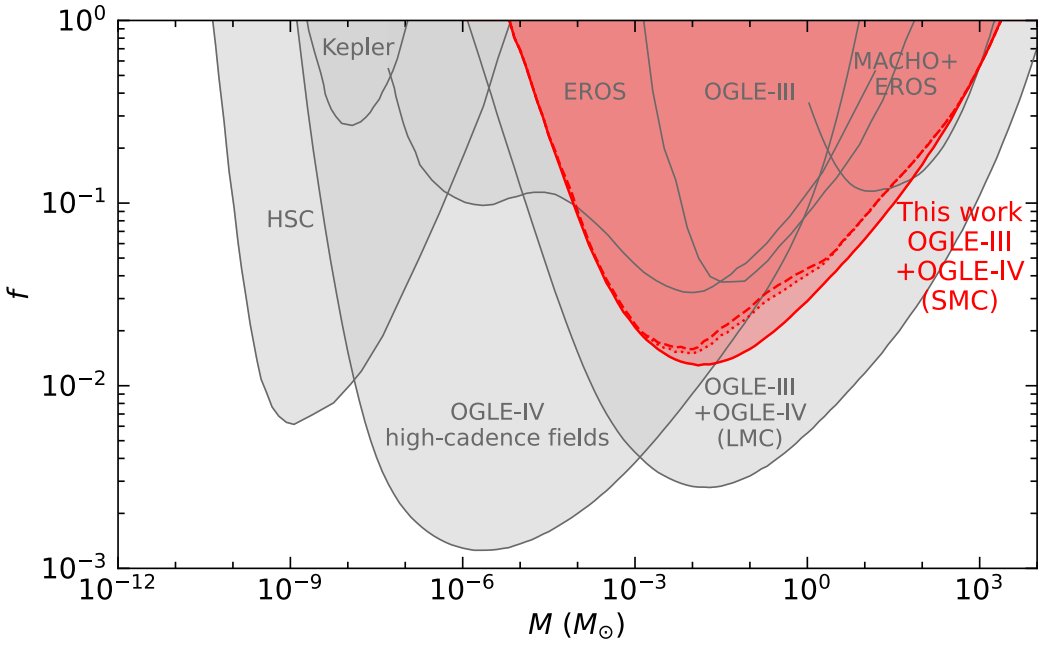

Figure 2.4: Compilation of constraints on the dark matter fraction of PBHs, $f(M)$, from microlensing surveys, taken from Mróz et al. (2025), licensed under CC BY 4.0. The shaded regions are excluded based on observations from Kepler (Griest et al., 2013), HSC (Niikura et al., 2019b; Smyth et al., 2020), EROS Tisserand et al. (2007), OGLE (Wyrzykowski et al., 2011a,b; Niikura et al., 2019a; Mróz et al., 2024b,c,a, 2025) and MACHO Blaineau et al. (2022).

derived from microlensing surveys carry the astrophysical uncertainty of the underlying model of the dark matter halo. In the context of PBHs, another uncertainty comes from their spatial clustering, which could significantly affect lensing constraints, although they are not expected to disappear entirely (Gorton and Green, 2022).

Equation 2.23 implies that the length of a microlensing event due to a PBH scales as $t \sim d_L\theta_E/v_{\rm PBH} \sim \sqrt{M_{\rm PBH}}$ because the velocity of dark matter is largely independent of the constituent mass. Observing lensing events from light PBHs thus requires a high time-resolution as the events typically take only minutes for $M_{\rm PBH} \sim 10^{-9}\,{\rm M}_\odot$ (see Figure 2 in Niikura et al. (2019b)). On the other hand, for $M_{\rm PBH} \sim {\rm M}_\odot$ the lensing events can take several weeks (see Figure 2 in Niikura et al. (2019a)). Another important factor that limits the possibility of detecting light PBHs through gravitational lensing is the finite size of the background star. When the angular size of the Einstein ring from Equation 2.23 drops below the angular diameter of the background star, the peak magnification gets significantly suppressed. As we discuss below, this prevents current constraints from microlensing to push below $M_{\rm PBH} \sim 10^{-10}\,{\rm M}_\odot$ and is thus determining the upper limit of the asteroid mass window.

Multiple surveys have been conducted to search for microlensing events in the Milky Way, the Small and Large Magellanic Cloud (SMC/LMC), and M31. In addition, extragalactic quasars, supernovae, and radio sources have been used to obtain limits on PBHs due to gravitational lensing (see Carr et al. (2021a) for a review). Figure 2.4, taken from Mróz et al. (2025), displays the most important constraints from microlensing. They limit PBHs with monochromatic mass

from making up the entire dark matter over a wide range of masses, from $M \sim 10^4\,\mathrm{M}_\odot$ down to $M_{\mathrm{PBH}} \sim 10^{-10}\,\mathrm{M}_\odot$, thereby also setting the upper limit of the asteroid mass window. The strongest constraint for $M_{\mathrm{PBH}} \in [10^{-10}, 10^{-8}]\,\mathrm{M}_\odot$ comes from a 7-hour observation of M31 with the Subaru Hyper Suprime-Cam (Niikura et al., 2019b) where only a single significant candidate event was found. Their initial limit extended to $M_{\mathrm{PBH}} \sim 10^{-11}\,\mathrm{M}_\odot$. However, Smyth et al. (2020) noted that the size of the lensed stars in M31 had been underestimated and revised the previous constraint, relaxing it towards the lowest masses. Similarly, Katz et al. (2018) showed that constraints in the asteroid mass window that were derived from femtolensing of gamma ray bursts disappear entirely once the finite source size is accounted for. From $M_{\mathrm{PBH}} \sim 10^{-8}\,\mathrm{M}_\odot$ up to $M_{\mathrm{PBH}} \sim 10^4\,\mathrm{M}_\odot$, the constraints are dominated by observations of the Milky Way bulge, the LMC, and the SMC using the Optical Gravitational Lensing Experiment (OGLE) (Wyrzykowski et al., 2011a,b; Niikura et al., 2019a; Mróz et al., 2024a,b,c, 2025), while other less stringent constraints have been obtained using data from EROS (LMC+SMC) (Tisserand et al., 2007), Kepler (MW) (Griest et al., 2013), and the MACHO survey (LMC) (Blaineau et al., 2022). Some of the surveys did detect one or several microlensing events, most notably, Niikura et al. (2019a) found six lensing events in the Galactic Bulge that could be explained by Earth-mass PBHs that make up a few percent of the dark matter. This finding was not confirmed by a later OGLE survey of the SMC/LMC (Mróz et al., 2024a), who argue that the events detected by Niikura et al. (2019a) are likely caused by free-floating planets. In other surveys, the number of detected events was generally consistent with the expected rate from self-lensing, where the lens is another star from the observed system.

2.3.3 Gravitational waves

The first successful detection of gravitational waves from a binary black hole merger by the LIGO-Virgo-KAGRA (LVK) collaboration in 2015 (Abbott et al., 2016) has opened a new window on the universe. In the decade following the first observation, LVK has detected more than 300 gravitational wave events over four observing runs, the latest (O4) concluding in November 2025. In addition, Pulsar Timing Arrays (PTA) have recently claimed a statistically significant detection of a stochastic gravitational wave background (SGWB) at nanohertz frequencies (Antoniadis et al.; Agazie et al., 2023; Reardon et al., 2023; Xu et al., 2023). The planned launch of LISA in the 2030s will further expand our detection capabilities to the millihertz regime.

Gravitational waves provide a unique way to probe many aspects of PBHs, from their formation in the very early universe to mergers at the present epoch. Discussing all of them is beyond the scope of this thesis, and we refer to recent reviews of Bagui et al. (2025) and Domènech (2024) for a detailed summary. PBHs can source individual gravitational wave events through inspiraling and merging binaries as well as close hyperbolic encounters. These processes can also create a SGWB. Other sources of SGWBs include second-order tensor perturbations induced from the scalar fluctuations that form the PBHs, as well as the Poisson noise in their number density in the early universe. Searching for SGWBs thus provides a unique way to probe the formation of PBHs in the early universe, which is especially relevant in the scenario of very light PBHs that are otherwise difficult to detect.

The gravitational wave signal from PBH mergers, both from individual mergers as well as the combined SGWB, has been used to compute constraints based on the observational data

from LVK. The PBH binary population can be divided into early binaries, which form directly from the initial distribution in the early universe and are extremely eccentric, and late binaries that form through three-body interactions and gravitational wave emission in close encounters. Many studies have estimated the merger rate of PBHs using analytical, semi-analytical, and numerical methods, including full N-body simulations (Delos et al. (2024), Nuño Siles and García-Bellido (2025), see Bagui et al. (2025) and Carr et al. (2021a) for further references). Most analysis found that PBHs from $M_{\rm PBH} \sim 10^{-1}\,{\rm M}_\odot$ to $M_{\rm PBH} \sim 10^{3}\,{\rm M}_\odot$ cannot make up the entire dark matter, even if they make up all observed LVK events. However, uncertainties remain due to the non-linear dependence of the merger rate on the spatial clustering of PBHs and the shape of the mass function, as a population of low-mass PBHs could significantly disrupt binaries of PBHs with larger masses. On the flip side, a clear detection of a merger with sub-solar progenitors would be a 'smoking gun' evidence for the existence of PBHs.

Future gravitational wave experiments will be able to probe the existence of PBHs at much greater precision and over a larger range of masses. Einstein Telescope (Abac et al., 2025) and Cosmic Explorer (Reitze et al., 2019) would be sensitive to mergers at high redshift where stellar remnants are subdominant. LISA (Amaro-Seoane et al., 2017) will be able to detect the SGWB from the formation of PBHs with masses of $M_{\rm PBH} \in [10^{18}, 10^{25}]\,{\rm g}$, including most of the asteroid mass window (Bartolo et al., 2019). Complementary, SKA (Dewdney et al., 2009) will be able to probe the formation of PBHs in the mass range $M_{\rm PBH} \in [10^{-1}, 10^{4}]\,{\rm M}_\odot$ (Ünal et al., 2021). The observational data will be complemented by numerical simulations of the cosmic evolution of PBHs, which will improve our understanding of their clustering and mergers, making testable predictions and sharpening constraints from current and future gravitational wave experiments.

2.3.4 Dynamical effects

There is a rich phenomenology related to the interaction between PBHs and the baryonic component of the universe. These concern direct collision or gravitational interaction of planets, stars, star clusters, and entire galaxies with PBHs. Each probe is sensitive to a different range of PBH masses that is mostly determined by the physical scale of the relevant system. Effects on the scale of galaxies constrain the most massive PBHs, while probes on the scale of stars and planets are sensitive to lighter ones, especially in the case of collisions. The most conservative constraints are based on the tidal disruption of galaxies, star clusters, and binaries by PBHs.

Figure 2.2 shows a selection of constraints from dynamical effects of PBHs in green colour. These include the disruption of wide binaries (WB), globular clusters (GC), and galaxies (G), with the corresponding labels from Figure 2.2 given in parentheses. Further constraints come from the requirement that PBHs do not sink to the centre of the galaxy due to dynamical friction (DF) and that they do not excessively add kinetic energy to the stellar component of the Galactic Disk (DH), also known as 'disk heating'. Ultra-faint dwarf galaxies are often dark matter-rich and thus ideal laboratories for the study of PBHs and their dynamical interaction with the stellar component. Therefore, some of the strongest constraints come from the study of their survival and dynamical state, with constraints for Eridanus II (Eri) and Segue 1 (S1) shown in Figure 2.2. However, the gravitational interaction among PBHs with $M_{\rm PBH} \sim 10^{1} - 10^{3}\,{\rm M}_\odot$ could also serve as an explanation for the observation of dark matter cores in

dwarf galaxies (Boldrini et al., 2020). Recently, the observation of a population of wide binaries in the ultra-faint dwarf galaxy Boötes I has been used to derive a strong constraint on PBHs, ruling out that those with $M \gtrsim 0.1\,\mathrm{M}_\odot$ and monochromatic mass function make up the dark matter (Shariat et al., 2025).

There are several studies that have investigated the collision of PBHs with neutron stars or white dwarfs and the corresponding observational signatures. They derived constraints on PBHs in the asteroid mass window that were later disputed (Montero-Camacho et al., 2019) and are thus not included in Figure 2.2. Recently, the capture of PBHs by main-sequence stars in dark matter-dominated ultra-faint dwarfs has been proposed as a way to probe PBHs of asteroidal mass. Using photometric data from the Hubble Space Telescope, Esser et al. (2025) excluded PBHs with $M_{\mathrm{PBH}} = 10^{19}\,\mathrm{g}$ from making up the entirety of the dark matter at 3.7σ confidence. Although a weak constraint, this would be the first firm limit in the so far open asteroid mass window.

In Chapter 6 and 7 of this thesis, we investigate the perturbations induced by PBHs on gravitational wave detectors and planetary orbits as they pass through the Solar System. We demonstrate that this could enable a new way to dynamically probe the existence of light PBHs.

2.3.5 Other constraints

There is a rich literature of further constraints on the abundance of PBHs at or above $M_{\mathrm{PBH}} \sim \mathrm{M}_\odot$ which we have not discussed so far and that we want to briefly summarise here, referencing the most recent studies.

If PBHs are sufficiently massive, they would accrete noticeably over the age of the universe. The radiative signature of this accretion has been used to derive strong constraints on the abundance of PBHs for $M_{\mathrm{PBH}} \gtrsim \mathrm{M}_\odot$ based on their contribution to cosmic radiation backgrounds across the frequency domain (Casanueva-Villarreal et al., 2025).

At even larger masses, PBHs can affect the formation of galaxies and the large-scale structure. This is caused by two mechanisms, termed the 'Poisson' and 'seed' effect. PBHs form at random initial positions, which introduces a Poissonian noise in the power spectrum that enhances structure formation at small scales and introduces clustering beyond the level of ΛCDM. The 'seed' effect denotes the gravitational effect of individual PBHs in attracting the surrounding matter and enhancing halo formation. The relative importance of both effects depends on f_{PBH} and the specific mass function, where the interplay of both effects can only be fully understood through numerical simulations (Inman and Ali-Haïmoud, 2019; Delos et al., 2024). Figure 2.2 displays constraints on PBHs derived from observations of the large-scale structure (labelled LSS) in dark blue colour, which become relevant for $M_{\mathrm{PBH}} \gtrsim 10^5\,\mathrm{M}_\odot$ (Carr and Silk, 2018). Notably, the recently observed luminous galaxies with $M_\star \gtrsim 10^9\,\mathrm{M}_\odot$ at redshift $z \gtrsim 10$ could have been seeded by a population of massive PBHs, making up a small fraction of the dark matter (Liu and Bromm, 2022; Zhang et al., 2025).

Finally, there are also constraints related to the formation of PBHs. As we discussed in Section 2.2, the production of PBHs requires an enhancement of the primordial power spectrum on sub-CMB scales. Rare overdensities in the tail of the distribution collapse into black holes,

while the remainder of the fluctuations dissipate through Silk damping. In the case of Gaussian fluctuations that form PBHs with $M_{\rm PBH} \in [10^3, 10^{12}]\,\mathrm{M}_\odot$, the dissipation leads to a distortion of the CMB spectrum that is strongly excluded by data from the COBE/FIRAS experiment (Kohri et al., 2014). However, some formation scenarios of PBHs result in highly non-Gaussian fluctuations, in which case this limit may be avoided (Nakama et al., 2018). The proposed PIXIE experiment (Kogut et al., 2025) would be sensitive enough to decisively detect or rule out any enhancement of the primordial power spectrum on scales which correspond to the aforementioned PBH masses.

2.4 Asteroid mass window

PBHs with masses $M_{\rm PBH} \lesssim 10^{-10}\,\mathrm{M}_\odot \sim 10^{23}\,\mathrm{g}$ are notoriously difficult to probe. They evade microlensing surveys as the Einstein ring is smaller than the size of the background star (see Section 2.3.2) and essentially behave like a collisionless dark matter particle in most regards. Several attempts have been made to derive limits on their abundance based on their collisions with neutron stars or white dwarfs, but they were later disputed (Montero-Camacho et al., 2019).

Hawking evaporation only becomes observationally relevant at $M_{\rm PBH} \lesssim 10^{17}\,\mathrm{g}$, even if we trust the SC calculations. As we demonstrate in this thesis (Chapter 3 and 4), the allowed mass window for light PBHs could be much wider once the quantum backreaction, in the form of the memory burden effect, is accounted for. Extended mass functions reduce the allowed range of PBH masses for which they can provide all the dark matter, but they do not close it unless the distribution is very wide (calculated for SC Hawking radiation by Gorton and Green (2024)). This reinforces the need to develop new methods to probe the existence of light PBHs.

The local dark matter density at the position of the Solar System in the Milky Way has been inferred to be around $\rho_{DM} \approx 0.01\,\mathrm{M}_\odot\,\mathrm{pc}^{-3}$ (Cirelli et al., 2024). This gives a number of PBHs in a sphere of radius R that can be expressed as

$$N_{\rm PBH} = \frac{\rho_{\rm DM}}{M_{\rm PBH}} \approx 0.8 \left(\frac{M_{\rm PBH}}{10^{20}\,\mathrm{g}}\right)^{-1} \left(\frac{R}{20\,\mathrm{AU}}\right)^{3}, \tag{2.24}$$

implying a non-vanishing number of PBHs within the planetary region for $M_{\rm PBH} \lesssim 10^{20}\,\mathrm{g}$, if they make up the entire dark matter. This motivates further study of the potential role of PBHs in the Solar System. In particular, it raises the question whether the asteroid mass window can be probed through observational signatures of PBHs in the Solar System. In Chapter 6 and 7, we show that PBHs passing through the Solar System can induce detectable perturbations on future gravitational wave detectors as well as planetary orbits, enabling future detection or constraints.

Complementary probes of the asteroid mass window could come from the detection of a SGWB by LISA, related to the formation of PBHs (see Section 2.3.3. Likewise, the capture of PBHs by main-sequence stars in ultra-faint dwarf galaxies has recently emerged as a promising way to constrain PBHs in the asteroid mass window (see Section 2.3.4).

Chapter 3

Publication I – Breakdown of hawking evaporation opens new mass window for primordial black holes as dark matter candidate

The following work has been published in Monthly Notices of the Royal Astronomical Society, Volume 523, Issue 1, pp. 451-459 in April 2024 (Thoss et al., 2024) and is licensed under CC BY 4.0[1]. It was inspired by my co-supervisor Gia Dvali, who had previously shown that the process of Hawking evaporation breaks down due to the memory burden effect. To study the consequences for light PBHs, I derived observational limits on their abundance and demonstrated that a new mass window emerges, where they can make up the entire dark matter. Kazunori Kohri contributed to this work by computing constraints from Big Bang Nucleosynthesis using his state-of-the-art code. The manuscript was prepared by me, but I received many helpful comments and suggestions from my supervisor, Andreas Burkert. Discussions with Gia Dvali, Florian Kühnel, and Sebastian Zell helped me to gain a better understanding of the theoretical aspects of Hawking radiation and the memory burden effect.

We want to note that the published paper has a typo in Equation 2. The correct formula reads

$$\frac{\mathrm{d}^2 N_{i,\mathrm{SC}}}{\mathrm{d}E\mathrm{d}t}(E, M, s_i) = \frac{g_i}{2\pi\hbar} \frac{\Gamma(E, M, s_i)}{e^{E/k_B T} - (-1)^{2s_i}}\,, \tag{3.1}$$

with $(-1)^{2s_i}$ instead of $(-1)^{s_i}$.

[1] https://creativecommons.org/licenses/by/4.0/

Monthly Notices of the ROYAL ASTRONOMICAL SOCIETY

MNRAS **532,** 451–459 (2024)
Advance Access publication 2024 April 23

https://doi.org/10.1093/mnras/stae1098

Breakdown of hawking evaporation opens new mass window for primordial black holes as dark matter candidate

Valentin Thoss [1,2,3]★ Andreas Burkert[1,2,3] and Kazunori Kohri [4,5,6]

[1]*Universitäts-Sternwarte, Ludwig-Maximilians-Universität München, Scheinerstr. 1, D-81679 Munich, Germany*
[2]*Max-Planck Institute for Extraterrestrial Physics, Giessenbachstr. 1, D-85748 Garching, Germany*
[3]*Excellence Cluster ORIGINS, Boltzmannstrasse 2, D-85748 Garching, Germany*
[4]*Division of Science, National Astronomical Observatory of Japan (NAOJ), and SOKENDAI, 2-21-1 Osawa, Mitaka, Tokyo 181-8588, Japan*
[5]*Theory Center, IPNS, and QUP, KEK, 1-1 Oho, Tsukuba, Ibaraki 305-0801, Japan*
[6]*Kavli IPMU (WPI), University of Tokyo, Kashiwa, Chiba 277-8568, Japan*

Accepted 2024 April 17. Received 2024 April 9; in original form 2024 February 27

ABSTRACT

The energy injection through Hawking evaporation has been used to put strong constraints on primordial black holes as a dark matter candidate at masses below 10^{17} g. However, Hawking's semiclassical approximation breaks down at latest after half-decay. Beyond this point, the evaporation could be significantly suppressed, as was shown in recent work. In this study we review existing cosmological and astrophysical bounds on primordial black holes, taking this effect into account. We show that the constraints disappear completely for a reasonable range of parameters, which opens a new window below 10^{10} g for light primordial black holes as a dark matter candidate.

Key words: black hole physics – dark matter – gamma-rays: general.

1 INTRODUCTION

The hypothesis of black holes forming in the early universe has been discussed for more than 50 years (Zel'dovich & Novikov 1967; Hawking 1971; Carr & Hawking 1974), with Chapline (1975) first to suggest that primordial black holes (PBHs) could constitute the entire dark matter of the universe. Since the 1970s, people have studied the consequences of PBHs as a dark matter candidate from the Planck mass $M_{\rm PBH} = M_{\rm pl}$ up to the' incredulity limit'[1] beyond $M_{\rm PBH} \sim 10^{10}\, M_{\odot}$. This has led to strong bounds that exclude PBHs of a single mass from constituting the entirety of the dark matter with the exception of a mass window in the asteroid range $M_{\rm PBH} \in [10^{17}, 10^{22}]$ g (Carr et al. 2021, and references therein).

The lower limit is a result of constraints due to black hole evaporation at low masses. This process was first described by Hawking (1974), as he was studying the consequences of light PBHs. He showed that a black hole will emit a thermal spectrum of particles, with the temperature of the radiation scaling as $T \sim 1/M_{\rm PBH}$. The described evaporation process is self-similar and ends with a final burst as $M \to 0$.

It was soon realized that the energy injection from low-mass PBHs is in conflict with observations of γ rays, the cosmic microwave background (CMB) and the abundance of light elements produced during big bang nucleosynthesis (BBN) unless these black holes constitute only a tiny fraction of the dark matter (Chapline 1975; Hawking 1975; Novikov et al. 1979; Carr et al. 2010, for a historical overview). Furthermore, if the PBHs have a mass below $M \simeq 5 \times 10^{14}$ g, they would have completely evaporated by now [see Auffinger (2023) for a review on constraints of evaporating PBHs].

However, it is possible to avoid some of the constraints that are a result of black hole evaporation. Pacheco et al. (2023) have studied 'quasi-extremal' PBHs and found that they can be a viable dark matter candidate. Friedlander et al. (2022) and Anchordoqui, Antoniadis & Lüst (2022) have investigated PBHs in the context of large extra dimensions (Arkani-Hamed, Dimopoulos & Dvali 1998) and showed that this opens up new mass windows for light PBHs as dark matter candidate.

Even in the case of non-spinning, uncharged 4D black holes, it has always been clear that Hawking's semiclassical (SC) calculations will break down before the black hole vanishes entirely. Previously, this breakdown has been assumed to happen when the mass of the black hole reaches the Planck mass. While Hawking (1975) acknowledged this, he argued that the black hole will nevertheless completely disappear. Others have discussed the idea that the evaporation comes to a halt, leaving behind Planck-mass relics that can make up the entirety of the dark matter and avoid any constraints (MacGibbon 1987; Barrow, Copeland & Liddle 1992; Torres 2013; Taylor et al. 2024).

However, Dvali et al. (2020) have shown that the SC approximation will break down at a much earlier time – at latest when the black hole has lost roughly half of its initial mass. Hawking's result entirely neglects the backreaction of the emission on the quantum state of the black hole itself. However, this effect can no longer be ignored when the energy of the released quanta becomes comparable to that of the black hole. The crucial insight by Dvali et al. (2020) is that

★ E-mail: vthoss@mpe.mpg.de

[1]This term was coined by B. Carr and refers to the limit that at least one black hole must exist in a given environment (e.g. galaxy and universe).

this backreaction leads to a universal effect of so-called 'memory burden', first introduced by Dvali (2018). This will significantly suppress further evaporation, which opens a possibility for light PBH to be a viable dark matter candidate as was already pointed out by Dvali et al. (2020).

In our work, we want to investigate the constraints on PBHs that are subject to the effect of memory burden and compare them to the results obtained within the SC Hawking picture. Following Dvali et al. (2020), we will describe the strength of the suppression by a single parameter k and study the bounds on the dark matter fraction of PBHs $f_{\rm PBH}(k, M_{\rm PBH})$.

We want to emphasize that there is no precise understanding of the evaporation process beyond the SC regime yet. Therefore, our results should be understood as a rough guide on how the landscape of PBH constraints changes as one goes beyond the Hawking picture. In addition to the memory burden effect, there are also other potential quantum properties of black holes such as vortices (Dvali, Kühnel & Zantedeschi 2022; Dvali et al. 2023), which can affect the evaporation that we do not investigate here.

We want to mention the work of Alexandre, Dvali & Koutsangelas (2024), who studied the effect of memory burden on PBH constraints from BBN and CMB distortions, and her results are complimentary to our study. In addition, we want to point out the work of Dvali, Kühnel & Zantedeschi (2021), who discussed a new mass window for PBH due to memory burden for the case of $k = 2$ in the context of the PBH formation mechanism of quark confinement.

This paper is organized as follows: In Section 2, we discuss the memory burden effect, our modified model of the evaporation process, and how we compute the various constraints. Our results are presented and discussed in Section 3. We conclude with a summary in Section 4.

2 METHODS

In this section, we briefly introduce the physics of black hole evaporation and how it is modified in our model of the memory burden effect. We then discuss the methodology to obtain important constraints on PBHs. We conclude by reviewing further bounds that we do not study in this work in more detail.

Henceforth, we will denote the mass of PBHs at formation by M_0, and their mass today by M_t. To keep our results as general as possible and to make comparisons with previous results easier, we use a monochromatic mass function. Constraints for arbitrary mass distributions can be derived from our results. The quantity $\beta_{\rm PBH} = \rho_{\rm PBH,0}/\rho_0$ gives the fraction of the universe's density in PBHs at the time of their formation. $f_{\rm PBH}$ refers to the present dark matter fraction of the PBHs, while $f_{\rm PBH,0}$ denotes the dark matter fraction at formation time. They are related via

$$f_{\rm PBH} = f_{\rm PBH,0}\frac{M_t}{M_0}, \qquad f_{\rm PBH,0} = \frac{\beta_{\rm PBH}}{\Omega_{\rm DM}}, \tag{1}$$

where $\Omega_{\rm DM}$ is the dark matter density at the time of PBH formation. We will use standard values for the Hubble rate $h = 0.67$, the number of relativistic degrees of freedom at formation $g_* = 106.75$[2] and for the factor $\gamma = 1$, which gives the fraction of mass inside a Hubble volume when the overdensity reenters the horizon that ends up in the black hole [see equations 2–6 of Carr et al. (2021)].

2.1 Semiclassical evaporation

The SC emission rate of a particle species i with energy E from a black hole with current mass M and temperature T is given by Hawking (1975).

$$\frac{{\rm d}^2N_{i,\rm SC}}{{\rm d}E\,{\rm d}t}(E, M, s_i) = \frac{g_i}{2\pi\hbar}\frac{\Gamma(E, M, s_i)}{e^{E/k_BT(M)} - (-1)^{s_i}}, \tag{2}$$

where g_i specifies the degrees of freedom of the particle emitted, s_i its spin, and Γ are the greybody factors. The black hole temperature T is directly related to its mass via

$$k_BT = \frac{\hbar c^3}{8\pi GM}. \tag{3}$$

The emission of fundamental particles leads to a mass loss rate $\dot{M} = -\mathcal{F}(M)/M^2$ of the black hole, where $\mathcal{F}(M)$ encompasses the degrees of freedom of the particles that the black hole emits at a certain mass. The lifetime of a black hole with mass M in the Hawking picture is given by $t_{\rm SC}(M) \approx M^3/(3\mathcal{F}(M))$.

Tabulated values for $\mathcal{F}(M)$ and the greybody factors are taken from BlackHawk (Arbey & Auffinger 2019). This is a publicly available code that is able to compute the SC emission rates for black holes with arbitrary mass- and spin-distribution. It makes use of existing particle physics codes to compute the secondary emission (see Section 2.2).

2.2 Secondary emission

Many of the particles that a sufficiently light black hole emits are not stable and decay or annihilate that leads to additional secondary emission of stable particles such as photons. The secondary emission of particles of type i is given by

$$\frac{{\rm d}^2N_{i,\rm sec}}{{\rm d}E\,{\rm d}t} = \sum_j \int {\rm d}E'\,{\rm Br}_{j\to i}(E, E')\frac{{\rm d}^2N_j}{{\rm d}E'{\rm d}t}, \tag{4}$$

where ${\rm Br}_{j\to i}(E, E')$ denotes the branching ratios that are calculated from particle physics codes. In our case, we use the spectra computed by BlackHawk and additionally make use of the code HDMSpectra (Bauer, Rodd & Webber 2021) for energies beyond the GeV-scale[3] BlackHawk makes use of the codes PYTHIA (Sjöstrand et al. 2015), Herwig (Bellm et al. 2016), and Hazma (Coogan, Morrison & Profumo 2020). All of them are suited for different energy ranges. For our purposes, we use Hazma for black holes with $k_BT < 0.1\,{\rm GeV}$, HDMSpectra for temperatures $k_BT > 100\,{\rm GeV}$, and Herwig in the intermediate range. Note that for a given black hole temperature, we include secondary emission only if $E > 10^{-6}k_BT$, as we do not trust the results at lower energies.

2.3 Memory burden

In the SC description of the evaporation process, a black hole decays self-similarly and can be fully described by its mass, spin, and charge without any knowledge about its prior history. During this process, the black hole entropy S, given by

$$S(M) = \frac{4\pi M^2Gk_B}{\hbar c} \approx 2.6\times10^{10}k_B\left(\frac{M}{1\,{\rm g}}\right)^2, \tag{5}$$

[2]There are 28 bosonic and 90 fermionic degrees of freedom in the Standard Model giving $g_* = 28 + 7/8\times 90 = 106.75$.

[3]By the time of publication, HDMSpectra has now been implemented into BlackHawk

continually decreases. Since the outgoing Hawking radiation is purely thermal and contains no information, this leads to the well-known' paradox', as no information escapes the black hole but its storage capacity decreases. The memory burden effect circumvents this problem, as the information stored within the black hole stabilizes it against further decay. This effect is not a specific property of black holes but is a universal phenomenon shared among all quantum systems that have a maximum entropy.

When a black hole is initially formed, its quantum state is such that it has a high capacity of information storage. This is achieved by having a large number of so-called 'memory modes' that store the information and which are nearly gapless to achieve the high storage capacity. Dvali et al. (2020) have shown under very general assumptions that the decay of the black hole (i.e. the Hawking radiation) leads to a backreaction on the black hole itself that increases the energy gaps of the memory modes slowing down any further decay. The slowdown happens at latest when the black hole has lost on the order of half of its original mass (although it might happen much earlier as we will discuss later). At this point, the cumulative backreaction of all previously emitted particles becomes so strong that the SC approximation breaks down.

As Dvali et al. (2020) have discussed, there are two possibilities for the fate of an evaporating black hole beyond half-decay. Either it continues to emit quanta with a strongly suppressed rate due to the memory burden effect or a new classical instability sets in. In the latter case, light PBHs cannot constitute the dark matter. However, if the evaporation is strongly suppressed, there is the possibility that PBHs can be a viable dark matter candidate. This is the scenario that we are investigating here.

2.4 Modified evaporation

Our modified model of the evaporation process assumes the validity of Hawking's results until the black hole has reached a mass of $M = qM_0$. Unless otherwise stated, we conservatively use $q = 1/2$ following the previous discussion. Beyond this point, the emission rate is suppressed (denoted by MB for memory burden), which we will parametrize following Dvali et al. (2020) as

$$\frac{\mathrm{d}^2 N_{i,\mathrm{MB}}}{\mathrm{d}E\mathrm{d}t}(E, M_0, s_i) = \frac{1}{(S(qM_0)/k_B)^k}\frac{\mathrm{d}^2 N_{i,\mathrm{SC}}}{\mathrm{d}E\mathrm{d}t}(E, qM_0, s_i), \tag{6}$$

where k is an exponent that controls the strength of the suppression and S is the black hole entropy [equation (5)].

Note that the large value of the entropy implies that the emission rate decreases by many orders of magnitude for $k \sim 1$. In this model, the evaporation rate and the black hole temperature remain constant. This implies a linear decay of the black hole with lifetime $t_{\mathrm{MB}}(M) \approx \frac{(qM_0)^3 S_0^k}{\mathcal{F}(qM_0)}$, neglecting the time spent in the SC regime.

As an alternative scenario, we could let the black hole temperature increase in the usual way, leading to a black hole explosion and

$$\frac{\mathrm{d}^2 N_{i,\mathrm{MB}}}{\mathrm{d}E\mathrm{d}t}(E, M, s_i) = \frac{1}{S(M)^k}\frac{\mathrm{d}^2 N_{i,\mathrm{SC}}}{\mathrm{d}E\mathrm{d}t}(E, M, s_i) \tag{7}$$

This leads to a very similar lifetime $t_{\mathrm{MB}}(M) \approx \frac{(qM_0)^3 S_0^k}{(3+2k)\mathcal{F}(qM_0)}$ and only makes a meaningful difference to the other scenario when the lifetime of the black hole is comparable to or less than the Hubble time. However, such scenarios are heavily constrained ($f_{\mathrm{PBH},0} \ll 1$) as we will show in this work. For simplicity, and since we do not know the late-time behaviour of the black hole in such detail, we will restrict our discussion to the former scenario. We want to emphasize that (in both cases) due to the dependence on the initial black hole mass M_0, the evaporation process is no longer self-similar.

2.5 Galactic γ ray emission

If light PBHs make up a sizeable fraction f_{PBH} of the dark matter halo of the Milky way, they would be detectable through their photon emission. Comparisons with observations have been used to put strong constraints on PBHs in the mass range $M_0 \in [5 \times 10^{14}, 10^{17}]$ g [e.g. Carr et al. (2016), see also Auffinger (2023) for a recent review].

The measured flux of photons would be

$$\Phi_{\mathrm{PBH}} = \frac{f_{\mathrm{PBH}}}{4\pi M_t \Delta\Omega}\frac{\mathrm{d}^2 N_\gamma}{\mathrm{d}E\mathrm{d}t}\int_{\Delta\Omega}\mathrm{d}\Omega\int \mathrm{d}r\,\rho_{\mathrm{DM}}(R(r,l,b)), \tag{8}$$

with $\Delta\Omega$ being the observed field of view on the sky and R, l, and b the Galactocentric distance, longitude, and latitude, respectively. The constraint on f_{PBH} is obtained by requiring that

$$\int_{E_{\mathrm{low}}}^{E_{\mathrm{up}}}\mathrm{d}E\;\Phi_{\mathrm{PBH}} \leq \Phi_{\mathrm{gc}}(E_{\mathrm{up}} - E_{\mathrm{low}}), \tag{9}$$

where Φ_{gc} is the measured γ ray flux in the energy bin $[E_{\mathrm{low}}, E_{\mathrm{up}}]$.

For $\rho_{\mathrm{DM}}(R)$, we choose an NFW profile with the 'convenient' set of parameters from McMillan (2011). This means our results will be identical to Auffinger (2022) in the SC limit, since we also use the observational data from their ISATIS code. This includes data from *INTEGRAL*, *COMPTEL*, *EGRET*, and *Fermi-LAT* (Strong et al. 1994; Strong & Mattox 1996; Strong et al. 1999; Bouchet et al. 2011; Strong 2011). Since we are also interested in PBHs of lower masses (and thus higher spectral energies) than usually investigated, we extend this data set by the recent observational data from *LHAASO* in the energy band from 10^4 to 10^6 GeV (Cao et al. 2023, 'inner region').

2.6 Extragalactic γ ray background

The evaporation of PBHs between the time of recombination t_{rec} and today t_0 will lead to a contribution to the extragalactic γ ray background. This has been used to constrain PBHs with masses $M_0 \in [3 \times 10^{13}, 10^{17}]$ g (Carr et al. 2010; Arbey, Auffinger & Silk 2020; Ballesteros, Coronado-Blázquez & Gaggero 2020; Chen, Zhang & Long 2022).

Assuming a homogenous distribution of dark matter, the observed flux is

$$\Phi_{\mathrm{PBH}} = \frac{cn_{\mathrm{t}}}{4\pi}\int_{t_{\mathrm{rec}}}^{t_0}\mathrm{d}t\,(1+z)\frac{\mathrm{d}^2 N_\gamma}{\mathrm{d}E\mathrm{d}t}\Big((1+z)E, M(t)\Big), \tag{10}$$

where n_t is today's number density of the PBHs which is related to $f_{\mathrm{PBH},0}$ via

$$n_{\mathrm{t}} \approx 2.2 \times 10^{-30}\,\mathrm{cm}^{-3}\; f_{\mathrm{PBH},0}\left(\frac{M_0}{1\mathrm{g}}\right)^{-1}. \tag{11}$$

The constraint on $f_{\mathrm{PBH},0}$ (and f_{PBH}) is obtained analogously to equation (9). We again use the observational data available in the ISATIS code from *HEAO*, *COMPTEL*, *EGRET*, and *Fermi-LAT* (Gruber et al. 1999; Strong, Moskalenko & Reimer 2004; Ackermann et al. 2015; Ruiz-Lapuente et al. 2016). In addition, we include the flux data from *LHAASO* (Cao et al. 2023, 'outer region').

2.7 CMB anisotropies

The injection of energy from PBH evaporation after recombination can ionize the otherwise neutral medium. This in turn leads to the

rescattering of CMB photons that affects the angular power spectrum of temperature and polarization. Comparisons with measurements of the CMB have led to strong constraints on PBH in the mass range $M_0 \in [3 \times 10^{13}, 10^{17}]$ g (Poulin, Lesgourgues & Serpico 2017; Stöcker et al. 2018; Acharya & Khatri 2020; Cang, Gao & Ma 2022). Stöcker et al. (2018) have developed the publicly available code ExoCLASS, a branch of the Boltzmann code CLASS (Blas, Lesgourgues & Tram 2011). It is able to compute the CMB power spectra for any value of M_0 and $f_{\mathrm{PBH},0}$. To achieve this, the code computes the rate of energy density deposition as a function of redshift,

$$\left.\frac{\mathrm{d}^2E}{\mathrm{d}t\,\mathrm{d}V}\right|_{\mathrm{dep},\alpha}(z) = h_\alpha(z)\left.\frac{\mathrm{d}^2E}{\mathrm{d}t\,\mathrm{d}V}\right|_{\mathrm{inj}}(z) = \frac{h_\alpha(z) f_{\mathrm{PBH},0}\rho_{\mathrm{DM,t}}(1+z)^3\dot{M}}{M_0}, \quad (12)$$

where α denotes heating, ionization, or excitation+ionization as the possible channels. The energy deposition function $h_\alpha(z)$ is a convolution of the PBH spectrum with a transfer function $T^i_\alpha(z', z, E)$. This function gives the fraction of the energy E injected at redshift z' in a channel α that is deposited at redshift z for the particle type i.

To obtain constraints on $f_{\mathrm{PBH},0}$, we use ExoCLASS and MontePython (Audren et al. 2013; Brinckmann & Lesgourgues 2019) to perform a Markov chain Monte Carlo (MCMC) analysis. The model uses the Planck TT,TE,EE+lowE+lensing likelihood (Planck Collaboration 2020) with $f_{\mathrm{PBH},0}$ as an additional cosmological parameter. To perform the calculations, we modified ExoCLASS and implemented our model of the evaporation process as described in Section 2.4. In addition, we also change the computation of the PBH spectra in the DarkAges module of the code. We replace the geometric optics approximation with the full results from BlackHawk including secondary emission as described in Section 2.2. Note that in the SC limit, we reproduce the results from Stöcker et al. (2018) within a factor of a few.

The transfer function used in ExoCLASS is only tabulated up to $E \sim 6$ TeV and for higher energies the code simply uses the last tabulated value. This should be a reasonable approximation even for much higher energies as the only relevant cooling process at energies above $E \sim 1$ TeV is the pair production on the CMB and subsequent cascade to lower energy photons that produces a universal spectrum (Slatyer, Padmanabhan & Finkbeiner 2009). The final deposition efficiency does not depend on the initial photon energy and the value of the transfer function should thus remain constant with respect to the energy. Indeed, the tabulated values of the transfer function change very little for energies $E > 1$ TeV.

Since we have k as an additional free parameter, it would be computationally very expensive to perform a large number of MCMC runs over the entire parameter space of M_0 and k and given the simple nature of our model we do not aim for very precise results. In fact, as we are going to show in this work, the constraints from CMB anisotropies are weaker than those from galactic and extragalactic γ rays by several orders of magnitude for most of the parameter space and thus not as relevant, which justifies approximations.

If the initial black hole mass is larger than $M_0 \simeq 3 \times 10^{13}$ g, then the SC phase of the evaporation ($M_0 \to qM_0$) is still ongoing after recombination. In this case, one can expect the constraints to change only by a factor of a few if $q \sim 1/2$, as the black hole still releases a sizeable fraction $1 - q$ of its total energy M_0c^2. To investigate this, we perform a MCMC run for $M_0 = 5 \times 10^{13}$ g were the black hole evaporation is stopped after half-decay. We compare it to a simulation with the full evaporation process. The resulting constraints on $f_{\mathrm{PBH},0}$ only differ by roughly 20 per cent. As this is significantly smaller than the modelling uncertainty of around two dex [see e.g. fig. 6 of Auffinger (2023)], we ignore the effect of memory burden in this mass range and just use the SC results from Stöcker et al. (2018).

To obtain the constraints for PBHs with $M_0 < 3 \times 10^{13}$ g, we run a full MCMC for $M_0 \in [10^3, 10^5, 10^7, 10^9, 10^{11}, 10^{13}]$ g and interpolate the results for other values of M_0 and k. To do this, we assume that f_{PBH} scales linearly with the total amount of energy injection, as is motivated by equation (12). Effectively, we are rescaling the constraints on $f_{\mathrm{PBH},0}(M_0, k)$ computed using ExoCLASS to obtain $f_{\mathrm{PBH},0}(M_0', k')$ through

$$f_{\mathrm{PBH},0}(M_0', k')\frac{\Delta M'}{M_0'} = f_{\mathrm{PBH},0}(M_0, k)\frac{\Delta M}{M_0}, \quad (13)$$

where ΔM is the change in mass from recombination to the end of reionization which depends on k. This does not require computing an angular power spectrum and is treating $h_\alpha(z)$ as constant. The latter approximation is exact if we keep M_0 constant as $h_\alpha(z)$ only depends on the shape of the PBH spectrum, which is unaffected by k. We discuss this approximation, its computation, and its validity in more detail in Appendix B.

2.8 Big bang nucleosynthesis

The abundance of light elements in the universe is the earliest cosmological probe to study PBH evaporation. In the Hawking picture, black holes with masses $M_0 \in [10^{10}, 10^{13}]$ g evaporate during or after the formation of light elements. The emitted radiation will alter the neutron-to-proton ratio and lead to photo- and hadrodissociation of elements. Since the standard BBN scenario predicts the abundance of light elements with great success, any modification will be heavily constrained. Carr et al. (2021, updated from Carr et al. (2010) through results of Kawasaki et al. (2018) and Hasegawa et al. (2019)) find that the initial dark matter fraction is constrained to $f_{\mathrm{PBH},0} \lesssim 10^{-3}$ in the denoted mass range with other studies obtaining comparable results (Acharya & Khatri 2020; Keith et al. 2020).

To understand how these results will be affected by the memory burden, we need to distinguish two regimes as in Section 2.7. For $M_0 \gtrsim 10^{10}$ g, the SC evaporation phase is still ongoing during or after nucleosynthesis. Therefore, one expects the constraints to change only by a factor of order unity as the black hole still releases half of its total energy M_0c^2. To understand this in more detail we use of the model described in Kawasaki et al. (2018) and modify it by halting the evaporation process at half-mass. This is a good approximation for $k \gtrsim 0.5$, since the lifetime of the black hole exceeds the age of the universe for $M_0 > 10^{10}$ g in this case.

On the other hand, if the initial mass of the PBHs is below $M_0 \sim 10^{10}$ g then the memory burden slows down the evaporation before they can affect the abundance of light elements. If the black holes are still present today, then their evaporation rate in the early universe will be completely negligible (compare this to the SC case where there are no BBN bounds on PBHs with a lifetime greater than $t \sim 10^6$ yr). Conversely, if they are light enough to evaporate significantly in the early universe and affect the abundance of light elements then they will not survive until today. For our purposes, we can therefore ignore this regime. This is also justified by the results of Alexandre et al. (2024), who discuss the constraints from BBN in more detail.

2.9 Seismic constraints

If PBH are light enough and make up a sizeable fraction of the dark matter, then they will frequently come close to or even transit through

the earth. The expected collision rate is (Luo et al. 2012)

$$\Gamma = 10^8\,\mathrm{yr}^{-1} f_{\mathrm{PBH}} \left(\frac{M}{1\,\mathrm{g}}\right)^{-1} \left(\frac{\langle v\rangle}{200\,\mathrm{km/s}}\right) \tag{14}$$

where $\langle v\rangle$ is the mean dark matter velocity. This assumes that the PBHs are smoothly distributed throughout the solar system. While this would imply a sizeable number of collisions per year for $M \ll 10^8$ g, these are virtually unobservable. In the same work, it was found that a black hole with $M_0 = 10^{15}$ g would produce a seismic event with a magnitude of $M_w = 4$. Since the amplitude of the seismic waves scales linearly with the black hole mass according to Luo et al. (2012), this would imply immeasurable magnitudes $M_w \ll 1$ for black holes with mass $M_0 \ll 10^{12}$ g. While close encounters with the Earth would be more numerous, they are still too weak to be detectable in the mass range that we are interested in.

2.10 Other constraints

In addition to the constraints already discussed, there are a large number of other bounds on evaporating PBHs (for a full overview see the review of Auffinger 2023).

Many of these are conceptually similar to the constraints from the galactic γ ray emission but instead look at the flux of electrons, positrons, or neutrinos (Boudaud & Cirelli 2019; Dasgupta, Laha & Ray 2020), the 511 keV annihilation signal (DeRocco & Graham 2019; Laha 2019), radio emission from synchrotron radiation Chan & Lee (2020), heating of the ISM (Kim 2021; Laha, Lu & Takhistov 2021) or take into account other astrophysical contributions to get stronger bounds (Berteaud et al. 2022). They are all usually within one order of magnitude of the conservative approach that we use here.

Another important constraint arises from spectral distortions of the CMB (Acharya & Khatri 2020; Chluba, Ravenni & Acharya 2020; Lucca et al. 2020). It affects black holes with masses in the range $M_0 \in [10^{11}, 10^{13}]$ g. One can follow the same arguments as in the previous section to conclude that the bounds will not change dramatically in the regime where the SC evaporation is still (partly) ongoing. During the phase of slowed down evaporation, the constraints only affect black holes which would not survive until today. This is also discussed in the work of Alexandre et al. (2024). Since the constraints from CMB spectral distortions are (currently) less strong than those from BBN and cover a smaller range of masses, we will ignore them for our purposes.

PBHs with a mass of $M_0 < 10^9$ g were previously ruled out as a dark matter candidate unless they could form stable relics at the Planck mass (MacGibbon 1987; Barrow et al. 1992; Torres 2013; Taylor et al. 2024). Nevertheless, PBHs in this mass range have been studied as an explanation for baryogenesis, as a source of particle dark matter and gravitational waves as well as a solution for the Hubble tension (Hawking 1975; Dolgov, Naselsky & Novikov 2000; Baumann, Steinhardt & Turok 2007; Fujita et al. 2014; Allahverdi, Dent & Osinski 2018; Lennon et al. 2018; Hooper, Krnjaic & McDermott 2019; Morrison, Profumo & Yu 2019; Baldes et al. 2020; Hooper et al. 2020; Masina 2021; Papanikolaou, Vennin & Langlois 2021; Papanikolaou 2023). All of these results need to be revisted in the context of the memory burden effect. In general, any regions of the parameter space for which $q\beta_{\mathrm{PBH}} > \Omega_{\mathrm{DM}}$ (i.e. $qf_{\mathrm{PBH},0} > 1$) are not allowed in our scenario as it would overclose the universe.

When PBHs form in the early radiation-dominated universe, they are able to accrete significantly for a short period of time, thereby increasing their mass by a factor of a few (Escrivà 2022). However, this will have no meaningful effect on our results as the evaporation will start to become dominant long before the black hole reaches the memory burden stage. This can be seen by a rough comparison of the evaporation rate to the accretion rate $\dot{M} = fc\rho_{\mathrm{r}} 4\pi r_{\mathrm{PBH}}^2$, where f is a factor of order unity and $\rho_{\mathrm{r}} = 3/32\pi Gt^2$ the radiation density in the early universe. Both rates are approximately equal at

$$t = \left(\frac{3GM_0^4}{2c^3\mathcal{F}(M_0)}\right)^{1/2} \approx 5\times 10^{-6}\tau_{\mathrm{SC}}(M_0)\left(\frac{M}{1\,\mathrm{g}}\right)^{-1}, \tag{15}$$

where we have used that $\mathcal{F}(M_0)$ becomes constant for $M_0 < 10^{11}$ g. Therefore, for black holes much larger than the Planck mass, the duration of the accretion phase will be completely negligible to the SC duration of the evaporation phase τ_{SC}. Our results should thus not be affected by accretion as long as M_0 is interpreted as the mass of the black hole at the end of the accretion phase (as is usually done in the literature).

Finally, we want to mention that in the standard formation scenario of PBHs from spherical collapse of overdensities, there is a lower mass limit of $M_0 \sim 0.1$ g that is set by the time of the end of inflation.

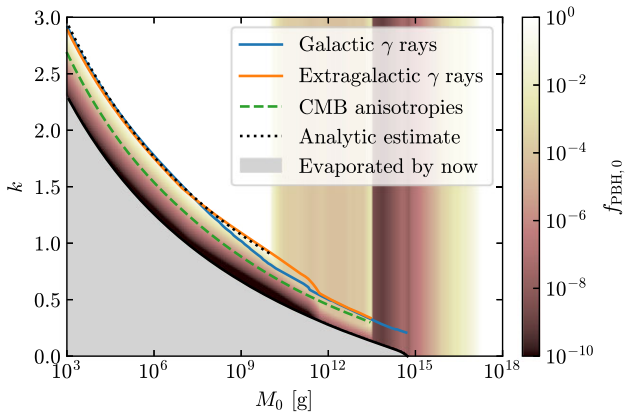

Figure 1. Combined constraints on $f_{\mathrm{PBH},0}(k, M_0)$. The coloured lines show $f_{\mathrm{PBH},0} = 1$ contours for each type of constraint. In the white region, PBHs can make up the entirety of the dark matter. The black, dotted line displays the analytic estimate given by equation (16). The different linestyles are chosen for better readability.

3 RESULTS AND DISCUSSION

In this section, we discuss the results and possible uncertainties in our model. The combined map of all constraints is shown in Fig. 1. The results for galactic and extragalactic γ ray emission are also shown separately in the appendix.

3.1 Galactic γ ray emission

Fig. A1 shows the constraints obtained from galactic γ ray emission. PBHs with initial mass $M_0 \gtrsim 5\times 10^{14}$ g have not yet lost half of their mass and thus the usual constraints apply which rule out PBHs to be the entirety of the dark matter up to $M_0 \sim 10^{17}$ g independent of k. For $k > 0.2$, a new mass window emerges that extends down to $M_0 = 10^9$ g for $k = 1$ and to $M_0 = 4\times 10^5$ g for $k = 2$. Note that when only primary photon emission is considered (dashed lines in Fig. A1), then there are no bounds for $k > 1.3$ or $M < 6\times 10^5$ g beyond the trivial constraint that they would have evaporated by now. However, when considering the emission of secondary photons, we obtain bounds on these PBHs far beyond these limits. We do not find any constraints from galactic γ ray emission for $M_0 < 3\times 10^2$ g.

The radiation of these light black holes goes beyond the energy range covered by any current γ ray observations. In this case, one would need to consider indirect effects of these highly energetic photons (beyond PeV) to obtain limits. For each value of k, the constraints on $f_{\mathrm{PBH},0}$ extend roughly two orders of magnitude beyond the mass at which the PBHs would completely evaporate by today.

3.2 Extragalactic γ ray background

In Fig. A2, the constraints from the extragalactic γ ray background are shown. In the Hawking picture, the dark matter fraction of PBHs is limited to $f_{\mathrm{PBH},0} < 1$ in the mass range from $M_0 \approx 3 \times 10^{13}$ g to $M \sim 10^{17}$ g. As explained before, for initial black hole masses $M \gtrsim 5 \times 10^{14}$ g, there are no changes. In the range $M_0 \in [3 \times 10^{13}, 5 \times 10^{14}]$ g, the constraints are softened at most by one order of magnitude when taking into account all observational data. This is because the SC evaporation phase is still ongoing after recombination. The lower end of the constrained mass range (which is roughly set by the mass of a black hole that evaporates at recombination) changes by only 4 per cent. A new window for PBHs as dark matter candidates opens at lower masses for $k > 0.35$. It extends down to $M = 10^9$ g for $k = 1$ and to $M = 10^5$ g for $k = 2$. If only primary photon emission is considered, then the constraints become significantly weaker as can be seen from the dashed lines in Fig. A2. We are not able to constrain black hole holes with $M_0 \lesssim 10^2$ g as the energy exceeds the current observational range, as already discussed for the galactic γ ray emission.

3.3 Other constraints

The constraints on PBHs from CMB anisotropies are weaker than those from galactic and extragalactic γ ray emission by 4–6 orders of magnitude for $M_0 < 10^{12}$ g and by around 2 dex for $M_0 \in [10^{12}, 3 \times 10^{13}]$ g. Note that for $M_0 < 10^9$ g, our results rely on extrapolation of the transfer function and are thus subject to some uncertainty. For $M_0 > 3 \times 10^{13}$ g, we just give the constraints from Stöcker et al. (2018), as explained in Section 2.7.

The bound from BBN in the mass range $M_0 \in [10^{10}, 10^{13}]$ g weakens by around 45 per cent if the evaporation is stopped at half-mass. As discussed in Section 2.8, there are no other constraints from BBN for black holes that survive to the present day.

3.4 Combined constraints

The combined map of constraints $f_{\mathrm{PBH},0}(k, M_0)$ is shown in Fig. 1. Fig. 2 shows $f_{\mathrm{PBH},0}(M_0)$ for $k = 2$, which is chosen for illustrative purposes. One can identify the constraints from the SC evaporation phase as the vertical, almost k-independent band in the range $M_0 \in [10^{10}, 10^{17}]$ g. The slowed down evaporation phase leads to constraints that are dependent on k. For $k \gtrsim 1.0$, a new mass window emerges for which PBHs can make up the entirety of the dark matter. The upper mass limit of $M_0 \sim 10^{10}$ g is set by the time of nucleosynthesis as the PBHs must reach the stage of suppressed evaporation before the onset of BBN. On the other hand, the lower bound depends on the strength of the suppression k, as it determines the lifetime of the black hole.

We can understand our results in simple terms by considering the fraction α of the PBH mass that evaporates during memory burden until today ($qM_0 \to (1-\alpha)qM_0$). From equation (6), it follows that

$$M_0 \approx \left(\frac{\mathcal{F}(qM_0)t_0}{\alpha}\right)^{\frac{1}{3+2k}} \left(\frac{\hbar c}{4\pi G}\right)^{\frac{k}{3+2k}}, \tag{16}$$

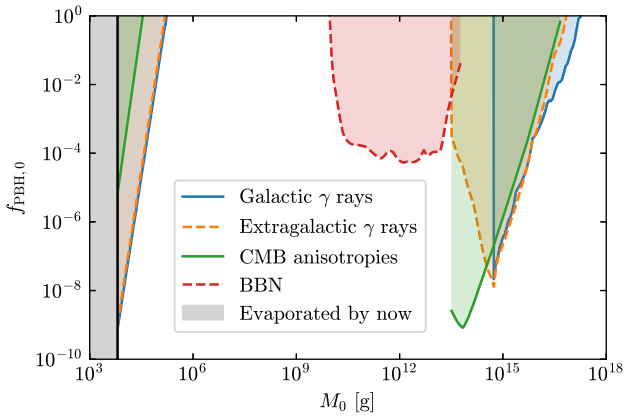

Figure 2. Constraints on $f_{\mathrm{PBH},0}(M_0)$ for $k = 2$. The different linestyles are chosen for better readability.

where t_0 is the age of the universe. This is is plotted in Fig. 1 for $\alpha = 10^{-13}$ and $\mathcal{F}(qM_0) \approx \mathcal{F}(0) \approx 8.2 \times 10^{26}$ g^3 s^{-1} and gives a good approximation for the lower bound on the black hole mass in the parameter range that we study. Put differently, this implies that the memory burden effect must increase the lifetime of the black hole to at least $\sim 10^{13}$ times the age of the universe in order to avoid all existing constraints.

3.5 Model uncertainties

Due to the lack of a detailed understanding of the evaporation process beyond the SC limit, we keep our model of the evaporation process as simple as possible. Motivated by Dvali et al. (2020), we model the strength of the suppression by a factor $1/S_0^k$ with S_0 being the black hole entropy. This means k only depends logarithmically on other parameters in our models. Therefore, any uncertainties in our models of the constraints will only weakly affect the bound on $k(M_0)$, where $f_{\mathrm{PBH},0} = 1$ (i.e. the coloured lines in Fig. 1). More specifically, if e.g. the rate of galactic γ ray emission decreases by a factor of 10, this will shift the bound $k(M_0)$ by less than 0.05 for the range of mass that we study.

Another uncertainty in our model is the question on how to set the black hole temperature and its spectrum. When the SC approximation breaks down, we can no longer expect the emission to be thermal. In our model, we keep the shape of the spectrum fixed as a zeroth-order approximation. Should the spectrum change very drastically (but keeping dN/dt constant) then this will most strongly affect the constraints from galactic and extragalactic emission. If the emission becomes more soft, then the bounds would become weaker and vice versa. This is due to the larger observed γ ray flux at lower energies. However, even a drastic change in f_{PBH} will not shift the bound on $k(M_0)$ by much as explained. The constraints from CMB anisotropies are very robust to uncertainties in the black hole spectrum since they depend mostly on the total rate of emission. In fact, in the mass range that we study, the transfer function is approximately constant (see Section 2.7) w.r.t. to the energy.

Similar arguments can be made about the uncertainties regarding the secondary emission of the PBHs. During the phase of memory burden, it is in principle possible that the emission of particles is no longer 'democratic', i.e. the emission of certain particle species are preferred [see also the discussion in Alexandre et al. (2024)]. However, as long as the emission rate only changes within an order of magnitude, our bounds should not change dramatically.

Regarding the black hole temperature, we discussed two different approaches in Section 2.4. For the results presented so far, we keep it fixed once the black hole has lost half of its mass. If we instead assume $T \sim 1/M$ throughout the memory burden phase [i.e. as in equation (7)] then we find that it changes our results only when the lifetime is comparable to or less than a Hubble time. Thus, it only affects the constraints in a regime, where PBHs are already excluded from being a sizeable fraction of the dark matter ($f_{\mathrm{PBH},0} \sim 10^{-10}$).

Finally, for our analysis, we defined the onset of the memory burden effect when the black hole loses half of its initial mass by setting $q = 1/2$. As Dvali et al. (2020) have shown, this is the latest time at which a quantum backreaction is unavoidable. Dvali & Panchenko (2015) and Michel & Zell (2023) have shown that in certain prototype systems of black holes, the breakdown of Hawking's calculations could happen already after a fraction $1/\sqrt{S}$ of the SC lifetime. While this requires more microscopic justification, it is still worthwhile to consider the effect on the constraints of PBH. Such an early transition into the phase of memory burden would correspond to

$$1 - q \approx 2 \times 10^{-6} (M_0/\mathrm{g})^{-1}, \tag{17}$$

which would imply that black holes with $M_0 > 10^{10}$ g reach the memory burden phase after losing a fraction of less than 10^{-15} of their initial mass. This implies that any constraints that arise from the SC evaporation phase (the'vertical band' in Fig. 1) will be significantly weakened. When we recompute these constraints under this assumption, then PBHs can make up the entirety of the dark matter for $M_0 > 10^{10}$ g. One is still left with the constraints from the slowed down phase of the evaporation. This would open a significantly larger window for PBHs as a viable dark matter candidate.

4 SUMMARY AND CONCLUSIONS

In this work, we investigate how the constraints on evaporating PBHs change when one goes beyond the SC calculations from Hawking (1974). When the quantum backreaction of the emitted particles is taken into account, the evaporation can slow down drastically due to the effect of memory burden described by Dvali et al. (2020). Here, we compute the bounds on the dark matter fraction of PBHs as a function of the currently unknown parameter k that quantifies the strength of the memory burden effect. It gives the suppression of the evaporation rate in powers of the black hole entropy $1/S^k$.

We find that for $k > 1.0$ a new mass window emerges, where PBHs can be a viable dark matter candidate. It extends up to $M_0 \sim 10^{10}$ g with higher mass being ruled out due to constraints from BBN. The lower end of the mass window depends on the parameter k, extending to $M_0 \sim 10^5$ g for $k = 2$.

The bounds that we obtain with our simple model of the evaporation process are quite robust and should hold unless the breakdown of the SC evaporation phase happens much earlier or the spectra of the PBH evaporation changes dramatically. It should be noted that all the constraints that we obtain in this work are computed for a monochromatic mass function and zero spin of the black hole to keep our results as general as possible. In reality, PBHs will form with an extended distribution of initial mass. Studying bounds on the dark matter fraction of PBHs for more realistic mass functions and a non-zero spin distribution is left for future work.

Our results are supposed to provide a first insight on the landscape of PBH constraints beyond the Hawking picture of black hole evaporation. A more detailed understanding of the actual evaporation process remains a significant theoretical challenge but will undoubtedly help to study the possibility that dark matter exists in the form of light PBHs.

In addition to open questions about the fundamental nature of black holes, it would also be of great interest to study the potential observational signatures and possibilities to detect PBHs in this new mass window where they are a viable dark matter candidate (see e.g. Lehmann et al. 2019).

SOFTWARE

BLACKHAWK 2.1 (Arbey & Auffinger 2019), EXOCLASS (Stöcker et al. 2018), CLASS (Blas et al. 2011), MONTEPYTHON 3.6.0 (Audren et al. 2013; Brinckmann & Lesgourgues 2019), JULIA 1.9.3 (Bezanson et al. 2017), and MATPLOTLIB 3.7.1 (Hunter 2007).

ACKNOWLEDGEMENTS

We thank Gia Dvali for giving us the idea for this project, as well as for his supervision. We also would like to thank Ana Alexandre, Manuel Behrendt, Florian Kühnel, Tracy Slatyer, and Sebastian Zell for fruitful discussion and helpful comments. We are grateful for the help of Patrick Stöcker and Vivian Poulin with regards to the EXOCLASS code. This research was supported by the Excellence Cluster ORIGINS, which is funded by the Deutsche Forschungsgemeinschaft (DFG, German Research Foundation) under Germany's Excellence Strategy—EXC-2094 - 390783311. Kazunori Kohri is supported by KAKENHI grant no. JP22H05270.

DATA AVAILABILITY

The numerical results presented in this article are publicly accessible under https://doi.org/10.5281/zenodo.10718218 (Thoss 2024).

REFERENCES

Acharya S. K., Khatri R., 2020, J. Cosmol. Astropart. Phys., 2020, 010
Ackermann M. et al., 2015, ApJ, 799, 86
Alexandre A., Dvali G., Koutsangelas E., 2024, preprint (arXiv:2402.14069)
Allahverdi R., Dent J., Osinski J., 2018, Phys. Rev. D, 97, 055013
Anchordoqui L. A., Antoniadis I., Lüst D., 2022, Phys. Rev. D, 106, 086001
Arbey A., Auffinger J., 2019, Eur. Phys. J. C, 79, 693
Arbey A., Auffinger J., Silk J., 2020, Phys. Rev. D, 101, 023010
Arkani-Hamed N., Dimopoulos S., Dvali G., 1998, Phys. Lett. B, 429, 263
Audren B., Lesgourgues J., Benabed K., Prunet S., 2013, J. Cosmol. Astropart. Phys., 2013, 001
Auffinger J., 2022, Eur. Phys. J. C, 82, 384
Auffinger J., 2023, Prog. Part. Nucl. Phys., 131, 104040
Baldes I., Decant Q., Hooper D. C., Lopez-Honorez L., 2020, J. Cosmol. Astropart. Phys., 2020, 045
Ballesteros G., Coronado-Blázquez J., Gaggero D., 2020, Phys. Lett. B, 808, 135624
Barrow J. D., Copeland E. J., Liddle A. R., 1992, Phys. Rev. D, 46, 645
Bauer C. W., Rodd N. L., Webber B. R., 2021, J. High Energy Phys., 2021, 121
Baumann D., Steinhardt P. J., Turok N., 2007, preprint(hep–th/0703250)
Bellm J. et al., 2016, Euro. Phys. J. C, 76, 196
Berteaud J., Calore F., Iguaz J., Serpico P. D., Siegert T., 2022, Phys. Rev. D, 106, 023030
Bezanson J., Edelman A., Karpinski S., Shah V. B., 2017, SIAM Rev., 59, 65
Blas D., Lesgourgues J., Tram T., 2011, J. Cosmol. Astropart. Phys., 2011, 034
Bouchet L., Strong A. W., Porter T. A., Moskalenko I. V., Jourdain E., Roques J.-P., 2011, ApJ, 739, 29
Boudaud M., Cirelli M., 2019, Phys. Rev. Lett., 122, 041104

Brinckmann T., Lesgourgues J., 2019, Phys. Dark Universe, 24, 100260
Cang J., Gao Y., Ma Y.-Z., 2022, J. Cosmol. Astropart. Phys., 2022, 012
Cao Z. et al., 2023, Phys. Rev. Lett., 131, 151001
Carr B. J., Hawking S. W., 1974, MNRAS, 168, 399
Carr B. J., Kohri K., Sendouda Y., Yokoyama J., 2010, Phys. Rev. D, 81, 104019
Carr B. J., Kohri K., Sendouda Y., Yokoyama J., 2016, Phys. Rev. D, 94, 044029
Carr B., Kohri K., Sendouda Y., Yokoyama J., 2021, Rep. Prog. Phys., 84, 116902
Chan M. H., Lee C. M., 2020, MNRAS, 497, 1212
Chapline G. F., 1975, Nature, 253, 251
Chen S., Zhang H.-H., Long G., 2022, Phys. Rev. D, 105, 063008
Chluba J., Ravenni A., Acharya S. K., 2020, MNRAS, 498, 959
Coogan A., Morrison L., Profumo S., 2020, J. Cosmol. Astropart. Phys., 2020, 056
Dasgupta B., Laha R., Ray A., 2020, Phys. Rev. Lett., 125, 101101
DeRocco W., Graham P. W., 2019, Phys. Rev. Lett., 123, 251102
Dolgov A. D., Naselsky P. D., Novikov I. D., 2000, preprint(astro–ph/0009407)
Dvali G., 2018, preprint (arXiv:1810.02336)
Dvali G., Panchenko M., 2015, preprint (arXiv:1507.08952)
Dvali G., Eisemann L., Michel M., Zell S., 2020, Phys. Rev. D, 102, 103523
Dvali G., Kühnel F., Zantedeschi M., 2021, Phys. Rev. D, 104, 123507
Dvali G., Kühnel F., Zantedeschi M., 2022, Phys. Rev. Lett., 129, 061302
Dvali G., Kaikov O., Kuhnel F., Sebastián Valbuena-Bermúdez J., Zantedeschi M., 2024, Phys. Rev. Lett., 132, 151402
Escrivà A., 2022, Universe, 8, 66
Friedlander A., Mack K. J., Schon S., Song N., Vincent A. C., 2022, Phys. Rev. D, 105, 103508
Fujita T., Harigaya K., Kawasaki M., Matsuda R., 2014, Phys. Rev. D, 89, 103501
Gruber D. E., Matteson J. L., Peterson L. E., Jung G. V., 1999, ApJ, 520, 124
Hasegawa T., Hiroshima N., Kohri K., Hansen R. S. L., Tram T., Hannestad S., 2019, J. Cosmol. Astropart. Phys., 2019, 012
Hawking S., 1971, MNRAS, 152, 75
Hawking S. W., 1974, Nature, 248, 30
Hawking S. W., 1975, Commun. Math. Phys., 43, 199
Hooper D., Krnjaic G., McDermott S. D., 2019, J. High Energy Phys., 2019, 1
Hooper D., Krnjaic G., March-Russell J., McDermott S. D., Petrossian-Byrne R., 2020, preprint (arXiv:2004.00618)
Hunter J. D., 2007, Comput. Sci. Eng., 9, 90
Kawasaki M., Kohri K., Moroi T., Takaesu Y., 2018, Phys. Rev. D, 97, 023502
Keith C., Hooper D., Blinov N., McDermott S. D., 2020, Phys. Rev. D, 102, 103512
Kim H., 2021, MNRAS, 504, 5475
Laha R., 2019, Phys. Rev. Lett., 123, 251101
Laha R., Lu P., Takhistov V., 2021, Phys. Lett. B, 820, 136459
Lehmann B. V., Johnson C., Profumo S., Schwemberger T., 2019, J. Cosmol. Astropart. Phys., 2019, 046
Lennon O., March-Russell J., Petrossian-Byrne R., Tillim H., 2018, J. Cosmol. Astropart. Phys., 2018, 009
Lucca M., Schöneberg N., Hooper D. C., Lesgourgues J., Chluba J., 2020, J. Cosmol. Astropart. Phys., 2020, 026
Luo Y., Hanasoge S., Tromp J., Pretorius F., 2012, ApJ, 751, 16
MacGibbon J. H., 1987, Nature, 329, 308
Masina I., 2021, Gravitation Cosmol., 27, 315
McMillan P. J., 2011, MNRAS, 414, 2446
Michel M., Zell S., 2023, Fortschr. Phys., 71, 2300163
Morrison L., Profumo S., Yu Y., 2019, J. Cosmol. Astropart. Phys., 2019, 005
Novikov I. D., Polnarev A. G., Starobinskii A. A., Zeldovich I. B., 1979, A&A, 80, 104
Pacheco J. A. d. F., Kiritsis E., Lucca M., Silk J., 2023, Phys. Rev. D, 107, 123525
Papanikolaou T., 2023, preprint (arXiv:2303.00600)
Papanikolaou T., Vennin V., Langlois D., 2021, J. Cosmol. Astropart. Phys., 2021, 053
Planck Collaboration V, 2020, A&A, 641, A5
Poulin V., Lesgourgues J., Serpico P. D., 2017, J. Cosmol. Astropart. Phys., 2017, 043
Ruiz-Lapuente P., The L.-S., Hartmann D. H., Ajello M., Canal R., Röpke F. K., Ohlmann S. T., Hillebrandt W., 2016, ApJ, 820, 142
Sjöstrand T. et al., 2015, Comput. Phys. Commun., 191, 159
Slatyer T. R., Padmanabhan N., Finkbeiner D. P., 2009, Phys. Rev. D, 80, 043526
Stöcker P., Krämer M., Lesgourgues J., Poulin V., 2018, J. Cosmol. Astropart. Phys., 2018, 018
Strong A. W., 2011, in Giani S., Leroy C., Rancoita P. G.eds, Cosmic Rays for Particle and Astroparticle Physics, World Scientific Publishing, Singapore. p. 473
Strong A. W., Mattox J. R., 1996, A&A, 308, L21
Strong A. W. et al., 1994, A&A, 292, 82
Strong A. W., Bloemen H., Diehl R., Hermsen W., Schönfelder V., 1999, Astrophys. Lett. Commun., 39, 209
Strong A. W., Moskalenko I. V., Reimer O., 2004, ApJ, 613, 956
Taylor Q., Starkman G. D., Hinczewski M., Mihaylov D. P., Silk J., de Freitas Pacheco J., 2024, preprint (arXiv:2403.04054)
Thoss V. A., 2024, Data for the paper 'Breakdown of Hawking Evaporation opens new Mass Window for Primordial Black Holes as Dark Matter Candidate' (Thoss et. al. 2024), Zenodo, https://doi.org/10.5281/zenodo.10718218
Torres R., 2013, Phys. Rev. D, 87, 123514
Zel'dovich Y. B., Novikov I. D., 1967, Soviet Astron., 10, 602

APPENDIX A: ADDITIONAL FIGURES

Here we provide additional plots that show the constraints on $f_{\mathrm{PBH},0}(k, M_0)$ for galactic γ ray emission in Fig. A1 and for extragalactic γ ray emission in Fig. A2.

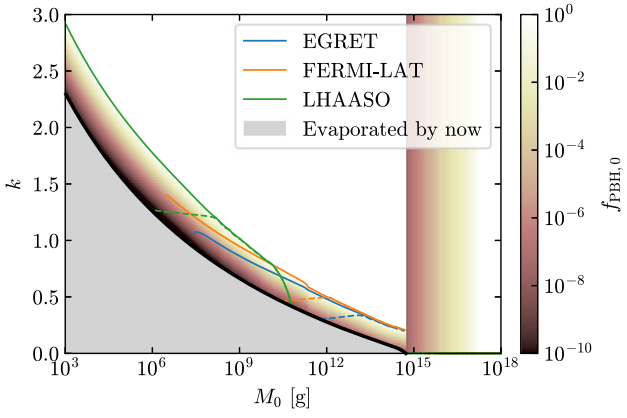

Figure A1. Combined constraints on $f_{\mathrm{PBH},0}(k, M_0)$ from galactic γ ray emission. The coloured lines show $f_{\mathrm{PBH}} = 1$ contours separately for selected observational data. The dashed lines are computed using only the primary photon emission.

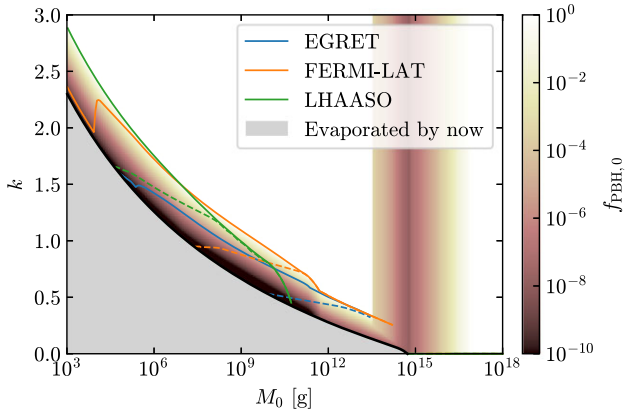

Figure A2. Combined constraints on $f_{\rm PBH,0}(k, M_0)$ from the extragalactic γ ray background. The coloured lines show $f_{\rm PBH} = 1$ contours separately for selected observational data. The dashed lines are computed using only primary photon emission.

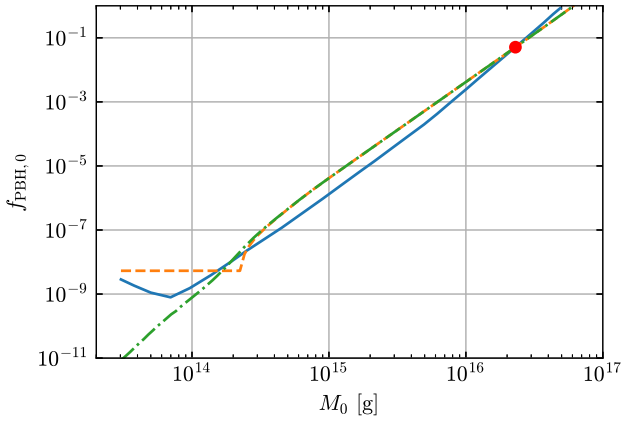

Figure B1. CMB constraints on the initial dark matter fraction of PBHs $f_{\rm PBH,0}(M_0)$ in the SC limit ($k = 0$). The solid blue line shows the result from Stöcker et al. (2018). The red dot shows the value $f(M_0 = 2.3 \times 10^{16}\text{g}) = 5.1 \times 10^{-2}$ from which the rescaled constraints were obtained. The dashed orange line shows the constraints obtained through equation (13), whereas the green dash–dotted line also takes into account the redshift-dependence of the integral.

APPENDIX B: CMB ANISOTROPIES

As explained in Section 2.7, to compute the constraints from CMB anisotropies, we rescale the results from the full MCMC runs using equation (13). In Fig. B1, we show that this method is able to reproduce the SC constraints within one order of magnitude by rescaling a single value $f(M_0 = 2.3 \times 10^{16}\text{g}) = 5.1 \times 10^{-2}$ obtained by Stöcker et al. (2018) over three orders of magnitude in mass. Note that in Fig. B1, we also show the resulting constraints when properly taking into account the $(1 + z)^3$ factor in equation (12). There is no noticeable difference down to $M_0 \sim 3 \times 10^{14}$g. The divergence at low masses is not relevant for us since it will in any case only affect those PBHs that will not survive until today – both in the SC limit as well as for $k > 0$.

To obtain constraints for $k > 0$, we compute six full MCMC runs for $M_0 \in [10^3, 10^5, 10^7, 10^9, 10^{11}, 10^{13}]$ g, where k is chosen for each mass such that $f(k, M_0) = 10^{-2}$ when rescaled from $f(M_0 = 2.3 \times 10^{16}\text{g}) = 5.1 \times 10^{-2}$ to the respective masses according to equation (13) and taking into account the effect of the memory burden. The values of $f(k, M_0)$ obtained from the MCMC runs lie between 3.8×10^{-2} and 9.7×10^{-2} and thus up to one order of magnitude higher then the 10^{-2} is expected from rescaling. These results are then used to obtain constraints for arbitrary values of k' and M_0' by rescaling from the two nearest values of M_0 and interpolating between the results. To test the validity of this approach, we run a second set of MCMC runs with $M_0 \in [10^4, 10^6, 10^8, 10^{10}, 10^{12}]$ g and k such that our method would give $f(k, M_0) = 10^{-1}$. The resulting constraints on $f_{\rm PBH,0}$ from the full computation are within a factor of two from our approximation, which is more than sufficient. This translates to an error in the bound on $k(M_0, f = 1)$ of less than 0.01.

This paper has been typeset from a TEX/LATEX file prepared by the author.

Chapter 4

Publication II – New bounds on memory burdened primordial black holes from Big Bang nucleosynthesis

The following work has been published in the Journal of Cosmology and Astroparticle Physics, Volume 2025, Issue 11, Nr. 57 (Chaudhuri et al., 2025). It is reprinted with permission from the publisher. It was initiated by Kazunori Kohri, who was interested in the computation of constraints from BBN for the memory burden stage of black hole evaporation, as an extension of our previous work. Making use of his previous numerical results, I derived constraints to investigate the parameter space of light PBHs that are evaporating in the early universe. This limits the available parameter space for evaporating PBHs in the early universe and has implications for their gravitational wave signatures and potential role in Baryogenesis. I received helpful comments from Arnab Chaudhuri, a postdoc of Kazunori Kohri, who prepared most of the manuscript.

We want to note that the published paper has a typo in Equation 2.6. The correct formula reads

$$\frac{\mathrm{d}^2 N_{i,\mathrm{SC}}}{\mathrm{d}E\mathrm{d}t}(E, M, s_i) = \frac{g_i}{2\pi\hbar} \frac{\Gamma(E, M, s_i)}{e^{E/k_B T} - (-1)^{2s_i}} \,, \tag{4.1}$$

with $(-1)^{2s_i}$ instead of $(-1)^{s_i}$.

Journal of Cosmology and Astroparticle Physics
An IOP and SISSA journal

Received: *July 14, 2025*
Accepted: *October 13, 2025*
Published: *November 18, 2025*

New bounds on memory burdened primordial black holes from Big Bang nucleosynthesis

Arnab Chaudhuri[a], **Kazunori Kohri**[a,b,c,d] **and Valentin Thoss**[e,f,g]

[a] *Division of Science, National Astronomical Observatory of Japan, Mitaka, Tokyo 181-8588, Japan*
[b] *The Graduate University for Advanced Studies (SOKENDAI), Mitaka, Tokyo 181-8588, Japan*
[c] *Theory Center, IPNS, KEK, 1-1 Oho, Tsukuba, Ibaraki 305-0801, Japan*
[d] *Kavli IPMU (WPI), UTIAS, The University of Tokyo, Kashiwa, Chiba 277-8583, Japan*
[e] *Universitäts-Sternwarte, Ludwig-Maximilians-Universität München, Scheinerstr. 1, 81679 Munich, Germany*
[f] *Max-Planck Institute for Extraterrestrial Physics, Giessenbachstr. 1, 85748 Garching, Germany*
[g] *Excellence Cluster ORIGINS, Boltzmannstrasse 2, 85748 Garching, Germany*

E-mail: arnab.chaudhuri@nao.ac.jp, kazunori.kohri@gmail.com, vthoss@mpe.mpg.de

Abstract: Primordial black holes (PBHs) with masses below 10^9 grams are typically assumed to have negligible cosmological impact due to their rapid evaporation via Hawking radiation. However, the "memory burden" effect, which is a quantum suppression of PBH evaporation, can dramatically alter their decay dynamics. In this work, we revisit early-Universe constraints on ultralight PBHs in this mass range, demonstrating that memory burden significantly alters previous constraints. We compute new cosmological bounds from BBN that strongly limit the presence of ultralight PBHs in the early Universe. We report that the PBHs in the mass range 10^0–10^2 g for a suppression parameter $k = 2$, where k quantifies the strength of the memory burden effect, are unconstrained by observations.

Keywords: big bang nucleosynthesis, physics of the early universe, primordial black holes

ArXiv ePrint: 2506.20717

https://doi.org/10.1088/1475-7516/2025/11/057

JCAP11(2025)057

Contents

1 Introduction

Primordial Black Holes (PBHs), proposed over half a century ago [1], have re-emerged as compelling candidates in the study of dark matter (DM) [1–12] and gravitational wave sources [13–23]. Unlike many DM scenarios, PBHs arise naturally from gravitational collapse without the need for new particle species.

However, PBHs are subject to strong constraints, particularly due to Hawking radiation [24, 25], which implies that PBHs with masses $M < 10^{15}$ g would have evaporated by the present epoch. While such light PBHs cannot account for DM, they could have played roles in early-Universe phenomena such as reheating [26–28], leptogenesis [29, 30], gravitational wave production [31–41], destabilizing the Higgs [42, 43], and DM generation [44–50].

Surviving PBHs with $M \gtrsim 10^{15}$ g are also constrained by observations such as γ-ray backgrounds [51, 52], Big Bang nucleosynthesis (BBN) [4, 6, 53, 54], and lensing or dynamical bounds [55–58]. A detailed summary can be found in [6]. For a monochromatic mass function, PBHs can comprise all of DM only in the mass window 10^{17} g $\lesssim M \lesssim 10^{23}$ g. In this work we restrict our analysis to a monochromatic PBH mass spectrum, as is standard in many earlier studies; we comment later on how broader distributions (e.g. log-normal or linear) would qualitatively affect our bounds.

The lower mass cutoff stems from the inverse mass dependence of Hawking temperature, $T \sim 1/M$, which accelerates evaporation [24]. This process also injects energy into the early Universe, potentially disrupting γ-ray backgrounds, CMB anisotropies, and BBN [59]. Accordingly, only a small abundance of light PBHs is allowed. However, some studies suggest that certain quantum effects can delay or suppress evaporation. One such effect is the "memory burden," first proposed in [60], which becomes relevant when a black hole has lost roughly half of its initial mass. Hawking's semiclassical (SC) results, valid in the $G \to 0$, $M \to \infty$ limit with fixed Schwarzschild radius, neglect backreaction from emitted radiation. As evaporation proceeds, this backreaction grows significant, modifying the dynamics [61].

The memory burden (MB) suppresses late-time evaporation and has been further developed in [62–79]. It implies that an old black hole with mass M is not equivalent to a young one with the same mass: the suppression mechanism delays the final burst of evaporation, altering the timing and energy injection into the plasma.

JCAP11(2025)057

As shown in [62, 80], this opens the possibility for PBHs with initial masses below 10^{10} g to evade standard BBN bounds. In this work, we revisit BBN constraints in the presence of memory burden for *ultralight PBHs* which have fully evaporated by the present day. Throughout, we assume a radiation-dominated Universe so that $H = 1/(2t)$ remains valid in our parameter space; we explicitly verify that the PBH energy fraction never grows large enough to cause PBH domination. This regime has not been tightly constrained and offers a previously overlooked window for viable PBH cosmology.

We show that evaporation suppression significantly alters the constraints from the abundances of light elements. Our results reveal a parameter space where evaporated PBHs remain compatible with observations, motivating a revised framework for future studies of such scenarios.

This paper is organized as follows: in section 2 we review the components of memory-burdened PBH evolution; in section 3, we present the modified BBN bounds in the ultralight regime; and we conclude in section 4.

2 Components of Memory Burden

To understand the influence of memory burden on PBH dynamics, it is crucial to first outline the key elements governing PBH formation and evolution. The mass of a primordial black hole (PBH) resulting from gravitational collapse is closely tied to the horizon size at the moment of formation. This relationship is expressed as [81, 82]:

$$M_0 = \frac{4}{3}\,\pi\,\gamma\,\left(\frac{1}{H\,(T_0)}\right)^3\,\rho_{\rm rad}\,(T_0)\;, \tag{2.1}$$

where $H(T_0)$ is the Hubble rate during the radiation-dominated era at the time of PBH formation, and γ is an efficiency factor defining the fraction of the total mass within the Hubble radius that collapses into PBHs and M_0 is the mass of the PBH at formation. In our numerical analysis, we take $\gamma = 1$ as a fiducial benchmark, corresponding to maximal collapse efficiency where the PBH mass equals the horizon mass at formation. This choice is standard in the literature and allows for conservative constraints. We also adopt $h = 0.67$ for the reduced Hubble constant. These parameters are consistent with Planck cosmology and [6]. The radiation temperature at the point of PBH formation is given by:

$$T_0 = \left(\frac{45\,\gamma^2}{16 g_\star(T_0)}\right)^{1/4}\,\left(\frac{M_P}{M_0}\right)^{1/2}\,M_P\,, \tag{2.2}$$

where we take $g_*(T_0) = 106.75$, appropriate for the Standard Model relativistic degrees of freedom at high temperatures, and $M_P \simeq 1.2 \times 10^{19}$ GeV is the Planck mass.

The time of PBH formation is determined by:

$$t_0 = \frac{M_0}{\gamma M_P^2}\,, \tag{2.3}$$

assuming a standard radiation-dominated Universe with $H(t) = 1/(2t)$. The initial abundance of PBHs can be described using the dimensionless parameter β_{PBH}, defined as:

$$\beta_{PBH} \equiv \frac{\rho_{\rm BH}(t_0)}{\rho_R(t_0)}\,, \tag{2.4}$$

JCAP11(2025)057

where $\rho_{\rm BH}(t_0)$ is the energy density of the PBHs, and $\rho_R(t_0)$ is the energy density of radiation at the time of formation. This parameter quantifies the fraction of the total energy density present in the form of PBHs at their formation, serving as an important measure of their initial contribution to the energy budget of the Universe.

The quantity $f_{\rm PBH,0}$ denotes the fraction of DM composed of PBHs at the time of their formation, which is related to the initial PBH abundance $\beta_{\rm PBH}$ by

$$f_{\rm PBH,0} = \frac{\beta_{\rm PBH}}{\Omega_{\rm DM}}\,, \tag{2.5}$$

where $\Omega_{\rm DM}$ is the density parameter of dark matter at the time of PBH formation. Note that $f_{\rm PBH,0} = 1$ does not imply that PBHs constitute the present-day dark matter due to the evaporation over cosmic time.

The semiclassical (SC) emission rate of particles from a black hole is a cornerstone of Hawking radiation theory, describing how particle species i are emitted with energy E from a black hole of mass M and temperature T [25]. This rate is expressed as:

$$\frac{{\rm d}^2 N_{i,\rm SC}}{{\rm d}E{\rm d}t}(E, M, s_i) = \frac{g_i}{2\pi}\frac{\Gamma(E, M, s_i)}{e^{E/T(M)} - (-1)^{s_i}}\,, \tag{2.6}$$

where g_i represents the degrees of freedom of the particle species, s_i is the particle's spin, and $\Gamma(E, M, s_i)$ are the greybody factors that quantify the deviation from a perfect black-body spectrum. The black hole's temperature T is intrinsically linked to its mass M through the relationship:

$$T = \frac{M_P^2}{8\pi M}\,. \tag{2.7}$$

The emission of particles leads to a gradual decrease in the black hole's mass, characterized by a mass loss rate:

$$\dot{M} = -\frac{\mathcal{F}(M)}{M^2}\,, \tag{2.8}$$

where $\mathcal{F}(M)$ is a function encapsulating the cumulative contributions of all particle species that the black hole emits at a given mass M. The greybody factors and the function $\mathcal{F}(M)$ are computed using the BlackHawk code [83], which provides accurate predictions for the particle emission spectra of black holes across various scenarios. The total lifetime of a black hole within the Hawking framework is determined solely by its initial mass and is approximately given by:

$$t_{\rm SC}(M_0) \approx \frac{M_0^3}{3\mathcal{F}(M)}\,. \tag{2.9}$$

While the SC picture predicts a rapid final burst of evaporation as M decreases, quantum gravity effects may become relevant once a significant fraction of the BH mass has been radiated. One such effect is the *memory burden* (MB), which encodes the idea that a black hole retains quantum information about its evaporation history, thereby modifying its ability to radiate. Physically, the MB can be viewed as a backreaction of internal microstate complexity on the emission process [60, 61].

In our revised framework for black hole evaporation, we incorporate modifications to Hawking's original model to account for deviations that arise during the later stages of evaporation. Specifically, we assume that Hawking's results hold up until the black hole reaches a critical mass $M = qM_0$, where q is the fraction of the initial black hole mass at which the standard SC description begins to break down. We take $q = 1/2$ as a representative benchmark, corresponding to the point where roughly half of the BH mass has evaporated — a regime where the backreaction effects are expected to become significant [61, 62]. We have checked that varying q in the range 0.3–0.7 does not qualitatively change our conclusions.

Beyond this critical mass, the particle emission rate could be significantly suppressed due MB effect. This suppression is described in a parametrized form based on the insights of [61]:

$$\frac{\mathrm{d}^2 N_{i,\mathrm{MB}}}{\mathrm{d}E\mathrm{d}t}(E, M_0, s_i) = \frac{1}{S(qM_0)^k}\frac{\mathrm{d}^2 N_{i,\mathrm{SC}}}{\mathrm{d}E\mathrm{d}t}(E, qM_0, s_i)\,, \tag{2.10}$$

where k is an adjustable parameter governing the degree of suppression, and S is the entropy of the black hole expressed in units of the Boltzmann constant k_B. Physically, the entropy $S \sim M^2$ quantifies the logarithm of the number of internal microstates of the black hole, so that the total number of accessible microstates grows as $\exp(S)$. The idea is that a more entropic black hole has more "memory" of its past emissions, and this memory suppresses further evaporation. The exponent k controls how strong this suppression is: $k = 0$ recovers the SC case, while $k \gtrsim 1$ can lead to orders-of-magnitude delay in the final stages of evaporation.

The entropy S is given by:

$$S = \frac{4\pi M^2}{M_P} \approx 2.6 \times 10^{10} \left(\frac{M}{1\,\mathrm{g}}\right)^2 . \tag{2.11}$$

The extraordinarily large value of entropy for black holes implies that even modest values of k can lead to a suppression of the emission rate by several orders of magnitude. For $M \simeq 1\,\mathrm{g}$ one has $S \simeq 2.7 \times 10^{10}$; thus for $k = 2$ the suppression factor is $S^{-k} \simeq 1.4 \times 10^{-21}$ (or $\simeq 2 \times 10^{-20}$ if evaluated at the onset $q = 1/2$), corresponding to an MB-lifetime enhancement by $S^k \sim 10^{20}$ relative to the SC rate.

Importantly, under this modified framework, the black hole temperature and emission rate are assumed to remain constant in the MB regime. As a consequence, the decay of the black hole becomes linear, with the lifetime approximated as:

$$t_{\mathrm{MB}}(M) \approx \frac{(qM_0)^3 S(qM_0)^k}{\mathcal{F}(qM_0)}\,, \tag{2.12}$$

where $\mathcal{F}(qM_0)$ encapsulates the degrees of freedom of the emitted particles and S_0 is the initial entropy. This expression highlights that the MB lifetime grows with S^k, explaining why even tiny PBHs can live much longer than predicted by the SC picture. We emphasize that the contribution from the early SC phase is negligible for $k \gtrsim 1$, making t_{MB} the dominant lifetime.

3 New bounds from BBN

The primordial abundance of light elements serves as one of the earliest and most sensitive cosmological tools for investigating the effects of PBH evaporation. According to Hawking's

JCAP11(2025)057

theory, black holes with mass $M_0 \gtrsim 10^{10}$ g undergo evaporation during or after the epoch of Big Bang Nucleosynthesis (BBN) [6], the period when light elements such as hydrogen, helium, and lithium were formed. The energetic radiation and particles emitted during this process can significantly impact the delicate nuclear reactions driving the synthesis of these elements.

In particular, the radiation from evaporating PBHs can disrupt the neutron-to-proton ratio, a key parameter in determining the final abundances of helium and other light nuclei. Moreover, high-energy photons and hadrons emitted during evaporation can trigger photodissociation and hadrodissociation processes, fragmenting existing nuclei and altering the predicted elemental abundances.

The standard BBN framework, which assumes no additional energy injection, has been remarkably successful in matching the observed primordial abundances of light elements. As a result, any deviations caused by PBH evaporation are subject to stringent observational constraints. Modifications to the predicted abundances must remain minimal to avoid conflict with astrophysical and cosmological measurements, making the study of light element abundances a powerful probe for understanding PBH dynamics in the early Universe. According to the findings presented by [6], which build upon earlier results from [4] and incorporate updates from [84, 85] and [86–88], the initial fraction of dark matter comprised of primordial black holes is tightly constrained to $f_{\mathrm{PBH},0} \sim 10^{-4}$ for $M_0 \in [10^{10}, 10^{13}]$. The upper limit of this mass range is determined by the lifetime of the PBHs exceeding the radiation-dominated phase of the Universe. Beyond radiation-matter-equality, the processes responsible for the modification of the abundance of light elements become inefficient, leading to a weakening of the constraint.

In deriving these constraints, we make use of the standard BBN cascade methodology developed in [84, 85, 88], where the effects of electromagnetic and hadronic showers on light-element abundances are computed and compared to observations. We do not perform a new cascade calculation here, but instead rescale the existing bounds by accounting for the modified evaporation history due to memory burden.

The constraints imposed by BBN are primarily obtained by two particle emission modes: the radiative and the hadronic emission modes. The electromagnetic particles (photons, electrons, etc.) emitted from the evaporating PBH collide with background photons and electrons and form an electromagnetic shower. Ultimately, this shower thermalises and dissipates into the thermal bath. During the development of the electromagnetic shower, the low-energy particles inside the electromagnetic shower dissociate light elements. The scale of the shower evolution is determined by the total amount of energy emitted from the evaporating PBH that ultimately thermalises. Therefore, the amount of light elements destroyed is determined by the total amount of energy emitted from the evaporating PBH. The dissociation of the light elements by the hadronic emission mode occurs when the emitted particles are colored particles (quarks, gluons, etc.), which fragment to produce a lot of high-energy hadrons (mesons and baryons). These trigger scattering with background particles (nuclei, nucleons, photons, electrons, etc.), forming a hadronic shower composed of energetic daughter hadrons. These daughter hadrons eventually dissipate into the thermal bath through their decays and/or scatterings off the background particles. During the shower evolution, light elements are dissociated by those energetic hadrons. The scale of this effect

JCAP11(2025)057

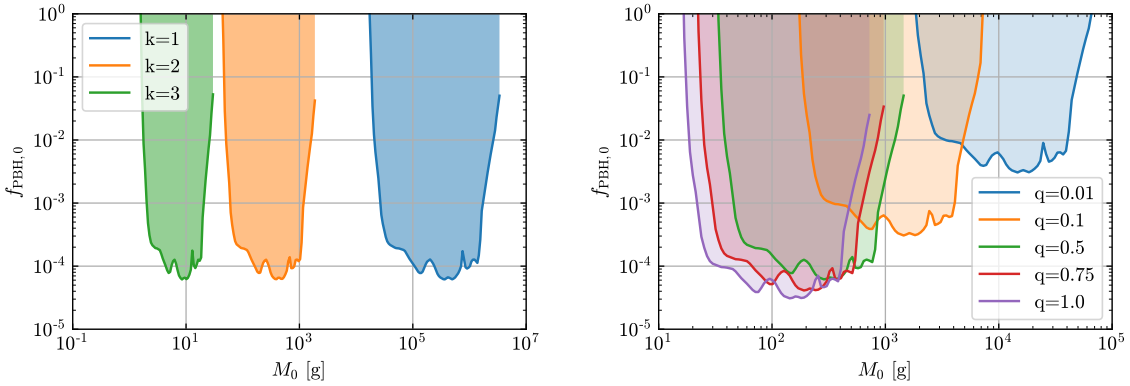

Figure 1. Bounds on $f_{\mathrm{PBH},0}(M_0)$ from BBN (shaded regions). The left panel displays constraints for $q = 0.5$ and various values of k. The right panel shows bounds for $k = 2$ and various values of q.

differs from that of the previous electromagnetic-shower case, as it is determined by the number of high-energy hadrons emitted just after the fragmentation. However, the number of high-energy hadrons depends only very weakly on the energy of the initially emitted colored particles. According to the experimental data of the fragmentation to hadrons obtained by the collider experiments, e.g., the Large Hadron Collider (LHC) experiment, this energy dependence does not increase linearly with energy but logarithmically. More quantitatively, even when the numbers of the high-energy hadrons emitted after the fragmentation are scaled by the total energy emitted from the PBH, the deviation is not significant.

For the reasons explained above, the physics of BBN is mostly sensitive to the total amount of energy injected by the PBHs at a given time after the Big Bang. Therefore, in order to compute bounds that take the memory burden into account we will assume that f_{PBH} is a function of the time of evaporation t_{ev} and the total energy injected only. We convert the existing bound $f_{\mathrm{PBH},0}(M)$ to $f_{\mathrm{PBH},0}(t_{\mathrm{ev}})$ according to their semiclassical lifetime. Then, we can obtain the bounds from the first phase of evaporation ($M_0 \to qM_0$) by rescaling the usual bounds by a factor of $1 - q$ as this is the fraction of mass lost (and thus energy injected) before the memory burden sets in. For $q = 0.5$, the full numerical calculation done by [62] found a relaxation of the bound by a factor of 0.55, close to the factor of 0.5 expected from the arguments above. The second stage of evaporation has a prolonged lifetime t_{MB} due to the memory burden effect, given by equation 2.12. We can compute the BBN bound for this phase according to $f'_{\mathrm{PBH},0}(M) = q f_{\mathrm{PBH},0}(t_{\mathrm{ev}} = t_{\mathrm{MB}})$, where f' denotes the new bound. In summary, the constraint from BBN is computed by taking into account the lifetime of both evaporation stages and the fraction of the total energy released during these.

In figure 1 we display the bounds from BBN for various values of q and k, that parametrize the memory burden effect. The prolongation of the evaporation means that the constraints now affect PBHs with much smaller initial masses, as they can now survive beyond the onset of BBN. Constraints from the semiclassical phase of evaporation restrict $f_{\mathrm{PBH},0} < 1$ for $M_{\mathrm{PBH}} \in [10^{10}, 10^{13}]\,\mathrm{g}$. Taking into account the memory burden, one obtains strong constraints for PBHs with $M_{\mathrm{PBH}} \in [10^4, 10^6]\,\mathrm{g}$ for $k = 1$ and substantially lighter ones for stronger suppression, i.e. larger values of k. Notably, the width of the mass window

JCAP11(2025)057

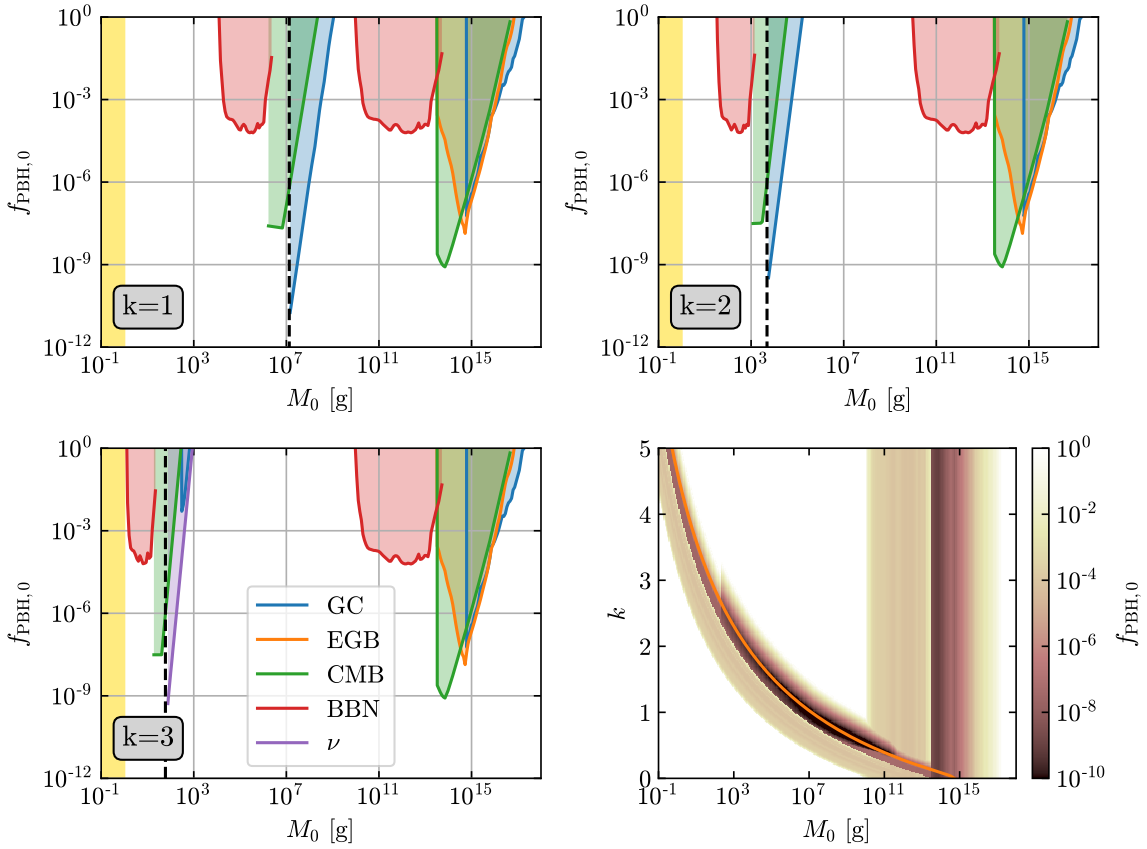

Figure 2. Constraints on $f_{\mathrm{PBH},0}(M_0)$ for $k = 1, 2, 3$. Shown are bounds from γ-ray emission from the galactic center (GC), the extragalactic γ-ray background (EGB), CMB anisotropies and BBN. For $k = 3$ we also display the bound from galactic neutrino emission [66]. The vertical dashed line indicates the mass below which PBHs fully evaporate by today. The bottom right panel shows a map of constraints on $f_{\mathrm{PBH},0}$ as a function of M_0 and k for $q = 0.5$. For parameters below the orange line, PBHs evaporate completely. The corresponding bounds in terms of β_{PBH} are given in appendix A.

constrained by BBN shrinks with increasing k as a result of the stronger dependence of t_{MB} on M_0 (see equation 2.12). Including the memory-burden suppression (with $q = 0.5$), the evaporation lifetimes for $M_0 \in [10^0, 10^2]$ g are lengthened from their semiclassical values to $t_{\mathrm{MB}} \sim 10^{-17}$–$10^{-7}$ s for $k = 1$ (still well before BBN) and to $t_{\mathrm{MB}} \sim 10^{-6}$–$10^{8}$ s for $k = 2$.

The case $q = 1$, where the memory burden is assumed to set in immediately at formation, is included in figure 1 only as a limiting benchmark. In all physical cases, the evaporation process must initially follow the semi-classical calculations. However, detailed analysis of the memory burden effects based on microscopic models suggest that it could become relevant significantly before the black hole loses half of its initial mass. Specifically, these models motivate $1 - q \ll 1$ [60, 61, 73, 80, 89] (see also [90, 91] for independent arguments for $1 - q \sim 1/\sqrt{S}$).

Changing the value of q shifts the bounds in mass according to $M_0 \sim 1/q$ and affects the strength of the bound as $f_{\mathrm{PBH},0} \sim q$. However, as the memory burden is expected to become relevant at latest when the black hole has lost half of its mass, values of $q \ll 0.5$

JCAP11(2025)057

are physically of little interest. In the regime $q \in [0.5, 1]$ the bounds are not overly sensitive to the exact value of q and change at most by a factor of two.

Figure 2 presents constraints compiled from galactic and extragalactic γ rays as well as CMB anisotropies, as computed by [62], alongside the BBN bounds derived in this work for $k = 1, 2, 3$. We have excluded the extragalactic γ-ray bound for PBHs with mass $M_0 < 10^{10}\,\mathrm{g}$, as attenuation at these energies — neglected in previous studies — was shown by [68] to be significant. Furthermore, due to the unreliability of secondary emission rates in the regime $E_{\mathrm{sec}}/T \ll 10^{-6}$, the constraints from γ-ray emission are restricted to $M_0 \gtrsim 10^3\,\mathrm{g}$ for the observational data considered. However, for $M_0 < 10^3\,\mathrm{g}$, there exist comparable constraints from neutrino experiments and ultra-high-energy γ-ray observatories, as computed by [66, 68]. Consequently, we include the neutrino emission bound from [66] for the case $k = 3$. For lower values of k, this bound closely follows the one from galactic γ-ray emission and is therefore omitted for clarity.

The bounds from BBN extend the existing constraints to lighter PBHs that do not survive to the present day — unless they leave behind relics. While they are thus excluded from making up the present dark matter, light evaporating PBHs have been studied as a mechanism to produce particle DM, to address baryogenesis or as a source of gravitational waves [13, 25, 35, 46, 92–100, 108], recently also in the context of the memory burden effect [40, 63, 64, 69, 70, 79, 101–107, 109]. For these analyses, our constraints provide important limits for the available parameter space. In particular, since light PBHs have also been proposed as a source of particle dark matter via their evaporation products, it is important to note that the parameter space allowed by BBN constraints is too narrow for them to constitute the dominant dark matter component. This justifies our focus on BBN limits without pursuing a dedicated dark matter production analysis. In particular, for $k = 1$, PBHs have to be lighter than $M_0 = 10^4\,\mathrm{g}$ in order to avoid cosmological constraints and evaporate before the onset of BBN. Observational limits on the tensor-to-scalar ratio imply that PBHs, which form from density fluctuations seeded by inflation, have a mass of at least $M_0 \sim 1\,\mathrm{g}$ [110]. Together with our results, this imposes a bound of $k \lesssim 3$ in order to have fully evaporating PBHs that are not strongly constrained by BBN, although the precise bound will depend on the value of γ and the accretion of the black hole after horizon formation. We emphasize that the bound $k \lesssim 3$ applies only to fully evaporating PBHs. For larger values of k, PBHs can remain quasi-stable due to the memory burden, in which case a viable parameter space persists even for $k \gtrsim 4$.

We want to note that our calculations assume an instantaneous transition from the semiclassical to the memory burden phase. Recently, the phenomenology of a smooth transition to the memory burden phase has been discussed in detail [71, 77, 78] and it was shown that it can significantly affect the constraints. On the one hand, the limits on M_0 and k below which ultralight PBHs are unconstrained by BBN depend mostly on the total lifetime of the PBH. Therefore, they are not sensitive to the nature of the transition towards the memory burden phase. On the other hand, to address the question of the viability of more massive PBHs as stable dark matter, the transition will have to be taken into account.

Finally, we remark that our analysis has been performed for a monochromatic initial PBH mass function. In realistic scenarios, however, PBHs may form with an extended or even

JCAP11(2025)057

multi-modal mass spectrum, depending on the underlying inflationary or collapse mechanism. Since BBN constraints are highly sensitive to the evaporation time of each mass component, the bounds for non-monochromatic distributions are typically stronger than those obtained for the monochromatic case, as even a small abundance of PBHs in the critical mass range can dominate the energy injection. A full treatment of extended mass functions in the presence of memory burden effects is left for future work, but we expect our monochromatic limits to provide conservative estimates in such scenarios.

4 Conclusion

The suppression of Hawking evaporation due to the memory burden effect fundamentally reshapes constraints on PBHs, most notably for $M_0 < 10^{10}\,\mathrm{g}$ — assuming it becomes relevant when the black hole has lost half its initial mass. Previous work has focused on the question, whether this opens up a new window for PBHs to make up the entire dark matter. However, even much lighter PBHs that cannot explain the present dark matter density can be interesting probes of the physics of the early Universe.

In this work we compute the bounds on ultralight PBHs arising from their effect on BBN. This early-Universe probe extends previous constraints towards lower PBH masses and poses strong limits on their parameter space.

These results highlight the importance of incorporating the memory burden effects into the modelling of evaporating black holes in the early Universe. This has implications for PBH phenomenology and provides a novel setting in which to test predictions of quantum gravity in a cosmological context.

Future constraints from improved measurements of primordial deuterium and helium abundances, as well as searches for late-time energy injection via spectral distortions, gamma-ray backgrounds, or CMB anisotropies, will be critical in further probing the existence of light PBHs. A more complete theoretical understanding of the memory burden mechanism and its parameter dependence will also be essential to delineate the precise range of allowed PBH masses. Our results motivate continued exploration of quantum-corrected black hole evaporation and its implications for early-Universe physics.

Acknowledgments

The work of Arnab Chaudhuri was supported by the Japan Society for the Promotion of Science (JSPS) as a part of the JSPS Postdoctoral Program (Standard), grant number JP23KF0289. The work of Valentin Thoss was supported by the Excellence Cluster ORIGINS which is funded by the Deutsche Forschungsgemeinschaft (DFG, German Research Foundation) under Germany's Excellence Strategy — EXC-2094 — 390783311. The work of Kazunori Kohri was partly supported by KAKENHI Grant Nos. JP24H01825, and JP24K07027.

A Constraints in terms of β_{PBH}

In the main text we presented bounds on ultralight PBHs in terms of the quantity $f_{\mathrm{PBH},0}$, the fraction of dark matter in PBHs at the time of their formation. For completeness, it is also

JCAP11(2025)057

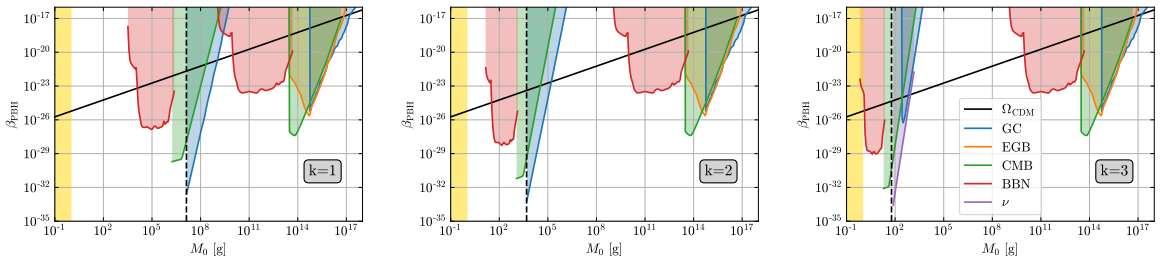

Figure 3. BBN constraints on the initial PBH abundance $\beta_{\rm PBH}(M_0)$ for $k = 1, 2, 3$ and $q = 0.5$. The solid black line indicates $\Omega_{\rm DM}$.

useful to express the constraints directly in terms of the initial PBH abundance parameter $\beta_{\rm PBH}$, defined in eq. (2.4). The two quantities are related by eq. (2.5).

Figure 3 shows the BBN constraints on $\beta_{\rm PBH}$ as a function of the initial PBH mass M_0, for representative values of the memory-burden suppression parameter $k = 1, 2, 3$ and $q = 0.5$. The shaded regions indicate excluded parameter space. The qualitative features mirror those in the $f_{\rm PBH,0}$ representation: stronger suppression (larger k) shifts the constrained window to lighter PBHs and narrows the mass range subject to BBN limits. Displaying the bounds in terms of $\beta_{\rm PBH}$ allows for straightforward comparison with earlier studies, which often adopted $\beta_{\rm PBH}$ as the primary parameter.

References

[1] B.J. Carr and S.W. Hawking, *Black holes in the early universe*, *Mon. Not. Roy. Astron. Soc.* **168** (1974) 399 [INSPIRE].

[2] S. Hawking, *Gravitationally collapsed objects of very low mass*, *Mon. Not. Roy. Astron. Soc.* **152** (1971) 75 [INSPIRE].

[3] P. Ivanov, P. Naselsky and I. Novikov, *Inflation and primordial black holes as dark matter*, *Phys. Rev. D* **50** (1994) 7173 [INSPIRE].

[4] B.J. Carr, K. Kohri, Y. Sendouda and J. Yokoyama, *New cosmological constraints on primordial black holes*, *Phys. Rev. D* **81** (2010) 104019 [arXiv:0912.5297] [INSPIRE].

[5] N. Bartolo et al., *Primordial black hole dark matter: LISA serendipity*, *Phys. Rev. Lett.* **122** (2019) 211301 [arXiv:1810.12218] [INSPIRE].

[6] B. Carr, K. Kohri, Y. Sendouda and J. Yokoyama, *Constraints on primordial black holes*, *Rept. Prog. Phys.* **84** (2021) 116902 [arXiv:2002.12778] [INSPIRE].

[7] B. Carr and F. Kuhnel, *Primordial black holes as dark matter: recent developments*, *Ann. Rev. Nucl. Part. Sci.* **70** (2020) 355 [arXiv:2006.02838] [INSPIRE].

[8] K. Jedamzik, *Primordial black hole dark matter and the LIGO/Virgo observations*, *JCAP* **09** (2020) 022 [arXiv:2006.11172] [INSPIRE].

[9] K. Jedamzik, *Consistency of primordial black hole dark matter with LIGO/Virgo merger rates*, *Phys. Rev. Lett.* **126** (2021) 051302 [arXiv:2007.03565] [INSPIRE].

[10] A.M. Green and B.J. Kavanagh, *Primordial black holes as a dark matter candidate*, *J. Phys. G* **48** (2021) 043001 [arXiv:2007.10722] [INSPIRE].

JCAP11(2025)057

[11] P. Villanueva-Domingo, O. Mena and S. Palomares-Ruiz, *A brief review on primordial black holes as dark matter*, *Front. Astron. Space Sci.* **8** (2021) 87 [arXiv:2103.12087] [INSPIRE].

[12] B. Carr and F. Kuhnel, *Primordial black holes as dark matter candidates*, *SciPost Phys. Lect. Notes* **48** (2022) 1 [arXiv:2110.02821] [INSPIRE].

[13] D. Baumann, P.J. Steinhardt, K. Takahashi and K. Ichiki, *Gravitational wave spectrum induced by primordial scalar perturbations*, *Phys. Rev. D* **76** (2007) 084019 [hep-th/0703290] [INSPIRE].

[14] J.R. Espinosa, D. Racco and A. Riotto, *A cosmological signature of the SM Higgs instability: gravitational waves*, *JCAP* **09** (2018) 012 [arXiv:1804.07732] [INSPIRE].

[15] K. Kohri and T. Terada, *Semianalytic calculation of gravitational wave spectrum nonlinearly induced from primordial curvature perturbations*, *Phys. Rev. D* **97** (2018) 123532 [arXiv:1804.08577] [INSPIRE].

[16] R.-G. Cai, S. Pi and M. Sasaki, *Gravitational waves induced by non-Gaussian scalar perturbations*, *Phys. Rev. Lett.* **122** (2019) 201101 [arXiv:1810.11000] [INSPIRE].

[17] S. Wang, T. Terada and K. Kohri, *Prospective constraints on the primordial black hole abundance from the stochastic gravitational-wave backgrounds produced by coalescing events and curvature perturbations*, *Phys. Rev. D* **99** (2019) 103531 [*Erratum ibid.* **101** (2020) 069901] [arXiv:1903.05924] [INSPIRE].

[18] G. Domènech, *Induced gravitational waves in a general cosmological background*, *Int. J. Mod. Phys. D* **29** (2020) 2050028 [arXiv:1912.05583] [INSPIRE].

[19] H.V. Ragavendra, P. Saha, L. Sriramkumar and J. Silk, *Primordial black holes and secondary gravitational waves from ultraslow roll and punctuated inflation*, *Phys. Rev. D* **103** (2021) 083510 [arXiv:2008.12202] [INSPIRE].

[20] K. Inomata, K. Kohri and T. Terada, *Detected stochastic gravitational waves and subsolar-mass primordial black holes*, *Phys. Rev. D* **109** (2024) 063506 [arXiv:2306.17834] [INSPIRE].

[21] G. Franciolini, J.A. Iovino, V. Vaskonen and H. Veermae, *Recent gravitational wave observation by pulsar timing arrays and primordial black holes: the importance of non-Gaussianities*, *Phys. Rev. Lett.* **131** (2023) 201401 [arXiv:2306.17149] [INSPIRE].

[22] H. Firouzjahi and A. Talebian, *Induced gravitational waves from ultra slow-roll inflation and pulsar timing arrays observations*, *JCAP* **10** (2023) 032 [arXiv:2307.03164] [INSPIRE].

[23] S. Maity et al., *Constraining the history of reheating with the NANOGrav 15-year data*, *JCAP* **01** (2025) 118 [arXiv:2403.16963] [INSPIRE].

[24] S.W. Hawking, *Black hole explosions*, *Nature* **248** (1974) 30 [INSPIRE].

[25] S.W. Hawking, *Particle creation by black holes*, *Commun. Math. Phys.* **43** (1975) 199 [*Erratum ibid.* **46** (1976) 206] [INSPIRE].

[26] M. He, K. Kohri, K. Mukaida and M. Yamada, *Formation of hot spots around small primordial black holes*, *JCAP* **01** (2023) 027 [arXiv:2210.06238] [INSPIRE].

[27] M. Riajul Haque, E. Kpatcha, D. Maity and Y. Mambrini, *Primordial black hole reheating*, *Phys. Rev. D* **108** (2023) 063523 [arXiv:2305.10518] [INSPIRE].

[28] M. He, K. Kohri, K. Mukaida and M. Yamada, *Thermalization and hotspot formation around small primordial black holes*, *JCAP* **10** (2024) 080 [arXiv:2407.15926] [INSPIRE].

[29] R. Calabrese et al., *Limits on light primordial black holes from high-scale leptogenesis*, *Phys. Rev. D* **107** (2023) 123537 [arXiv:2305.13369] [INSPIRE].

JCAP11(2025)057

[30] J. Gunn, L. Heurtier, Y.F. Perez-Gonzalez and J. Turner, *Primordial black hole hot spots and out-of-equilibrium dynamics*, *JCAP* **02** (2025) 040 [arXiv:2409.02173] [INSPIRE].

[31] K. Inomata, K. Kohri, T. Nakama and T. Terada, *Enhancement of gravitational waves induced by scalar perturbations due to a sudden transition from an early matter era to the radiation era*, *Phys. Rev. D* **100** (2019) 043532 [*Erratum ibid.* **108** (2023) 049901] [arXiv:1904.12879] [INSPIRE].

[32] S. Sugiyama et al., *Testing stochastic gravitational wave signals from primordial black holes with optical telescopes*, *Phys. Lett. B* **814** (2021) 136097 [arXiv:2010.02189] [INSPIRE].

[33] K. Inomata et al., *Gravitational wave production right after a primordial black hole evaporation*, *Phys. Rev. D* **101** (2020) 123533 [arXiv:2003.10455] [INSPIRE].

[34] G. Domènech, C. Lin and M. Sasaki, *Gravitational wave constraints on the primordial black hole dominated early universe*, *JCAP* **04** (2021) 062 [*Erratum ibid.* **11** (2021) E01] [arXiv:2012.08151] [INSPIRE].

[35] T. Papanikolaou, V. Vennin and D. Langlois, *Gravitational waves from a universe filled with primordial black holes*, *JCAP* **03** (2021) 053 [arXiv:2010.11573] [INSPIRE].

[36] G. Domènech, V. Takhistov and M. Sasaki, *Exploring evaporating primordial black holes with gravitational waves*, *Phys. Lett. B* **823** (2021) 136722 [arXiv:2105.06816] [INSPIRE].

[37] T. Papanikolaou, *Gravitational waves induced from primordial black hole fluctuations: the effect of an extended mass function*, *JCAP* **10** (2022) 089 [arXiv:2207.11041] [INSPIRE].

[38] N. Bhaumik, A. Ghoshal and M. Lewicki, *Doubly peaked induced stochastic gravitational wave background: testing baryogenesis from primordial black holes*, *JHEP* **07** (2022) 130 [arXiv:2205.06260] [INSPIRE].

[39] N. Bhaumik, A. Ghoshal, R.K. Jain and M. Lewicki, *Distinct signatures of spinning PBH domination and evaporation: doubly peaked gravitational waves, dark relics and CMB complementarity*, *JHEP* **05** (2023) 169 [arXiv:2212.00775] [INSPIRE].

[40] S. Balaji et al., *Probing modified Hawking evaporation with gravitational waves from the primordial black hole dominated universe*, *JCAP* **11** (2024) 026 [arXiv:2403.14309] [INSPIRE].

[41] X. Wang, Y.-L. Zhang, R. Kimura and M. Yamaguchi, *Reconstruction of power spectrum of primordial curvature perturbations on small scales from primordial black hole binaries scenario of LIGO/VIRGO detection*, *Sci. China Phys. Mech. Astron.* **66** (2023) 260462 [arXiv:2209.12911] [INSPIRE].

[42] K. Kohri and H. Matsui, *Electroweak vacuum collapse induced by vacuum fluctuations of the Higgs field around evaporating black holes*, *Phys. Rev. D* **98** (2018) 123509 [arXiv:1708.02138] [INSPIRE].

[43] T. Hayashi, K. Kamada, N. Oshita and J. Yokoyama, *On catalyzed vacuum decay around a radiating black hole and the crisis of the electroweak vacuum*, *JHEP* **08** (2020) 088 [arXiv:2005.12808] [INSPIRE].

[44] A. Chaudhuri, B. Coleppa and K. Loho, *Dark matter production from two evaporating PBH distributions*, *Phys. Rev. D* **108** (2023) 035040 [arXiv:2301.08588] [INSPIRE].

[45] A.M. Green, *Supersymmetry and primordial black hole abundance constraints*, *Phys. Rev. D* **60** (1999) 063516 [astro-ph/9903484] [INSPIRE].

[46] O. Lennon, J. March-Russell, R. Petrossian-Byrne and H. Tillim, *Black hole genesis of dark matter*, *JCAP* **04** (2018) 009 [arXiv:1712.07664] [INSPIRE].

JCAP11(2025)057

[47] A. Cheek, L. Heurtier, Y.F. Perez-Gonzalez and J. Turner, *Primordial black hole evaporation and dark matter production. I. Solely Hawking radiation*, *Phys. Rev. D* **105** (2022) 015022 [arXiv:2107.00013] [INSPIRE].

[48] N. Bernal, Y.F. Perez-Gonzalez and Y. Xu, *Superradiant production of heavy dark matter from primordial black holes*, *Phys. Rev. D* **106** (2022) 015020 [arXiv:2205.11522] [INSPIRE].

[49] P. Gondolo, P. Sandick and B. Shams Es Haghi, *Effects of primordial black holes on dark matter models*, *Phys. Rev. D* **102** (2020) 095018 [arXiv:2009.02424] [INSPIRE].

[50] P.C.W. Davies, D.A. Easson and P.B. Levin, *Nonsingular black holes as dark matter*, *Phys. Rev. D* **111** (2025) 103512 [arXiv:2410.21577] [INSPIRE].

[51] D.N. Page and S.W. Hawking, *Gamma rays from primordial black holes*, *Astrophys. J.* **206** (1976) 1 [INSPIRE].

[52] J.H. MacGibbon and B.J. Carr, *Cosmic rays from primordial black holes*, *Astrophys. J.* **371** (1991) 447 [INSPIRE].

[53] K. Kohri and J. Yokoyama, *Primordial black holes and primordial nucleosynthesis. 1. Effects of hadron injection from low mass holes*, *Phys. Rev. D* **61** (2000) 023501 [astro-ph/9908160] [INSPIRE].

[54] S. Clark et al., *Planck constraint on relic primordial black holes*, *Phys. Rev. D* **95** (2017) 083006 [arXiv:1612.07738] [INSPIRE].

[55] V. Poulin, J. Lesgourgues and P.D. Serpico, *Cosmological constraints on exotic injection of electromagnetic energy*, *JCAP* **03** (2017) 043 [arXiv:1610.10051] [INSPIRE].

[56] H. Niikura et al., *Microlensing constraints on primordial black holes with Subaru/HSC Andromeda observations*, *Nature Astron.* **3** (2019) 524 [arXiv:1701.02151] [INSPIRE].

[57] D. Croon, D. McKeen, N. Raj and Z. Wang, *Subaru-HSC through a different lens: microlensing by extended dark matter structures*, *Phys. Rev. D* **102** (2020) 083021 [arXiv:2007.12697] [INSPIRE].

[58] K. Griest, A.M. Cieplak and M.J. Lehner, *Experimental limits on primordial black hole dark matter from the first 2 yr of Kepler data*, *Astrophys. J.* **786** (2014) 158 [arXiv:1307.5798] [INSPIRE].

[59] J. Auffinger, *Primordial black hole constraints with Hawking radiation — a review*, *Prog. Part. Nucl. Phys.* **131** (2023) 104040 [arXiv:2206.02672] [INSPIRE].

[60] G. Dvali, *A microscopic model of holography: survival by the burden of memory*, arXiv:1810.02336 [INSPIRE].

[61] G. Dvali, L. Eisemann, M. Michel and S. Zell, *Black hole metamorphosis and stabilization by memory burden*, *Phys. Rev. D* **102** (2020) 103523 [arXiv:2006.00011] [INSPIRE].

[62] V. Thoss, A. Burkert and K. Kohri, *Breakdown of Hawking evaporation opens new mass window for primordial black holes as dark matter candidate*, *Mon. Not. Roy. Astron. Soc.* **532** (2024) 451 [arXiv:2402.17823] [INSPIRE].

[63] B. Barman, K. Loho and Ó. Zapata, *Constraining burdened PBHs with gravitational waves*, *JCAP* **10** (2024) 065 [arXiv:2409.05953] [INSPIRE].

[64] B. Barman, K. Loho and Ó. Zapata, *Asymmetries from a charged memory-burdened PBH*, *JCAP* **02** (2025) 052 [arXiv:2412.13254] [INSPIRE].

[65] U. Basumatary, N. Raj and A. Ray, *Beyond Hawking evaporation of black holes formed by dark matter in compact stars*, *Phys. Rev. D* **111** (2025) L041306 [arXiv:2410.22702] [INSPIRE].

JCAP11(2025)057

[66] M. Chianese et al., *Light burden of memory: constraining primordial black holes with high-energy neutrinos*, *Phys. Rev. D* **111** (2025) 063036 [arXiv:2410.07604] [INSPIRE].

[67] A. Boccia and F. Iocco, *Could the KM3-230213A event be caused by an evaporating primordial black hole?*, *Phys. Rev. D* **112** (2025) 063045 [arXiv:2502.19245] [INSPIRE].

[68] M. Chianese, *High-energy gamma-ray emission from memory-burdened primordial black holes*, *Phys. Rev. D* **112** (2025) 023043 [arXiv:2504.03838] [INSPIRE].

[69] P. Athron et al., *Impact of memory-burdened black holes on primordial gravitational waves in light of Pulsar Timing Array*, *JCAP* **05** (2025) 005 [arXiv:2411.19286] [INSPIRE].

[70] R. Calabrese, M. Chianese and N. Saviano, *Impact of memory-burdened primordial black holes on high-scale leptogenesis*, *Phys. Rev. D* **111** (2025) 083008 [arXiv:2501.06298] [INSPIRE].

[71] G. Montefalcone et al., *Does memory burden open a new mass window for primordial black holes as dark matter?*, arXiv:2503.21005 [INSPIRE].

[72] X.-H. Tan and Y.-F. Zhou, *Probing memory-burdened primordial black holes with galactic sources observed by LHAASO*, arXiv:2505.19857 [INSPIRE].

[73] G. Dvali, J.S. Valbuena-Bermúdez and M. Zantedeschi, *Memory burden effect in black holes and solitons: implications for PBH*, *Phys. Rev. D* **110** (2024) 056029 [arXiv:2405.13117] [INSPIRE].

[74] M. Zantedeschi and L. Visinelli, *Ultralight black holes as sources of high-energy particles*, *Phys. Dark Univ.* **49** (2025) 102034 [arXiv:2410.07037] [INSPIRE].

[75] S. Datta and R. Samanta, *Fingerprints of GeV scale right-handed neutrinos on inflationary gravitational waves and PTA data*, *Phys. Rev. D* **108** (2023) L091706 [arXiv:2307.00646] [INSPIRE].

[76] D. Bandyopadhyay, D. Borah and N. Das, *Axion misalignment with memory-burdened PBH*, *JCAP* **04** (2025) 039 [arXiv:2501.04076] [INSPIRE].

[77] A. Dondarini, G. Marino, P. Panci and M. Zantedeschi, *The fast, the slow and the merging: probes of evaporating memory burdened PBHs*, *JCAP* **11** (2025) 006 [arXiv:2506.13861] [INSPIRE].

[78] G. Dvali, M. Zantedeschi and S. Zell, *Transitioning to memory burden: detectable small primordial black holes as dark matter*, arXiv:2503.21740 [INSPIRE].

[79] A. Chaudhuri, K. Pal and R. Mohanta, *Neutrino fluence influenced by memory burdened primordial black holes*, arXiv:2505.09153 [INSPIRE].

[80] A. Alexandre, G. Dvali and E. Koutsangelas, *New mass window for primordial black holes as dark matter from the memory burden effect*, *Phys. Rev. D* **110** (2024) 036004 [arXiv:2402.14069] [INSPIRE].

[81] T. Fujita, M. Kawasaki, K. Harigaya and R. Matsuda, *Baryon asymmetry, dark matter, and density perturbation from primordial black holes*, *Phys. Rev. D* **89** (2014) 103501 [arXiv:1401.1909] [INSPIRE].

[82] I. Masina, *Dark matter and dark radiation from evaporating primordial black holes*, *Eur. Phys. J. Plus* **135** (2020) 552 [arXiv:2004.04740] [INSPIRE].

[83] A. Arbey and J. Auffinger, *BlackHawk: a public code for calculating the Hawking evaporation spectra of any black hole distribution*, *Eur. Phys. J. C* **79** (2019) 693 [arXiv:1905.04268] [INSPIRE].

JCAP11(2025)057

[84] M. Kawasaki, K. Kohri and T. Moroi, *Big-Bang nucleosynthesis and hadronic decay of long-lived massive particles*, *Phys. Rev. D* **71** (2005) 083502 [astro-ph/0408426] [INSPIRE].

[85] M. Kawasaki, K. Kohri, T. Moroi and Y. Takaesu, *Revisiting Big-Bang nucleosynthesis constraints on long-lived decaying particles*, *Phys. Rev. D* **97** (2018) 023502 [arXiv:1709.01211] [INSPIRE].

[86] M. Kawasaki, K. Kohri and N. Sugiyama, *Cosmological constraints on late time entropy production*, *Phys. Rev. Lett.* **82** (1999) 4168 [astro-ph/9811437] [INSPIRE].

[87] M. Kawasaki, K. Kohri and N. Sugiyama, *MeV scale reheating temperature and thermalization of neutrino background*, *Phys. Rev. D* **62** (2000) 023506 [astro-ph/0002127] [INSPIRE].

[88] T. Hasegawa et al., *MeV-scale reheating temperature and thermalization of oscillating neutrinos by radiative and hadronic decays of massive particles*, *JCAP* **12** (2019) 012 [arXiv:1908.10189] [INSPIRE].

[89] G. Dvali, L. Eisemann, M. Michel and S. Zell, *Universe's primordial quantum memories*, *JCAP* **03** (2019) 010 [arXiv:1812.08749] [INSPIRE].

[90] G. Dvali and M. Panchenko, *Black hole type quantum computing in critical Bose-Einstein systems*, arXiv:1507.08952 [INSPIRE].

[91] M. Michel and S. Zell, *The timescales of quantum breaking*, *Fortsch. Phys.* **71** (2023) 2300163 [arXiv:2306.09410] [INSPIRE].

[92] A.D. Dolgov, P.D. Naselsky and I.D. Novikov, *Gravitational waves, baryogenesis, and dark matter from primordial black holes*, astro-ph/0009407 [INSPIRE].

[93] T. Fujita, M. Kawasaki and S. Yokoyama, *Curvaton in large field inflation*, *JCAP* **09** (2014) 015 [arXiv:1404.0951] [INSPIRE].

[94] R. Allahverdi, J. Dent and J. Osinski, *Nonthermal production of dark matter from primordial black holes*, *Phys. Rev. D* **97** (2018) 055013 [arXiv:1711.10511] [INSPIRE].

[95] C. Keith, D. Hooper, N. Blinov and S.D. McDermott, *Constraints on primordial black holes from Big Bang nucleosynthesis revisited*, *Phys. Rev. D* **102** (2020) 103512 [arXiv:2006.03608] [INSPIRE].

[96] A. Coogan, L. Morrison and S. Profumo, *Hazma: a python toolkit for studying indirect detection of sub-GeV dark matter*, *JCAP* **01** (2020) 056 [arXiv:1907.11846] [INSPIRE].

[97] I. Baldes, Q. Decant, D.C. Hooper and L. Lopez-Honorez, *Non-cold dark matter from primordial black hole evaporation*, *JCAP* **08** (2020) 045 [arXiv:2004.14773] [INSPIRE].

[98] S.K. Acharya and R. Khatri, *CMB and BBN constraints on evaporating primordial black holes revisited*, *JCAP* **06** (2020) 018 [arXiv:2002.00898] [INSPIRE].

[99] I. Masina, *Dark matter and dark radiation from evaporating Kerr primordial black holes*, *Grav. Cosmol.* **27** (2021) 315 [arXiv:2103.13825] [INSPIRE].

[100] T. Papanikolaou and K.N. Gourgouliatos, *Constraining supermassive primordial black holes with magnetically induced gravitational waves*, *Phys. Rev. D* **108** (2023) 063532 [arXiv:2306.05473] [INSPIRE].

[101] N. Bhaumik, M.R. Haque, R.K. Jain and M. Lewicki, *Memory burden effect mimics reheating signatures on SGWB from ultra-low mass PBH domination*, *JHEP* **10** (2024) 142 [arXiv:2409.04436] [INSPIRE].

[102] B. Barman, M.R. Haque and Ó. Zapata, *Gravitational wave signatures of cogenesis from a burdened PBH*, *JCAP* **09** (2024) 020 [arXiv:2405.15858] [INSPIRE].

JCAP11(2025)057

[103] M.R. Haque, S. Maity, D. Maity and Y. Mambrini, *Quantum effects on the evaporation of PBHs: contributions to dark matter*, *JCAP* **07** (2024) 002 [arXiv:2404.16815] [INSPIRE].

[104] K. Kohri, T. Terada and T.T. Yanagida, *Induced gravitational waves probing primordial black hole dark matter with the memory burden effect*, *Phys. Rev. D* **111** (2025) 063543 [arXiv:2409.06365] [INSPIRE].

[105] N.P.D. Loc, *Gravitational waves from burdened primordial black holes dark matter*, *Phys. Rev. D* **111** (2025) 023509 [arXiv:2410.17544] [INSPIRE].

[106] D. Borah and N. Das, *Successful cogenesis of baryon and dark matter from memory-burdened PBH*, *JCAP* **02** (2025) 031 [arXiv:2410.16403] [INSPIRE].

[107] W. Barker, B. Gladwyn and S. Zell, *Inflationary and gravitational wave signatures of small primordial black holes as dark matter*, *Phys. Rev. D* **111** (2025) 123033 [arXiv:2410.11948] [INSPIRE].

[108] T.C. Gehrman, B. Shams Es Haghi, K. Sinha and T. Xu, *Baryogenesis, primordial black holes and MHz–GHz gravitational waves*, *JCAP* **02** (2023) 062 [arXiv:2211.08431] [INSPIRE].

[109] Y. Jiang, C. Yuan, C.-Z. Li and Q.-G. Huang, *Constraints on the primordial black hole abundance through scalar-induced gravitational waves from advanced LIGO and Virgo's first three observing runs*, *JCAP* **12** (2024) 016 [arXiv:2409.07976] [INSPIRE].

[110] PLANCK collaboration, *Planck 2018 results. X. Constraints on inflation*, *Astron. Astrophys.* **641** (2020) A10 [arXiv:1807.06211] [INSPIRE].

JCAP11(2025)057

Chapter 5

Transition to the memory burden phase

In this chapter, we expand the model used in the previous two chapters to account for the transition from the SC to the memory burden phase of evaporation. After the publication of Thoss et al. (2024) and Chaudhuri et al. (2025), there has been a discussion on the relevance of the transition for the role of light PBHs as a dark matter candidate (Montefalcone et al., 2025; Dvali et al., 2025). In particular, Montefalcone et al. (2025) suggested that light PBHs cannot make up the dark matter unless the transition is 'nearly instantaneous'. Here, we want to comment on these results and present some updated constraints on PBHs that account for the transition period.

5.1 Introduction

In Chapters 3 and 4 of this thesis, we did not explicitly model the transition from the SC to the memory burden phase of evaporation. Implicitly, we assumed that the suppression would take place instantaneously when the black hole reached a mass $M = qM_0$, with M_0 denoting the initial black hole mass. A more realistic description should account for the transitional regime between the two phases, described by a parameter $\delta = \Delta M/M_0$, that expresses the width of the transition in terms of the black hole mass loss.

Montefalcone et al. (2025) first noted the importance of accounting for the transitional regime between both phases. They parametrized the mass loss rate as

$$\frac{\mathrm{d}M}{\mathrm{d}t} = \left(\frac{\mathrm{d}M}{\mathrm{d}t}\bigg|_{\mathrm{SC}}\right)^{h(M)} \left(\frac{\mathrm{d}M}{\mathrm{d}t}\bigg|_{\mathrm{MB}}\right)^{1-h(M)} , \tag{5.1}$$

$$h(M) = \frac{k}{2}\left[1 + \tanh\left(\frac{M - qM_0}{\delta q M_0/2}\right)\right] , \tag{5.2}$$

$$\frac{\mathrm{d}M}{\mathrm{d}t}\bigg|_{\mathrm{MB}} = \frac{1}{(S(qM_0)/k_B)^k} \frac{\mathrm{d}M}{\mathrm{d}t}\bigg|_{\mathrm{SC}} (qM_0) , \tag{5.3}$$

and computed corresponding constraints from BBN and CMB. They found that for $q = 0.5$ the new mass window remains open for $\delta \lesssim 10^{-10}$. This implies that the transition has to be very sharp, if expressed in terms of black hole mass, to allow an open mass window for light PBHs to make up the dark matter.

Dvali et al. (2025) discussed the transition from the perspective of theoretical models of the memory burden effect, relating δ and q to fundamental parameters of the theory and discussed constraints from BBN, CMB, and the galactic and extragalactic neutrino flux. A key insight from their work is that the fractional mass loss until the onset of the memory burden effect, $(1 - q)$, and the width of the transition δ are related. Expressed as $\delta \sim \nu(1 - q)$, dependent on the fundamental parameters of theory, it is found that $\nu \sim 0.01 - 0.1$. Therefore, δ is typically smaller than $1 - q$ but not by many orders of magnitude. In the case $q = 0.5$, where the memory burden sets in at half-mass, considered throughout most of Chapter 3 and 4, this implies $\delta \sim 0.01 - 0.1$. Based on their analysis and the results of Montefalcone et al. (2025), such a scenario is strongly constrained, and PBHs cannot make up a sizeable fraction of the dark matter.

However, as already discussed in Section 3.5 of Chapter 3, there is theoretical motivation to consider the regime where $1 - q \ll 1$, i.e. an early onset of the memory burden, when only a small fraction of the mass has been lost. In particular, theory suggests that $1 - q \sim S^{-\alpha}$, with Dvali and Panchenko (2015) and Michel and Zell (2023) giving arguments for $\alpha = 0.5$. Dvali et al. (2025) additionally show that δ is also naturally parametrised by the black hole entropy with $\delta \sim S^{-\alpha}$, although there are logarithmic corrections. This provides a strong argument to consider the parameter space where $1 - q \ll 1$ and $\delta \ll 1$ in more detail. In the mathematical limit $q = 1$, and $\delta = 0$, we can simply repeat the computations described in 3. The resulting map of constraints is shown in Figure 5.1. Bounds that originate from the memory burden phase change only mildly, shifting by a factor of 2 in M_0. However, the constraints from the SC phase, producing the vertical bands in Figure 1 of Chapter 3, disappear entirely, as $q = 1$ implies an instant onset of the memory burden effect. This is, in principle, only a mathematical

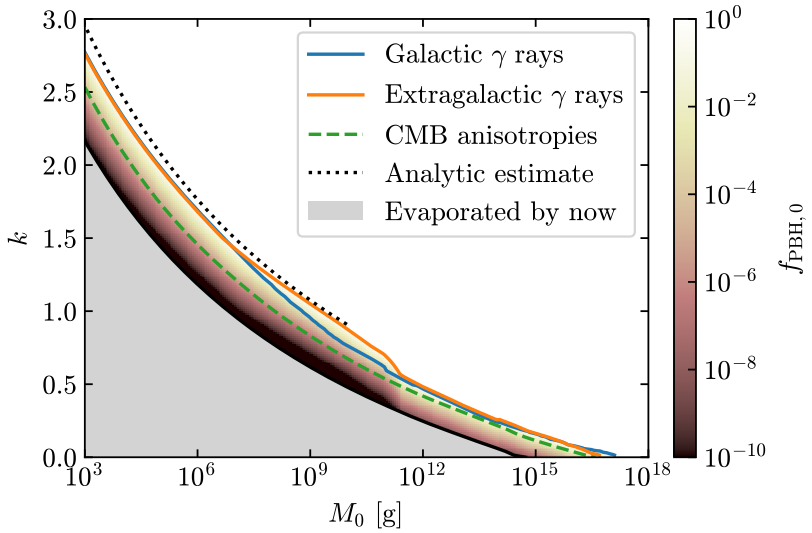

Figure 5.1: Combined constraints on $f_{\mathrm{PBH},0}(k, M_0)$ for $q = 1$. The coloured lines show $f_{\mathrm{PBH},0} = 1$ contours for each type of constraint. In the white region, PBHs can make up the entirety of the dark matter. The black, dotted line displays the analytic estimate given by Equation 16 in Chapter 3.

limit, and a detailed analysis is required to explore how small δ and $1 - q$ have to be in order to allow light PBHs as a dark matter candidate. However, as we demonstrate in this Chapter, theoretical models motivate scenarios in which $q = 1$ and $\delta = 0$ can be assumed to a good approximation, resulting in the bounds presented in Figure 5.1 and a large window for light PBHs. This also emphasizes the value of the work presented in Chapters 3 and 4.

5.2 Results

To investigate the parameter space for light PBHs as a dark matter candidate, we introduce the following parametrisation of the black hole emission,

$$\frac{\mathrm{d}N_{i,\mathrm{MB}}}{\mathrm{d}E\mathrm{d}t}(E, M_0, s_i) = \frac{\mathrm{d}N_{i,\mathrm{SC}}}{\mathrm{d}E\mathrm{d}t}(E, M_0, s_i) \begin{cases} 1 & M \geq qM_0 \\ \exp\left(-\frac{qM_0 - M(t)}{\delta M_0}\right) & qM_0 > M > M_{\mathrm{MB}} \\ (S_0/k_B)^{-k} & M < M_{\mathrm{MB}} \,, \end{cases} \tag{5.4}$$

which is based on discussions with Sebastian Zell (Thoss, Zell, in prep.) and Dvali et al. (2025). $S_0 = S(M_0)$ denotes the black hole entropy at formation, and $M_{\mathrm{MB}} = M_0(q - \delta k \ln S)$ is the mass for which the memory burden phase is reached, and is obtained by the requirement that the emission rate is continuous. Note that for $q < \delta k \ln S$, the memory burden stage is never reached and the black hole fully evaporates while in the transitional phase. The mass loss rate $\frac{\mathrm{d}M}{\mathrm{d}t}$ is suppressed in the same way,

$$\left.\frac{\mathrm{d}M}{\mathrm{d}t}\right|_{\mathrm{MB}} = \dot{M}_0 \begin{cases} 1 & M \geq qM_0 \\ \exp\left(-\frac{qM_0 - M(t)}{\delta M_0}\right) & qM_0 > M > M_{\mathrm{MB}} \\ (S_0/k_B)^{-k} & M < M_{\mathrm{MB}} \,, \end{cases} \tag{5.5}$$

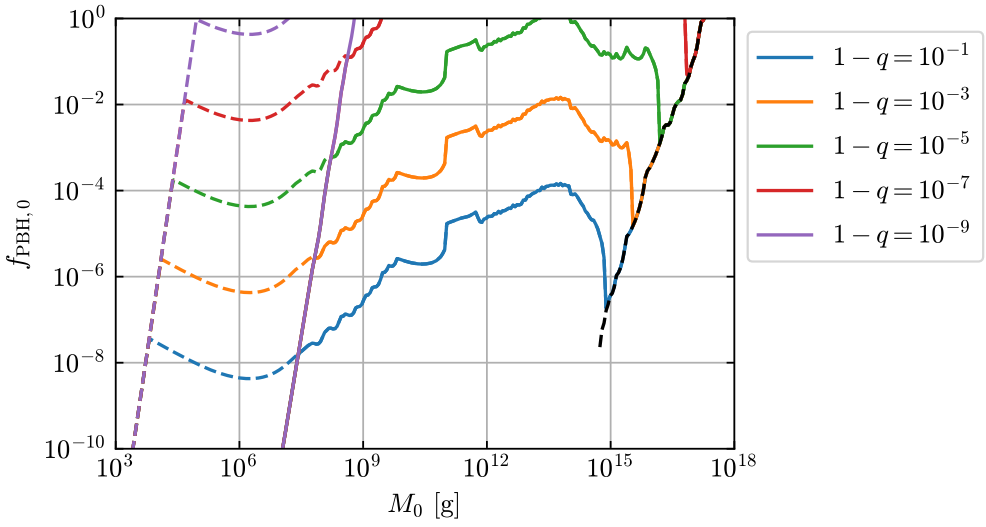

Figure 5.2: Constraints on $f_{\mathrm{PBH},0}(M_0)$ from galactic γ-ray emission for various values of q and $\delta = 0.01(1-q)$. The solid lines correspond to $k=1$, the dashed lines to $k=2$. The black, dashed line indicates the result in the SC limit.

where $\dot{M}_0$ is the SC mass loss rate at formation. In the semiclassical phase and the full memory burden stage, the mass loss rate is constant, implying a linear decay of the mass. In the transitional regime, Equation 5.5 can be solved analytically. Taking all three regimes together, we get

$$M(t) = \begin{cases} M_0 - t|\dot{M}_0| & t < (1-q)M_0/|\dot{M}_0| \\ qM_0 - \delta M_0 \ln\left(1 - \frac{(1-q)M_0 - t|\dot{M}_0|}{\delta M_0}\right) & \frac{(1-q)M_0}{|\dot{M}_0|} < t < t_{\mathrm{MB}} \\ M_{\mathrm{MB}} - t|\dot{M}_0|(S_0/k_B)^{-k} & t > t_{\mathrm{MB}}\,, \end{cases} \tag{5.6}$$

with

$$t_{\mathrm{MB}} = \frac{M_0}{|\dot{M}_0|}\left(\delta(S_0/k_B)^k + (1-q) - \delta\right) \approx \frac{\delta M_0}{|\dot{M}_0|}(S_0/k_B)^k\,, \tag{5.7}$$

where the approximation assumes $(S_0/k_B)^k \gg 1$, i.e. that the memory burden effect is significant.

Observational constraints are sensitive to the energy injected by PBHs and thus the mass loss rate at a given time. From Equation 5.6, we can obtain

$$\left.\frac{\mathrm{d}M}{\mathrm{d}t}\right|_{\mathrm{MB}} = -\frac{|\dot{M}_0|\delta M_0}{(1-q)M_0 + \delta M_0 + |\dot{M}_0|t}\,, \tag{5.8}$$

implying $\dot{M} \approx -\delta M_0/t$ deep in the transitional phase.

Using the parametrisation from Equation 5.4, we compute constraints on $f_{\mathrm{PBH},0}$ based on the galactic γ-ray emission. The computation of other constraints is subject of ongoing work, and we briefly discuss them below. For the case $\delta = 0.01(1-q)$, motivated by theoretical considerations as discussed before, we show the resulting constraints on $f_{\mathrm{PBH},0}$ in Figure 5.2. At the highest masses, for $M > qM_0$, the constraints are unaffected by the memory burden

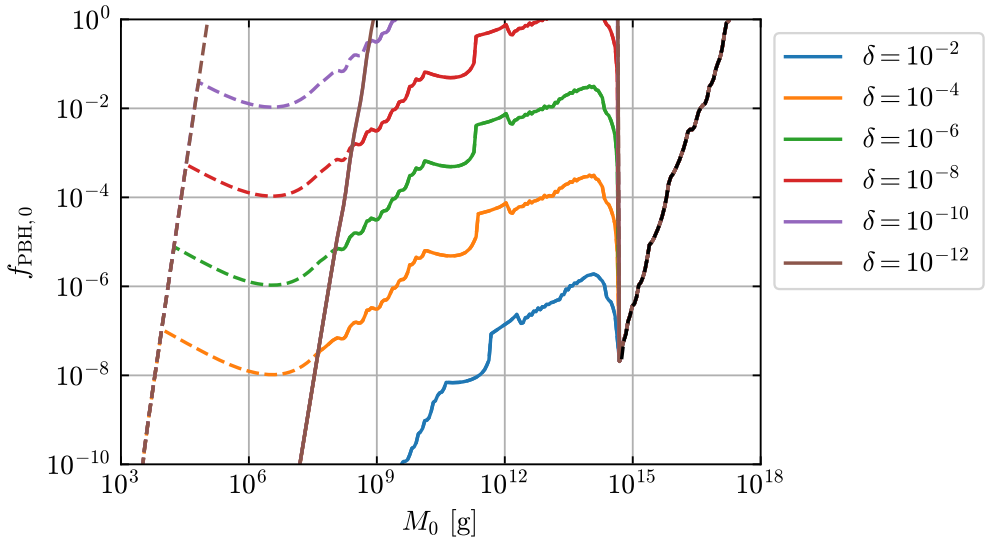

Figure 5.3: Constraints on $f_{\mathrm{PBH},0}(M_0)$ from galactic γ-ray emission for various values of δ and $q = 0.5$. The solid lines correspond to $k = 1$, the dashed lines to $k = 2$. The black, dashed line indicates the result in the SC limit.

effect because the black hole is still in the SC regime. At the lowest masses, for $M < M_{\mathrm{MB}}$, the black hole has reached the memory burden phase and the constraints are independent of the transition and determined by the parameter k. In this regime the results are equivalent to the results from Chapter 3 up to a shift in the black hole mass by a factor of 2[1] In the intermediate mass range, the PBHs are in the transitional regime. The constraints weaken as $q \to 1$ and $\delta \to 0$, but one still has $f_{\mathrm{PBH},0} \ll 1$ over the entire mass range unless $1 - q \ll 10^{-5}$. For $1 - q \ll 10^{-7}$, the constraint at the highest masses disappears entirely as the SC phase ends sufficiently early to prevent any observable emission. Note that the weakening of the constraint in the transitional phase is a result of $\delta \to 0$ rather than $q \to 1$. Indeed, during the transition, the bounds are not sensitive to the value of q. This can be understood by considering the mass loss rate, $\dot{M} \approx -\delta M_0/t$, implying $f_{\mathrm{PBH},0} \sim 1/\dot{M} \sim 1/\delta$, in agreement with the results shown in Figure 5.3.

Relaxing, for a moment, the assumption that δ and $1 - q$ are related, we now come back to the conservative scenario of $q = 0.5$ discussed in Chapters 3 and 4. In Figure 5.3 we show the constraints from galactic γ-ray emission for $q = 0.5$ and various values of δ. We recover the results from our previous analysis for $\delta \lesssim 10^{-10}$ ($\delta \lesssim 10^{-12}$) for $k = 1$ ($k = 2$). Under these conditions, the transition is short enough to be neglected for galactic γ-ray emission. Other constraints might impose stronger limits as we discuss below. For larger values of δ, the transition closes the open mass window. Based on theoretical models that suggest a roughly similar scale of δ and $1 - q$, these small values of δ do not seem very plausible for $q = 0.5$. In other words, if the memory burden effect becomes relevant at half-mass, then the corresponding transition to the full memory burden phase likely rules out light PBHs as a dark matter candidate. However, there is strong theoretical motivation to consider the parameter space where $1 - q \ll 1$ and $\delta \ll 1$. The case $q \to 1$ was already briefly discussed in Chapters 3

[1] In Chapter3, we assumed $q = 0.5$, whereas here we are in the limit $q \to 1$, which shifts the constraints by a factor of 2 in the initial black hole mass.

and 4 and we provided updated constraints for the limit $q = 1$ and $\delta = 0$ in Figure 5.1.

To quantify the viability of light PBHs to make up the dark matter as a function of q and δ, we introduce the following dimensionless parameter,

$$\mathcal{O}_M = \int_{-\infty}^{0} \mathrm{d}s \, \tilde{f}_{\mathrm{PBH},0}(s) \,, \tag{5.9}$$

where $s = \log_{10}(M_{\mathrm{PBH}}/M_{\mathrm{PBH,max}})$ and

$$\tilde{f}_{\mathrm{PBH},0} = \begin{cases} f_{\mathrm{PBH},0} & f_{\mathrm{PBH},0} < 1 \\ 1 & f_{\mathrm{PBH},0} \geq 1 \,. \end{cases} \tag{5.10}$$

$M_{\mathrm{PBH,max}} \approx 2 \times 10^{17}\,\mathrm{g}$ denotes the lower mass limit of the asteroid mass window, i.e. the maximum PBH mass for which we obtain $f_{\mathrm{PBH},0} < 1$ in the SC limit. In essence, $\mathcal{O}_M$ measures the range of PBH masses that can make up the dark matter in addition to the asteroid mass window, expressed in units of dex. E.g., if $f_{\mathrm{PBH},0} \ll 1$ over most of the mass range except for $M_{\mathrm{PBH}} \in [10^7, 10^9]\,\mathrm{g}$, then $\mathcal{O}_M = 9 - 7 = 2$. Note that due to the weighting by $f_{\mathrm{PBH},0}$, a large range of masses that are weakly constrained $f_{\mathrm{PBH},0} \sim \mathcal{O}(0.1)$ can also contribute to $\mathcal{O}_M$.

In Figure 5.4 we show $\mathcal{O}_M$ as a function of $1 - q$ and δ for $k = 1$ (left) and $k = 2$ (right), based on the constraints from galactic γ-ray emission. The allowed mass range for light PBHs making up the dark matter is determined mostly by δ. This is in agreement with our previous observation that $f_{\mathrm{PBH},0} \sim 1/\delta$ for most of the relevant mass range. For $\delta \gtrsim 10^{-7}$, light PBHs cannot make up the dark matter, setting a strong limit on the width of the transition that is independent of k and q. Increasing k allows, in principle, to have lighter PBH masses, by extending the overall lifetime through a stronger memory burden effect. However, actually extending the parameter space also requires a smaller value of δ in order to avoid constraints on these light PBHs. In Figure 5.4, the difference in the allowed PBH mass range between $k = 1$ and $k = 2$ only becomes apparent for $\delta \lesssim 10^{-11}$. The role of q is in setting the upper mass limit, by determining the length of the SC phase, as is visible in Figure 5.2. This has a smaller effect on increasing the allowed parameter space compared to changing δ. For $k = 1$, having $1-q \lesssim 10^{-7}$ and $\delta \lesssim 10^{-9}$ allows an open mass range close to the theoretical maximum, reached for $q = 1$ and $\delta = 0$ and visualized in Figure 5.1. For $k = 2$ this requires $1 - q \lesssim 10^{-7}$ and $\delta \lesssim 10^{-11}$.

Dvali et al. (2025) have found, for simple prototype models, that δ and $1 - q$ scale as

$$1 - q \sim \left(p S_0^2\right)^{\frac{-1}{2(p-1)}} \,, \tag{5.11}$$

$$\delta \sim \frac{1}{(p-1)\ln S_0} \left(p S_0^2\right)^{\frac{-1}{2(p-1)}} \,, \tag{5.12}$$

where $p \geq 1$ is a critical exponent and a fundamental parameter of the theory. For $p = 1$, we recover the limit $q = 1$ and $\delta = 0$, whereas $p = 2$ corresponds to $1 - q \sim 1/\sqrt{S}$, discussed before. For $p \gtrsim \ln S_0$ one obtains $1 - q \sim \mathcal{O}(1)$ (including the onset at half-mass discussed in previous chapters) and $\delta \sim 1/\ln S_0^2 \sim \mathcal{O}(10^{-4})$. If we ignore the logarithmic corrections we can write

$$100\,\delta = 1 - q = \frac{1}{S_0^\alpha} \,, \tag{5.13}$$

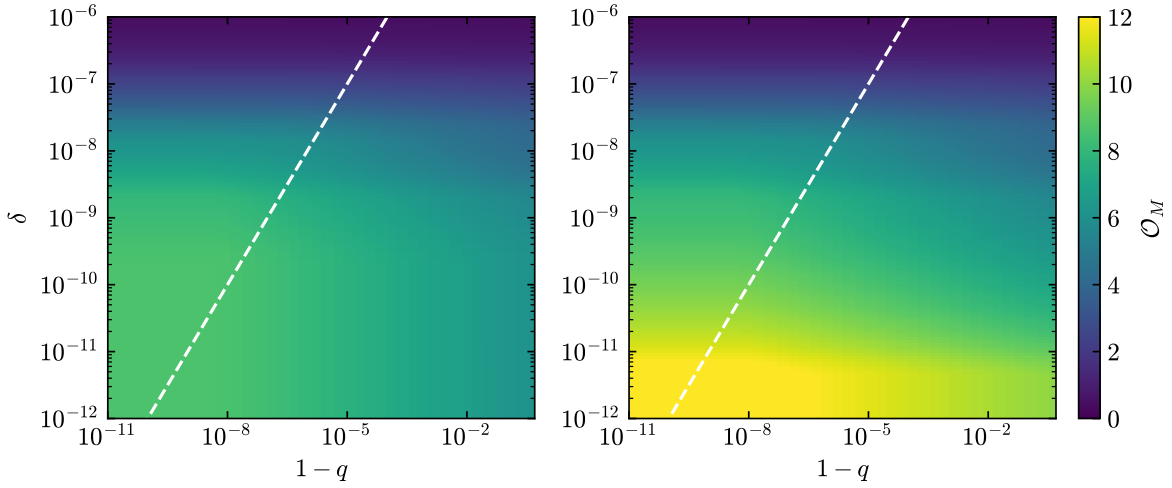

Figure 5.4: Size of the newly opened mass window for light PBHs, described by $\mathcal{O}_M$, as a function of δ and $1-q$. $\mathcal{O}_M$ can be interpreted as the range of PBH masses below the asteroid mass window, which is unconstrained, in units of dex. This has been computed based on constraints from galactic γ-ray emission. The left panel shows results for $k = 1$, while the right panel displays results for $k = 2$. The white, dashed line indicates $\delta = 0.01(1-q)$, motivated by theoretical models of the memory burden effect.

where the factor of 100 roughly accounts for the factor $\ln S_0$ in the relevant mass range, giving $\delta = 0.01(1-q)$ as before. Including the prefactor from Equation 5.11 and 5.12, changes α of the order of $\Delta\alpha \lesssim 0.1$.

Using the parametrisation from Equation 5.13, we can now obtain constraints on α as a function of the PBH mass and k. Figure 5.5 shows the resulting limits on $f_{\mathrm{PBH},0}$ from galactic γ-ray emission for $k = 1$ (left) and $k = 2$ (right). The three phases of PBH evaporation (SC, transition, memory burden) are separated by dotted black lines. In the lower right corner, when PBHs are in the SC regime, the constraints are independent of α. Notably, the value of k only determines the lower mass limit, below which PBHs have reached the memory burden phase and the constraints become independent of δ and thus α. Overall, we find that $\alpha \gtrsim 0.2 - 0.3$ is required for light PBHs to make up the entire dark matter. In this case, the constraints are physically equivalent to those for $q = 1$ and $\delta = 0$ shown in Figure 5.1. Importantly, the theoretically motivated scenario of $\alpha = 0.5$ (Dvali and Panchenko, 2015; Michel and Zell, 2023) is clearly unconstrained over a large mass range.

We want to emphasize that the results presented in this chapter only account for the galactic γ-ray emission using the observational data described in Chapter 3. Preliminary results for constraints from BBN show that they are weaker than those from the galactic emission and pose no additional bounds on the parameter space. However, additional data on the ultra-high energy γ-ray flux as well as the extragalactic contribution are expected to strengthen the constraints presented so far, especially towards low masses. In addition, the effect of light PBHs on CMB anisotropies (see Chapter 3) is expected to provide complementary bounds on the abundance of light PBHs.

During the preparation of these results, the study by Dondarini et al. (2025) appeared,

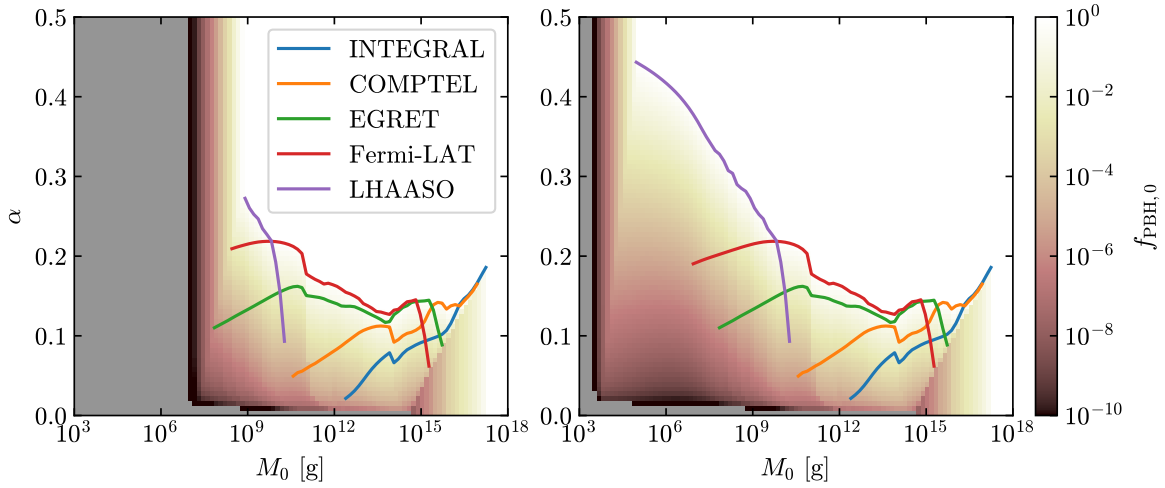

Figure 5.5: Constraints on $f_{\mathrm{PBH},0}(M_0, \alpha)$ from galactic γ-ray emission, based on the parametrisation from Equation 5.13. The left panel shows results for $k = 1$, while the right panel displays results for $k = 2$. The coloured lines are contours of $f_{\mathrm{PBH},0} = 1$ for the individual observational data. PBHs evaporate before the present epoch in the grey shaded region. The dotted black lines separate the three stages of the evaporation process in the parameter space, with the SC phase in the lower right corner, the memory burden phase in the upper left and the transition in-between.

which also investigated the parameter space of light PBHs, accounting for the transition to the memory burden phase. Their analysis includes the aforementioned constraints with the exception of BBN. Additionally, they also considered the impact of PBH mergers on the evaporation dynamics. However, they did not include data for γ-rays below the energies probed by Fermi ($E \lesssim 0.1\,\mathrm{GeV}$). Therefore, our analysis, which includes data from INTEGRAL and COMPTEL (see Chapter 3), is complementary to their study and provides additional constraints in the mass range $M_{\mathrm{PBH}} \in [10^{14}, 10^{17}]\,\mathrm{g}$.

5.3 Summary

In this chapter, we have briefly discussed the impact of a smooth transition from the SC to the memory burden phase and the implications for light PBHs as a dark matter candidate. We found that

- Adding a transition towards the memory burden phase has important consequences for the resulting constraints on PBHs unless the fractional mass loss $\delta = \Delta M/M_0$ during this phase is very small.
- The constraints derived in Chapter 3 and 4 continue to be a good approximation at low masses, when the PBHs have reached the full memory burden phase. They set a limit on the allowed PBH mass. The width of the transition δ determines the strength of the constraints throughout most of the previously opened mass window, with $f_{\mathrm{PBH},0} \sim 1/\delta$. At the highest masses, the constraints are controlled by how quickly the SC phase ends,

determined by q.

- Based on galactic γ-ray emission, we find that $\delta \lesssim 10^{-7}$ opens a sizeable mass window, where PBHs can make up the dark matter, that is enlarged for lower values of δ. For this particular constraint, we also find that the transition can be neglected for $\delta \lesssim 10^{-9}$ ($\delta \lesssim 10^{-11}$) for $k = 1$ ($k = 2$).

- Theoretical models suggest a similar scale of δ and $1 - q$. The strong limits on δ required to have light PBHs as a dark matter candidate thus imply strong limits on $1 - q$ and require an early onset of the memory burden. As a result, constraints from the SC phase disappear, leading to a potentially much larger allowed mass range as discussed in Chapters 3 and 4.

- The results for the galactic γ-ray emission derived in Chapter 3 and 4 for $q = 0.5$ are recovered for $\delta \lesssim 10^{-9}$ ($\delta \lesssim 10^{-11}$) for $k = 1$ ($k = 2$). These small values of δ for $q = 0.5$ seem implausible from a theoretical point of view. However, the results derived in previous work remain valid for PBHs that have reached the memory burden phase and are a good overall approximation for the case $\delta \sim (1 - q) \sim 1/\sqrt{S}$, previously discussed by Dvali and Panchenko (2015) and Michel and Zell (2023). In this case, the bounds from the semiclassical phase disappear, and the resulting constraints are displayed in Figure 5.1.

- Other constraints, in particular from CMB anisotropies and ultra-high energy γ-rays or neutrinos, are expected to strengthen the bounds obtained here. These have recently been computed by Dondarini et al. (2025), with our results providing additional bounds for $M_{\rm PBH} \in [10^{14}, 10^{17}]\,\mathrm{g}$.

Chapter 6

Publication III – Detecting dark objects in the Solar System with gravitational wave observatories

The following work has been published in Physical Review D, Volume 112, Issue 8, Nr. 083050 in October 2025 (Thoss and Loeb, 2025) and is licensed under CC BY 4.0[1]. It was the result of a research visit at the Center for Astrophysics at Harvard University in April 2025. During a discussion with Avi Loeb, the idea emerged to detect light PBHs in the newly opened mass window (see previous chapters) using gravitational wave observatories. Using the sensitivity curves of a number of proposed GW experiments, I computed the prospects to detect gravitational perturbations from PBHs or generic dark objects as they pass through the Solar System. I demonstrated that the DECIGO experiment would be sensitive to PBHs with $M_{\mathrm{PBH}} \in [10^7, 10^{11}]\,\mathrm{g}$, making up the dark matter. This overlaps with the newly opened mass window that I derived previously (Chapters 3, 4, and 5). The manuscript of the paper was prepared by me, but I received numerous helpful comments and suggestions from my supervisor, Andreas Burkert, and from Valeriya Korol and Jakob Stegmann. This work also benefited from discussion with experts in gravitational wave astronomy at the MIAPbP workshop "Enabling Future Gravitational Wave Astrophysics in the milli-Hertz Regime" in July 2025. Even though this work was done after the one in the following chapter, we present it first due to its direct link to the results from the previous chapter.

[1] https://creativecommons.org/licenses/by/4.0/

PHYSICAL REVIEW D **112,** 083050 (2025)

Detecting dark objects in the Solar System with gravitational wave observatories

Valentin Thoss*

Universitäts-Sternwarte, Ludwig-Maximilians-Universität München, Scheinerstraße 1, 81679 Munich, Germany, Max-Planck-Institut für Extraterrestrische Physik, Gießenbachstraße 1, 85748 Garching, Germany, and Excellence Cluster ORIGINS, Boltzmannstraße 2, 85748 Garching, Germany

Abraham Loeb

Astronomy Department, Harvard University, 60 Garden St., Cambridge, Massachusetts 02138, USA

(Received 25 July 2025; revised 28 September 2025; accepted 30 September 2025; published 23 October 2025)

Dark objects streaming into the solar system can be probed using gravitational wave (GW) experiments through the perturbations that they would induce on the detector test masses. In this work, we study the detectability of the resulting gravitational signal for a number of current and future GW observatories. Dark matter in the form of clumps or primordial black holes with masses in the range 10^7–10^{11} g can be detected with the proposed DECIGO experiment.

DOI: 10.1103/g3wh-hg4x

I. INTRODUCTION

Gravitational wave (GW) observatories such as LIGO-Virgo-KAGRA have opened a new window to the Universe by their ability to detect minuscule deformations of spacetime caused by the inspiral and merger of black hole binaries and neutron stars [1–3]. They do so by interfering light beams sent between the detector test masses.

During their operation, GW experiments are subject to a number of different noise sources, some of which lead to movement of the test masses between which the deformations of spacetime are measured. Such perturbations, if they are unpredictable, generally pose a limit to the sensitivity of an experiment [4].

However, the movement of the detector test masses can also lead to a detectable signature. In this work, we are interested in gravitational perturbations induced on the test masses by fast transients of objects passing through the Solar System. These objects could be primordial black holes (PBHs), making up the entire dark matter [5,6]. However, the results from this work generically apply to any object flying through the Solar System unbound, with velocities beyond the escape speed.

Similar analyses have been performed in the past for the case of dark matter clumps [7–12]. References [7,8] were the first to consider the detectability of dark matter clumps using space-based laser interferometers. Additionally, [9] studied a Yukawa interaction between dark and baryonic matter for the LIGO and LISA detectors. Reference [10] added to existing work by considering both gravitational and nongravitational forces for several detectors, including a novel concept for an asteroid-based detector [13]. In addition, they performed Monte Carlo simulations to account for the full phase space distribution of the dark matter trajectories. Reference [11] expanded previous analyses by also taking into account the Shapiro delay and considering higher-frequency gravitational wave experiments. Reference [12] studied the detectability of dark matter with proposed atom gradiometers. Their detectable mass window ($M \in [10^6, 10^{10}]$ g) is similar to what we find for the planned Big Bang Observer (BBO)/Deci-hertz Interferometer Gravitational wave Observatory (DECIGO) experiments, and their results are thus complementary to our work. Finally, we want to emphasize that there have been numerous other works on the role that dark matter clumps or primordial black holes could have in the Solar System [14,14–20].

Our contribution is summarized in the following. First, we study the general detectability of an object passing through the solar system with any velocity, mass, or distance, regardless of its nature, for a number of current and planned GW detectors. Adding to previous work, we include the proposed detectors BBO and DECIGO with their respective modeled noise curve. Furthermore, a detection threshold based on the false alarm rate based on [21] is used in this work, giving more realistic sensitivities compared to SNR thresholds used in the

*Contact author: vthoss@mpe.mpg.de

existing literature. Focusing on the case of dark matter clumps, we show that there is an interesting mass range $M \in [10^7, 10^{11}]$ g for which DECIGO could detect the presence of dark matter. In the case of PBHs, this mass range has previously been ignored due to their presumed rapid evaporation. However, recently this view has been challenged by the so-called "memory burden" effect [22–28], giving additional motivation to investigate this parameter space. Nevertheless, we remain agnostic about the nature of the objects passing through the Solar System, demanding only that they can be treated as a point mass in terms of their gravitational influence.

Our paper is structured as follows. We first describe how we compute the signal of the fly-by for a given gravitational wave detector. In the following, we investigate detection prospects in terms of the detection volume of each experiment as well as the interstellar mass density to which they are sensitive. For the case of the DECIGO detector, we additionally perform Monte Carlo simulations to sample a realistic phase space distribution of dark matter trajectories through the Solar System. This allows us to make predictions about the probability to observe the gravitational perturbation from the fly-by of a dark object.

II. COMPUTATION OF THE SIGNAL

In this section, we derive an analytical expression used to estimate the signal detected by a gravitational wave detector from the gravitational force of an object with mass M traversing the solar system with speed v. This is largely analogous to previous considerations in the literature [7–12].

The gravitational force exerted by the traversing object leads to a time-dependent acceleration of the detector test mass,

$$a(t) = \frac{GMR}{(R^2 + (vt)^2)^{3/2}}, \tag{1}$$

in the direction toward the point of closest encounter at a distance of R. The spectral density of such a signal can be computed analytically to be

$$a(\omega) = \frac{2GM\omega}{v^2} K_1(\omega R/v), \tag{2}$$

where K_1 denotes the first-order modified Bessel function of the second kind. Note that $K_1(x) \approx 1/x$ for $x \ll 1$ and thus $a(\omega) = \frac{2GM}{vR}$ for $\omega \ll v/R$. For $\omega > v/R$, the signal drops exponentially.

There is also an acceleration in the direction parallel to the perturber

$$a_\parallel(t) = \frac{GMvt}{(R^2 + (vt)^2)^{3/2}}, \tag{3}$$

with its spectral density given by

$$a_\parallel(\omega) = i\frac{2GM\omega}{v^2} K_0(\omega R/v). \tag{4}$$

As $K_0(x) \ll K_1(x)$ unless $x \gtrsim 0.1$ and both drop exponentially for $x > 1$, the contribution from $a_\parallel(\omega)$ is small except for $\omega \sim v/R$.

For a detector with multiple test masses i, located at positions $\mathbf{r}_i$, the different masses will be perturbed at a slightly different time t_i and distance of closest encounter R_i. The spectral density of the relative acceleration $\delta a_{ij}(\omega)$ between a pair of test masses i and j can be computed by projection on the vector between the two test masses, $\mathbf{r}_i - \mathbf{r}_j$:

$$\delta a_{ij}(\omega) \approx (a_i(\omega)\hat{\mathbf{a}}_\mathbf{i} + a_{i,\parallel}(\omega)\hat{\mathbf{v}} - a_j(\omega)\hat{\boldsymbol{a}}_\mathbf{j} e^{i\omega\Delta t} - a_{j,\parallel}(\omega)\hat{\mathbf{v}} e^{i\omega\Delta t}) \cdot \frac{(\mathbf{r}_i - \mathbf{r}_j)}{L}. \tag{5}$$

Here, $\Delta t = t_i - t_j$ is the difference between the time of closest encounter for each detector test mass and $L = |\mathbf{r}_i - \mathbf{r}_j|$ is the arm length of the detector. By $\hat{\mathbf{a}}_i$, we denote the normalized vector pointing from the position of the test mass to the point of closest encounter. $\hat{\mathbf{v}}$ denotes a normalized vector parallel to the motion of the perturber.

To gain a better understanding of Eq. (5), we consider a single detector arm with two test masses and the particular geometry sketched in Fig. 1, where the dark object moves perpendicular to the axis of the detector arm. For $R \gg L$, this leads to the largest possible perturbation, whereas for $R \lesssim L$ it is representative of a typical signal as we will show below. For the geometry depicted in Fig. 1, we have $\Delta t = 0$, $\hat{\mathbf{v}} \cdot (\mathbf{r}_i - \mathbf{r}_j) = 0$ and Eq. (5) reduces to

$$\delta a = \frac{2GM\omega}{v^2}(K_1(\omega R/v) - K_1(\omega(R+L)/v)). \tag{6}$$

If the compact object passes within close proximity of the test mass ($R \ll L$, near-field limit), then that mass will be perturbed much stronger than the other one, and we reach a good approximation:

$$\delta a_{\text{near}} = \frac{2GM\omega}{v^2} K_1(\omega R/v). \tag{7}$$

If the distance between the compact object and the test masses is much larger than the detector size ($R \gg L$), we only get a tidal effect, where the perturbation is suppressed by the factor L/R:

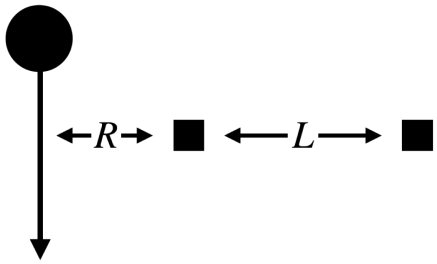

FIG. 1. Visualization of a fly-by at an impact parameter R near a GW detector of arm length L.

$$\delta a_{\rm tid} \approx \frac{2GM\omega L}{Rv^2} K_1(\omega R/v). \tag{8}$$

A gravitational wave detector usually has more than two test masses. For an L-shaped detector like LIGO with 3 test masses, the measured quantity is actually $\delta a_{12}(\omega) - \delta a_{13}(\omega)$. Here, the index 1 indicates the corner test mass where the signals from the two arms interfere. Therefore, the measured perturbation can in principle be larger by up to a factor of two compared to Eq. (6). It is useful to evaluate the probability distribution $p(\delta a(\omega))$ due to the space of possible geometries of the encounter. Using Monte-Carlo simulations, we sample this distribution for a LIGO-like "L"-shaped detector, as well as for a triangular setup as is planned for LISA, BBO, and DECIGO. We find that the following expression gives an excellent fit to the mean perturbation strength both for $R \ll L$ and $R \gg L$ as long as $\omega < v/R$:

$$\langle \delta a(\omega) \rangle = \frac{2GM\omega L}{v^2(\alpha R + \beta L)} K_1(\omega R/v). \tag{9}$$

For an L-shaped detector, we obtain $\alpha = 1.3$ and $\beta = 1.8$, and for a triangular shape we get $\alpha = 1.5$ and $\beta = 2.0$. The maximum deviation of the fit from the simulated data is observed for $R = L/2$, when the expression above underestimates the mean perturbation strength by a factor of ∼1.6. For $\omega \sim v/R$, Eq. (9) typically underestimates the spectral density by a factor of around two, partly as a result of the contribution from $a_{\parallel}(\omega)$. In the following, we will make use of Eq. (9) to obtain estimates of the signal-to-noise ratio (SNR) for existing and planned GW observatories.

To compute the spectral density of the gravitational wave strain $h(\omega)$, we recall that by definition of the metric tensor $L' = \sqrt{1+h}L$ and thus $\delta x = L' - L \approx h/2$. From this and $\delta x(\omega) = \delta a(\omega)/\omega^2$, we get the strain

$$h(\omega) = \frac{4GM}{\omega v^2(\alpha R + \beta L)} K_1(\omega R/v), \tag{10}$$

which can be used to estimate the SNR for any GW experiment, as

$$\mathrm{SNR} = 2\left(\int \mathrm{d}f \frac{h(f)^2}{P_n(f)} \right)^{1/2}, \tag{11}$$

where $P_n(\omega)$ denotes the power spectral density of the detector noise for the respective observatory. Note that, for the case of gravitational waves, $P_n(f)$ is replaced by the spectral strain sensitivity $S_n(f)$. The latter usually accounts for the angular dependence of the response of the detector. In addition, it includes a frequency-dependent suppression for gravitational waves with wavelengths which are comparable or smaller than the arm length of the detector [29]. In our case, this suppression is not applicable and the angular dependence is accounted for in the signal by the factors α and β. Therefore, we can directly use the detector noise $P_n(f)$ to estimate the SNR.

The data for our study is taken from [30] for the detectors aLIGO (design sensitivity), Einstein Telescope (ET), LISA, BBO, and DECIGO. For Cosmic Explorer (CE), we use the updated model for the detector noise from [31]. For the LISA experiment, we include the binary confusion noise presented in [32] for our analysis. This stochastic background will also be relevant for the BBO/DECIGO experiments, but the precise noise spectrum has not been worked out yet and will depend on the exact detector geometry and the ability to subtract individual sources from the background. Therefore, as a conservative choice, we set the lower frequency limit of both detectors to $f = 3 \times 10^{-3}$ Hz where we can expect the noise level to be subdominant (see the dotted gray line in Fig. 2). We found that if we instead extrapolate the detector noise to lower frequencies, including the binary noise as computed for LISA, then our results do not change much. Only if BBO achieves lower detector noise than LISA at frequencies $f \ll 10^{-3}$ do the detection prospects improve notably.

In addition to the noise from the galactic binaries, there are a plethora of other possible sources for GW backgrounds [33,34], from binary black holes to phase transitions. The existence of a GW background can in principle limit the detectability of the perturbations induced by dark objects flying through the solar system. However, there are often large uncertainties in the estimates for the noise level of the GW backgrounds. Therefore, in our analysis, we will assume that detectability is limited only by the detector noise. The only exception to this is the mentioned galactic foreground that is accounted for in the LISA noise curve.

The integrand in Eq. (11) has the form $\mathrm{d}f/P_n(f)/f^4 = \mathrm{d}\log f/P_n(f)/f^3$ for $f \ll v/R$ and decreases sharply for $f \gg v/R$. It is therefore convenient to plot $\sqrt{P_n(f)f^3}$ and $h(f)f^2$ together, as the latter will be constant for $f \ll v/R$ and the area between the two curves will be proportional to the SNR on a log-scaled figure.

Figure 2 shows the rescaled spectral noise of current, planned, and proposed GW observatories. This plot can be used to easily read off the signal-to-noise ratio for any of the experiments displayed by the area between the signal,

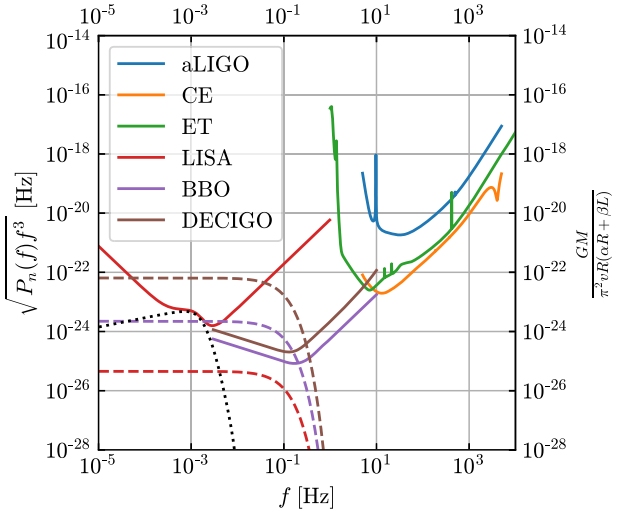

FIG. 2. Strain sensitivity of various existing and proposed GW experiments. The y-axis has been rescaled such that the signal of an encounter with given parameters M, R, and v would appear as a horizontal line for $f < v/R$, dropping quickly for $f > v/R$. The area between it and any sensitivity curve is proportional to the signal-to-noise ratio for that experiment. Note that, in the limit of a close encounter, $R < L$, the signal amplitude is dependent on the detector arm length and must be computed for each experiment separately. The dashed lines show the signal for an object with $M = 10^{10}$ g, $v = 300$ km s^{-1}, and $R = 10^3$ km for the detectors LISA, BBO, and DECIGO in the same colors as the strain sensitivity. The dotted black line indicates the binary confusion noise, taken from [32].

based on the right-side y-axis and the noise curve. The axis has been rescaled such that the signal will be represented by a horizontal line with an amplitude of $\frac{GM}{\pi^2 vR(\alpha R+\beta L)}$ that extends up to a frequency $f = v/R$ and drops sharply thereafter. Note that in the limit $R \ll L$ the amplitude is dependent on the arm length of each detector, and thus, the signal must be computed for each experiment individually.

As a first step, we remain agnostic about the orbital parameters of the perturber and compute for a range of values of M and velocity v the distance of the encounter R to which each experiment is sensitive. We will present the results of this in the following section.

As a second step, we study the feasibility of detecting objects with a given interstellar mass density ρ at the location of the solar system. If primordial black holes of a given mass M make up all of the dark matter, they will have $\rho \sim \rho_{\rm DM} = 7 \times 10^{-25}\,{\rm g\,cm^{-3}} \approx 0.4$ GeV cm^{-3} and an rms velocity of $v \sim 300$ km s^{-1} [35,36]. While our results apply to PBHs, they can also be used more generally as a way to constrain any kind of interstellar objects flying through the solar system.

Fixing the density of the perturbers implies a number of encounters with impact parameters smaller than R within a time t, given by

$$N = \frac{\pi R^2 \rho v t}{M}. \tag{12}$$

Therefore, the probability distribution of the distance R to the closest encounter by Poisson statistics is

$$p(R) = p(N)\frac{{\rm d}N}{{\rm d}R} = \frac{2\pi R \rho v t}{M}\exp\left(-\frac{\pi R^2 \rho v t}{M}\right), \tag{13}$$

which implies that the 90th percentile distance of the closest encounter to occur within a time span t is given by

$$R_{\rm min,90} = \sqrt{\frac{M\ \ln\ (10)}{\rho v t}}. \tag{14}$$

Using this as an estimate for the value of R, we employ Eqs. (10) and (11) to evaluate the SNR for a given interstellar density ρ, mass M, and velocity v of the perturbers. The choice of $R_{\rm min,90}$ implies that there is a 90% probability to observe at least one event with the given SNR in that time period.

Previous studies of "burst"-like GW signals have found SNRs of around 8 sufficient for the LIGO observatory [21,37]. For a lower SNR, the false alarm rate (FAR) will be too large. Using Eq. (30) from [21], we compute the FAR for any other GW detector using the spectral density $h(\omega)$ of the signal:

$${\rm FAR} = \sqrt{\frac{C_2 - C_1^2}{2\pi}}\xi e^{-\xi^2/2}. \tag{15}$$

Here, ξ denotes the signal-to-noise ratio according to Eq. (11) and C_k are defined as

$$C_k = \frac{4}{\xi^2}\int {\rm d}f (2\pi f)^k \frac{h(f)^2}{P_n(f)}. \tag{16}$$

As the detectors considered in this work are generally most sensitive at lower frequencies compared to LIGO, the resulting false alarm rates are generally lower and so is the required SNR. Using the false alarm rate as a detection threshold provides more realistic estimates for the sensitivity of individual detectors and is generally more conservative compared to the SNR thresholds used in previous work. We will use FAR $< 10^{-3}$ yr^{-1} throughout this work but note that due to the exponential dependence in Eq. (15) the precise value is not important.

III. DETECTION PROSPECTS

Figure 3 displays the minimum fly-by distance required to have a signal with FAR $< 10^{-3}$ yr^{-1}, which corresponds to SNRs between 5 and 8 for the experiments considered. We display the detection volume as a function of the perturber mass and velocity for LISA and DECIGO

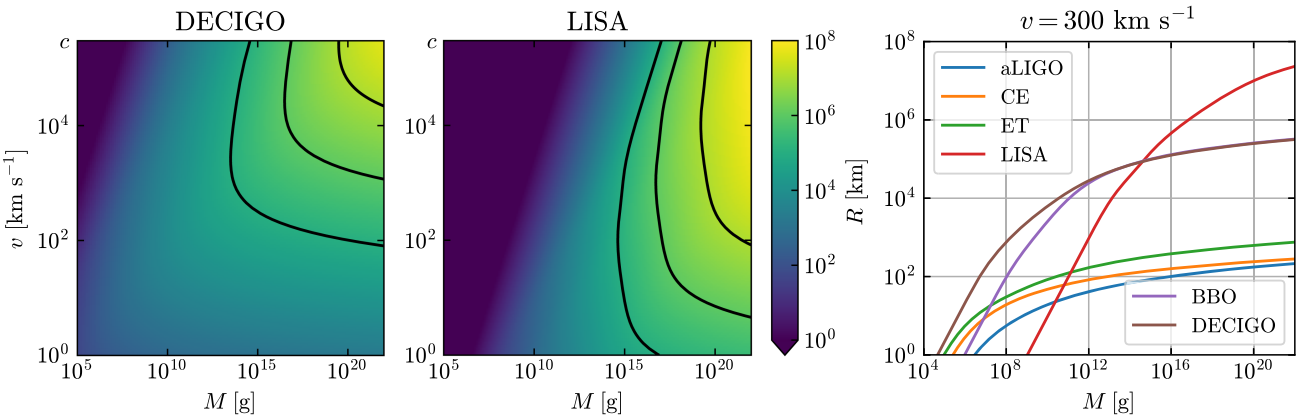

FIG. 3. Maximum distance for which GW experiments are sensitive to a fly-by of a perturber. Left: results for DECIGO/LISA as a function of the mass and velocity of the perturber. Contours for $R = [10^5, 10^6, 10^7]$ km are shown as black lines. Right: results for all GW experiments as a function of the mass of the perturber for $v = 300\,\mathrm{km\,s^{-1}}$. Detectability is defined as FAR $< 10^{-3}$ yr^{-1}.

and additionally show the results for all detectors for $v = 300\,\mathrm{km\,s^{-1}}$.

A limitation for each GW detector is the minimum frequency $f_{\min}$ to which it is sensitive, as it sets the maximum distance observable to $R_{\max} \sim v/f_{\min}$. For this reason, LISA has the largest detection range for the most massive objects due to its susceptibility at low frequencies. For objects of smaller mass or higher velocity, where the limiting factor is the sensitivity of the experiment, DECIGO achieves a larger detection volume due to its superior design sensitivity compared to LISA.

We note that the large detection radius for LISA in principle opens the possibility to measure the masses of asteroids or comets whose trajectory and velocity are known, should they pass close enough to the detector. The recently discovered interstellar object 3I/ATLAS [38–40] has a minimum intersection distance with Earth's orbit of 0.37 AU. Assuming a mass of 10^{16} g, corresponding to a diameter of the nucleus of 1–2 km, the closest approach to LISA would have to be at a distance below 0.002 AU in order to be detectable. However, there are assumed to be many more smaller bodies, some of which could come close enough to a GW observatory for detection. Computing the likelihood for such an event is left for future work.

The results presented in Fig. 3 for aLIGO, ET, and LISA agree reasonably well with those presented in Fig. 1 of [10] for the same choice of parameters. We find somewhat larger sensitivity at higher masses for aLIGO and ET due to the approximations made in their heuristic sensitivity estimate.

Figure 4 shows the SNR resulting from a fixed density of the dark objects of $\rho \sim \rho_{\mathrm{DM}} = 7 \times 10^{-25}\,\mathrm{g\,cm^{-3}} \approx 0.4\,\mathrm{GeV\,cm^{-3}}$. The distance to the perturber is set by Eq. (14), implying that there is 90% probability to observe at least one event with at least the given SNR. The future detectors BBO and DECIGO show the most promising results, achieving large SNRs for a sizable part of the parameter space, even at nonrelativistic velocities. LISA, CE, and ET reach SNRs close to or slightly above one at relativistic velocities. However, such parameter regions are likely ruled out by other constraints, either from structure formation in the case of dark matter or from collisions with solar system bodies in general.

Focusing on the case of compact objects such as PBHs as dark matter, we adopt a velocity of $v = 300\,\mathrm{km\,s^{-1}}$ and compute the lowest density ρ for which the closest encounter at the 90th percentile within a period of $T = 10$ yr produces a signal with a false alarm rate below 10^{-3} yr^{-1}. The results are displayed in Fig. 5. The curves can be easily adopted for different periods of observation T by noting that $\rho \sim 1/T$. Our results demonstrate that the planned BBO and DECIGO experiments have the potential to probe scenarios where the dark matter is in the form of compact objects with a mass of $M \in [10^7, 10^{11}]$ g. It is commonly assumed that PBHs of such masses cannot make up the dark matter due to their rapid evaporation. However, the so-called "memory burden" effect [22,23] could significantly suppress the evaporation, opening a new window for light PBHs as a dark matter candidate [24–27]. It is therefore highly interesting that GW experiments could be used to probe their existence purely by their gravitational interaction as they pass through the solar system. By pure coincidence, DECIGO is also able to probe PBHs of similar mass through the GW emission associated with their formation [41]. Independent of the nature of dark matter, it is highly interesting that GW detectors in the decihertz regime show the potential to probe a region in the parameter space of massive dark matter that is otherwise difficult to access.

The noise spectrum of future gravitational wave detectors has to be estimated, which implies some degree of uncertainty. In Fig. 5, we show how an uncertainty in the detector noise $\sqrt{P_n(f)}$ of a factor of two affects the resulting densities which can be probed. For lower masses,

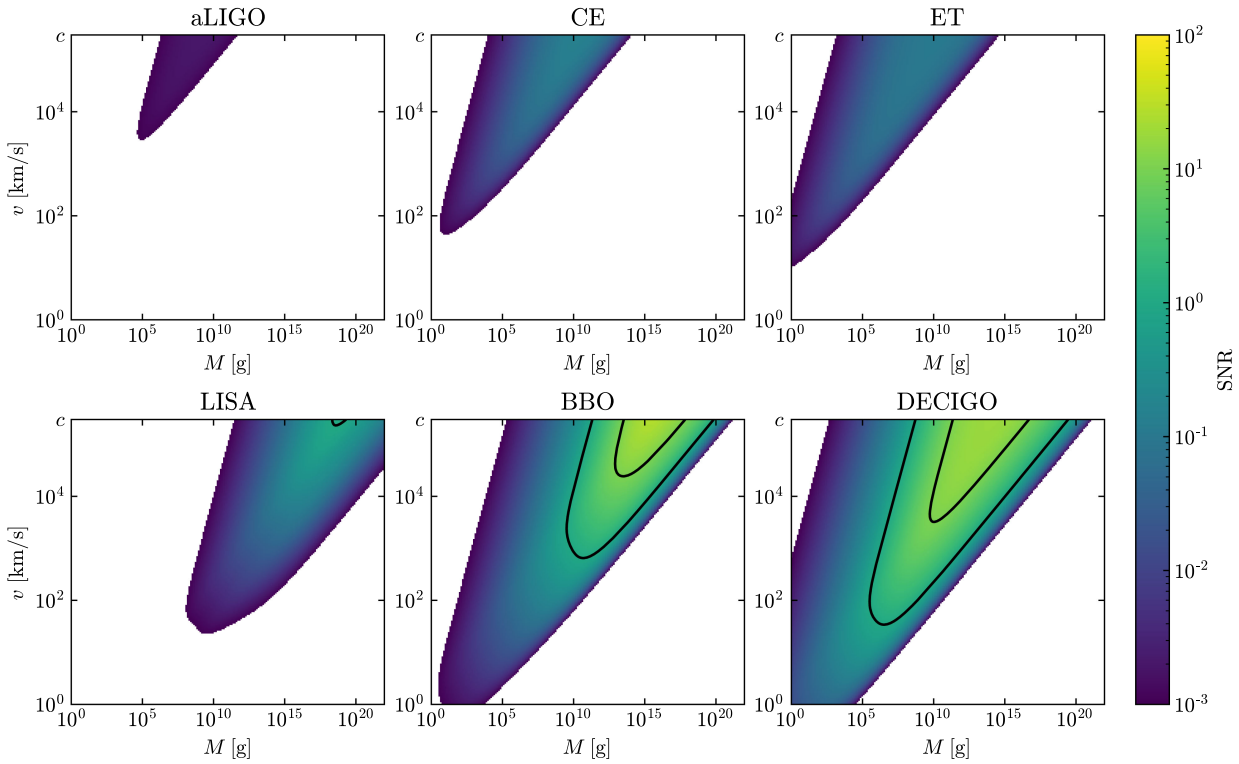

FIG. 4. Signal-to-noise ratio from the closest encounter at the 90th percentile expected within an observation time $T = 10$ yr for density $\rho = \rho_{\rm DM} = 7 \times 10^{-25}\,{\rm g\,cm^{-3}}$. The SNR is shown for several GW experiments as a function of the mass M and velocity v of the perturber. In the white area, the SNR is lower than 10^{-3}. The black lines indicate the contours for which SNR $= [1, 10]$.

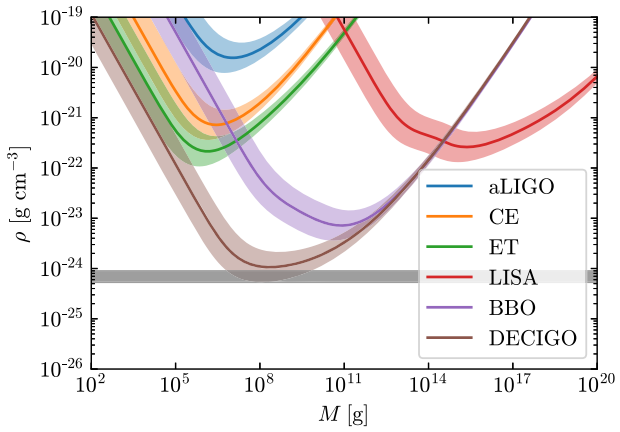

FIG. 5. Density for which each experiment is sensitive to at least one perturbation within a period of $T = 10$ yr at 90th percentile. A velocity of $v = 300\ {\rm km\,s^{-1}}$ is assumed, as expected for dark matter. The detection threshold is FAR $< 10^{-3}\ {\rm yr^{-1}}$ which implies SNRs between 5 and 8 for the various detectors. The colored shaded area indicates the resulting range implied by an uncertainty in the detector noise $\sqrt{P_n}$ of a factor of two. The gray shaded area corresponds to the range of the latest observational estimates of the local dark matter density $\rho_{\rm DM} \in [0.3, 0.5]{\rm GeV\,cm^{-3}}$ [35].

where the detection is limited by the noise level of the observatory, one has $\rho \sim P_n(f)$ as $h(f) \sim 1/R \sim \sqrt{\rho}$. At higher masses, where the limit is set by the frequency range of the detector, the results are not very sensitive to the exact noise level.

We can compare our results for the sensitivity of aLIGO, ET, CE, and LISA with those shown in Fig. 3 of [11] for the same choice of parameters. Overall, our results agree quite well with some deviations due to methodological differences and the fact that in their work they use $S_n(f)$ for the computation of the SNR instead of $P_n(f)$ which gives a somewhat worse sensitivity. We found a notable deviation for ET at low masses which seems to come from an erroneous value for the arm length in [11] giving a sensitivity that is two orders in magnitude too low. We also want to note that the sensitivities of LISA, BBO, and DECIGO presented in Fig. 1 of [8] are significantly more optimistic compared to ours, owing to their assumption of a flat spectrum of the detector noise $P_n(f)$ which is only true in a certain frequency range.

Our estimates based on Eq. (10) show that DECIGO has the greatest potential to detect perturbations from dark matter in the form of compact objects streaming through the solar system. We therefore study this case in more detail

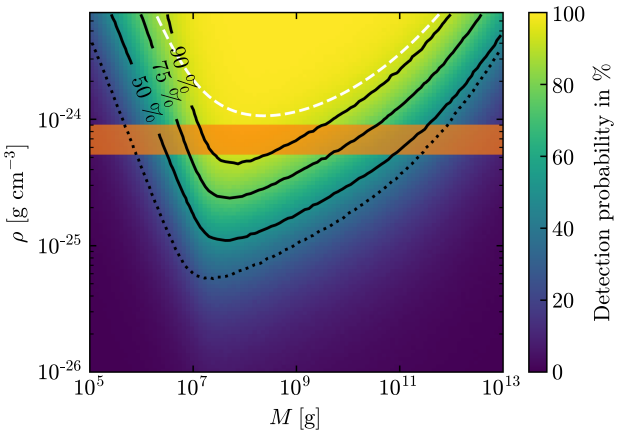

FIG. 6. Probability for DECIGO to detect at least one signal from the fly-by of compact objects, shown as a function of their mass M and density ρ. We assume an observation time of $T = 10$ yr. A successful detection is defined as having FAR $< 10^{-3}$ yr^{-1}, which roughly corresponds to SNR > 6. The orange shaded area corresponds to the range of the latest observational estimates of the local dark matter density $\rho_{\rm DM} \in [0.3, 0.5]$GeV cm^{-3} [35]. Contours of constant probability are displayed as solid black lines. The dotted black line indicates a contour of 50% probability given a reduction in the detector noise level by a factor of two. The estimate from Fig. 5 for the DECIGO experiment is shown as a dashed white line and should be compared to the contour of 90% probability.

and relax previous approximations. For a more accurate assessment of detection prospects, we compute the signal using Eq. (5) by performing Monte Carlo simulations over the space of possible geometries of the encounter. The velocity for each encounter is obtained by adding a random component with $v_{\rm rms} = 270$ km s^{-1} to the proper motion of the Sun around the Galactic Center (DM wind) with $v_\odot = 220$ km s^{-1} [36]. We neglect the small nonisotropy in the angular distribution of the velocity and sample the orientation uniformly on a sphere. These simulations are performed for a range of different masses M and densities ρ, and the probability of a successful observation in a period of $T = 10$ yr is determined as the fraction of simulations for which FAR $< 10^{-3}$ yr^{-1} is obtained.

Figure 6 shows the results. Notably, there is a wide range of masses M for which the probability of observing the gravitational signal is high. In other words, should the dark matter be in the form of compact objects with mass $M \in [10^7, 10^{11}]$ g, there is a good chance that it will perturb the DECIGO detector enough to lead to a detectable signal at least once within 10 yr of observation. This agrees reasonably well with the estimate presented before in Fig. 5 that is also shown as a white dashed line in Fig. 6. Our more careful analysis results in slightly better sensitivity compared to the estimate based on Eq. (9), which underestimates the mean spectral density for $\omega \sim v/R$ as we have mentioned before.

The nondetection of a gravitational signal of this kind allows in principle one to put constraints on the dark matter density for the same range of masses. Our results indicate that these constraints would rule out that all the dark matter is in objects with a mass $M \in [10^7, 10^9]$ g at 90% confidence.

The sensitivity to the perturbations depends on the exact level of DECIGO's detector noise. We highlight this in Fig. 6 by an additional dashed line which indicates the contour for a 50% probability of observation in a scenario where the detector noise is lower by a factor of two. Notably, if the "Ultimate DECIGO" detector [42] is realized, which is only limited by quantum noise, then the detection prospects could increase by several orders of magnitude, expanding the range of masses to which it would susceptible. Conversely, the detection prospects can diminish if detector noise is greater than anticipated or in the presence of irremovable gravitational wave backgrounds. We find that an increase in the noise level by a factor of six reduces the probability for an observation to below 50% for any mass of the perturber. Finally, we want to note that the densities which are observable or that can be constrained scale with observation time as $\rho \sim 1/T$.

IV. SUMMARY

We have studied the feasibility of gravitationally probing the streaming of dark objects through our solar system. The detection method relies on the perturbation of the test masses of gravitational wave detectors, which leads to a burstlike signal in the experiment.

We have computed the distances of encounters to which the different types of current and future GW experiments are sensitive, which can reach several million kilometers for LISA, BBO, and DECIGO. The main limitation of each experiment is the frequency range to which it is sensitive. In order for the encounter to be detectable, the fly-by must be sufficiently close or fast in order for $f \sim v/R$ to be large enough.

If the solar system is penetrated by dark objects with a halo density $\rho \sim \rho_{\rm DM}$, then the proposed GW experiment DECIGO offers the best prospects to detect dark matter and it will be sensitive to the range of masses $M \in [10^7, 10^{11}]$ g.

ACKNOWLEDGMENTS

We want to thank Valeriya Korol, Jakob Stegmann, and Andreas Burkertfor fruitful discussions. We are grateful to the anonymous referee for valuable comments and suggestions. This research was supported in part by the Excellence Cluster ORIGINS which is funded by the Deutsche Forschungsgemeinschaft (DFG, German Research Foundation) under Germany's Excellence Strategy—EXC-2094–390783311 (for V. T.). This work was supported in part by the Black Hole Initiative and the Galileo Project at Harvard University (for A. L.).

DATA AVAILABILITY

The data that support the findings of this article are openly available [43].

[1] B. P. Abbott *et al.* (LIGO Scientific and Virgo Collaborations), Observation of gravitational waves from a binary black hole merger, Phys. Rev. Lett. **116**, 061102 (2016).
[2] B. P. Abbott *et al.* (LIGO Scientific and Virgo Collaborations), GW170817: Observation of gravitational waves from a binary neutron star inspiral, Phys. Rev. Lett. **119**, 161101 (2017).
[3] R. Abbott *et al.* (LIGO Scientific and Virgo Collaborations), GWTC-3: Compact binary coalescences observed by LIGO and Virgo during the second part of the third observing run, Phys. Rev. X **13**, 041039 (2023).
[4] B. P. Abbott *et al.* (LIGO Scientific and Virgo Collaborations), A guide to LIGO-Virgo detector noise and extraction of transient gravitational-wave signals, Classical Quantum Gravity **37**, 055002 (2020).
[5] B. Carr, K. Kohri, Y. Sendouda, and J. Yokoyama, Constraints on primordial black holes, Rep. Prog. Phys. **84**, 116902 (2021).
[6] A. Escrivà, F. Kühnel, and Y. Tada, Primordial black holes, in Black Holes in the Era of Gravitational-Wave Astronomy, edited by M. Arca Sedda, E. Bortolas, and M. Spera (2024), pp. 261–377, https://doi.org/10.1016/B978-0-32-395636-9.00012-8.
[7] A. W. Adams and J. S. Bloom, Direct detection of dark matter with space-based laser interferometers, arXiv:astro-ph/0405266.
[8] N. Seto and A. Cooray, Search for small-mass black-hole dark matter with space-based gravitational wave detectors, Phys. Rev. D **70**, 063512 (2004).
[9] E. D. Hall, R. X. Adhikari, V. V. Frolov, H. Müller, and M. Pospelov, Laser interferometers as dark matter detectors, Phys. Rev. D **98**, 083019 (2018).
[10] S. Baum, M. A. Fedderke, and P. W. Graham, Searching for dark clumps with gravitational-wave detectors, Phys. Rev. D **106**, 063015 (2022).
[11] Y. Du, V. S. H. Lee, Y. Wang, and K. M. Zurek, Macroscopic dark matter detection with gravitational wave experiments, Phys. Rev. D **108**, 122003 (2023).
[12] L. Badurina, Y. Du, V. S. H. Lee, Y. Wang, and K. M. Zurek, Detecting gravitational signatures of dark matter with atom gradiometers, Phys. Rev. D **112**, 063014 (2025).
[13] M. A. Fedderke, P. W. Graham, and S. Rajendran, Asteroids for μHz gravitational-wave detection, Phys. Rev. D **105**, 103018 (2022).
[14] Y. Luo, S. Hanasoge, J. Tromp, and F. Pretorius, Detectable seismic consequences of the interaction of a primordial black hole with earth, Astrophys. J. **751**, 16 (2012).
[15] T. X. Tran, S. R. Geller, B. V. Lehmann, and D. I. Kaiser, Close encounters of the primordial kind: A new observable for primordial black holes as dark matter, Phys. Rev. D **110**, 063533 (2024).
[16] A. Yalinewich and M. E. Caplan, Crater morphology of primordial black hole impacts, Mon. Not. R. Astron. Soc. **505**, L115 (2021).
[17] M. E. Caplan, J. Johnston, and A. D. Santarelli, Lunar collision rate with primordial black holes, Mon. Not. R. Astron. Soc. **524**, 1927 (2023).
[18] M. Cuadrat-Grzybowski, S. Clesse, P. Defraigne, M. Van Camp, and B. Bertrand, Probing primordial black holes and dark matter clumps in the Solar System with gravimeter and Global Navigation Satellite Systems networks, Phys. Rev. D **110**, 063029 (2024).
[19] Y.-L. Li, G.-Q. Huang, Z.-Q. Huang, and F.-W. Shu, Detecting sublunar-mass primordial black holes with the earth-moon binary system, Phys. Rev. D **107**, 084019 (2023).
[20] V. Thoss and A. Burkert, Primordial black holes in the solar system, Astrophys. J. **980**, 238 (2025).
[21] G. Morrás, J. F. N. Siles, J. García-Bellido, and E. R. Morales, False alarms induced by Gaussian noise in gravitational wave detectors, Phys. Rev. D **107**, 023027 (2023).
[22] G. Dvali, A microscopic model of holography: Survival by the burden of memory, arXiv:1810.02336.
[23] G. Dvali, L. Eisemann, M. Michel, and S. Zell, Black hole metamorphosis and stabilization by memory burden, Phys. Rev. D **102**, 103523 (2020).
[24] V. Thoss, A. Burkert, and K. Kohri, Breakdown of Hawking evaporation opens new mass window for primordial black holes as dark matter candidate, Mon. Not. R. Astron. Soc. **532**, 451 (2024).
[25] A. Alexandre, G. Dvali, and E. Koutsangelas, New mass window for primordial black holes as dark matter from the memory burden effect, Phys. Rev. D **110**, 036004 (2024).
[26] G. Dvali, M. Zantedeschi, and S. Zell, Transitioning to memory burden: Detectable small primordial black holes as dark matter, arXiv:2503.21740.
[27] G. Montefalcone, D. Hooper, K. Freese, C. Kelso, F. Kuhnel, and P. Sandick, Does memory burden open a new mass window for primordial black holes as dark matter?, arXiv:2503.21005.
[28] A. Dondarini, G. Marino, P. Panci, and M. Zantedeschi, The fast, the slow and the merging: Probes of evaporating memory burdened PBHs, arXiv:2506.13861.
[29] T. Robson, N. J. Cornish, and C. Liu, The construction and use of LISA sensitivity curves, Classical Quantum Gravity **36**, 105011 (2019).
[30] K. Schmitz, New sensitivity curves for gravitational-wave signals from cosmological phase transitions, J. High Energy Phys. 01 (2020) 097.
[31] K. Kuns, P. Fulda, L. Barsotti, and M. Evans, Cosmic explorer strain sensitivity, Cosmic Explorer (2023).
[32] N. Cornish and T. Robson, Galactic binary science with the new LISA design, J. Phys. Conf. Ser. **840**, 012024 (2017).
[33] N. Christensen, Stochastic gravitational wave backgrounds, Rep. Prog. Phys. **82**, 016903 (2019).
[34] A. I. Renzini, B. Goncharov, A. C. Jenkins, and P. M. Meyers, Stochastic gravitational-wave backgrounds: current detection efforts and future prospects, Galaxies **10**, 34 (2022).
[35] M. Cirelli, A. Strumia, and J. Zupan, Dark matter, arXiv:2406.01705.
[36] K. Choi, C. Rott, and Y. Itow, Impact of the dark matter velocity distribution on capture rates in the Sun, J. Cosmol. Astropart. Phys. 05 (2014) 049.

[37] G. Morrás, J. García-Bellido, and S. Nesseris, Search for black hole hyperbolic encounters with gravitational wave detectors, Phys. Dark Universe **35**, 100932 (2022).

[38] D. Z. Seligman *et al.*, Discovery and preliminary characterization of a third interstellar object: 3I/ATLAS, arXiv:2507.02757.

[39] A. Loeb, 3I/ATLAS is smaller or rarer than it looks, Res. Not. Am. Astron. Soc. **9**, 178 (2025).

[40] C/2025 N1 (ATLAS Collaboration) Orbit Parameters, JPL Small-Body Database (accessed: 2025–07–25), https://ssd.jpl.nasa.gov/tools/sbdb_lookup.html#/?sstr=1004083.

[41] W. Barker, B. Gladwyn, and S. Zell, Inflationary and gravitational wave signatures of small primordial black holes as dark matter, Phys. Rev. D **111**, 123033 (2025).

[42] N. Seto, S. Kawamura, and T. Nakamura, Possibility of direct measurement of the acceleration of the universe using 0.1 Hz band laser interferometer gravitational wave antenna in space, Phys. Rev. Lett. **87**, 221103 (2001).

[43] V. Thoss, Data for the paper "Detecting dark objects in the Solar System with Gravitational Wave observatories" (Thoss and Loeb, 2025), (2025).

Chapter 7

Publication IV – Primordial Black Holes in the Solar System

The following work has been published in The Astrophysical Journal, Volume 980, Issue 2, id.238, 11 pp (Thoss and Burkert, 2025) and is licensed under CC BY 4.0[1]. In August 2024, a preprint appeared, claiming that PBHs in the asteroid mass window are ruled out based on their gravitational effect on Solar System objects (Loeb, 2024). Intrigued by this claim, I developed N-body simulations of the Solar System embedded in a halo of PBHs to study both their cumulative as well as their individual effects. The manuscript was prepared by me. My supervisor, Andreas Burkert, contributed to this project through his countless questions and ideas, helping me to quickly progress. In addition, Chris McKee made several helpful suggestions.

[1] https://creativecommons.org/licenses/by/4.0/

The Astrophysical Journal, 980:238 (11pp), 2025 February 20 https://doi.org/10.3847/1538-4357/adae84

Primordial Black Holes in the Solar System

Valentin Thoss[1,2,3] and Andreas Burkert[1,2,3]
[1] Universitäts-Sternwarte, Ludwig-Maximilians-Universität München, Scheinerstr. 1, 81679 Munich, Germany; vthoss@mpe.mpg.de
[2] Max-Planck-Institut für Extraterrestrische Physik, Gießenbachstraße 1, 85748 Garching, Germany
[3] Excellence Cluster ORIGINS, Boltzmannstraße 2, 85748 Garching, Germany
Received 2024 September 24; revised 2024 December 20; accepted 2025 January 23; published 2025 February 19

Abstract

If primordial black holes (PBHs) of asteroidal mass make up the entire dark matter, they could be detectable through their gravitational influence in the solar system. In this work, we study the perturbations that PBHs induce on the orbits of planets. Detailed numerical simulations of the solar system, embedded in a halo of PBHs, are performed. We find that the gravitational effect of the PBHs is dominated by the closest encounter. Using the Earth–Mars distance as an observational probe, we show that the perturbations are smaller than the current measurement uncertainties and thus PBHs are not directly constrained by solar system ephemerides. We estimate that an improvement in the ranging accuracy by an order of magnitude or the extraction of signals well below the noise level is required to detect the gravitational influence of PBHs in the solar system in the foreseeable future.

Unified Astronomy Thesaurus concepts: Solar system evolution (2293); Solar system (1528); Primordial black holes (1292); Milky Way dark matter halo (1049); Dark matter (353); Close encounters (255); Orbital anomalies (1176); Gravitation (661); Black holes (162)

1. Introduction

Primordial black holes (PBHs) as a dark matter (DM) candidate have been studied for half a century (B. J. Carr & A. M. Green 2024), gaining special attention after the first direct detection of gravitational waves from binary black hole mergers (B. P. Abbott et al. 2016). By now, a large number of constraints have been derived that limit the fraction of DM that can be in the form of PBHs (B. Carr et al. 2021). However, these constraints come with some uncertainty and can even disappear entirely, as was recently demonstrated for light PBHs (A. Alexandre et al. 2024; V. Thoss et al. 2024).

The asteroid-mass window ($M_{\rm PBH} \in [10^{17}, 10^{23}]$ g) has been studied with particular interest, as it remains a viable parameter region for PBHs. Within this mass range, their interaction with stars, neutron stars, and white dwarfs has been studied as a pathway to detect them or constrain their DM fraction. However, many of the bounds that were obtained in this way are disputed for various reasons (see B. Carr et al. 2021 for an overview).

Another approach to studying PBHs of asteroidal mass is through their effect within the solar system. It has been suggested to look for craters as a signature of PBH collisions with moons and planets (A. Yalinewich & M. E. Caplan 2021; M. E. Caplan et al. 2023). Other work focuses on the gravitational effects of PBHs. This includes perturbations to the orbits of moons and planets (Y.-L. Li et al. 2023; T. X. Tran et al. 2024), satellite constellations (B. Bertrand et al. 2023), and future space-based gravitational-wave detectors such as LISA (A. W. Adams & J. S. Bloom 2004; N. Seto & A. Cooray 2004). So far these are mostly proof-of-concept studies that suggest that an accurate model for solar system ephemerides, combined with a sophisticated data analysis, will make the detection of individual asteroid-mass PBHs feasible. T. X. Tran et al. (2024) showed that if the extraction of signals with an amplitude of 10^{-4} relative to the noise is achieved, then there will be a significant rate of detectable PBH encounters for $10^{18}\,\mathrm{g} < M_{\rm PBH} < 10^{23}\,\mathrm{g}$ with the current observational accuracy.

Recently, A. Loeb (2024) argued that PBHs within most of the asteroid-mass window are already excluded from making up the entire DM, based on their perturbations of solar system bodies. The result was obtained by considering the Poissonian fluctuation of the number of PBHs within a given radius R from the Sun. The rate of change of the total PBH mass, enclosed within R, was compared to an observational constraint on the rate of change of the solar mass. This approach assumes that the total mass of PBHs within R has a gravitational effect similar to a point mass and therefore can be added directly to the mass of the Sun. From this, A. Loeb (2024) concluded that, for $R = 50$ au, PBHs cannot make up the entire DM in the mass range $M_{\rm PBH} \in [6 \times 10^{18}, 10^{22}]$ g. However, J. M. Cline (2024) has noted that the choice of $R = 50$ au is not justified and that one cannot easily rule out PBHs as a DM candidate.

Because of the far-reaching consequences of the results obtained by A. Loeb (2024), it is necessary to investigate it in more detail. The key question is whether PBHs can induce detectable perturbations on the orbits of solar system objects (SSOs). In this work we present results from N-body simulations of the solar system, embedded in a halo of PBHs. We study the orbital perturbations that these compact objects induce on planets in the solar system. Our methods are presented in Section 2, and our results are shown in Section 3. In Section 4 we provide a discussion of our results and show that the perturbations are dominated by the closest encounter rather than the Poissonian fluctuations in the PBH number density studied by A. Loeb (2024). We conclude with a summary in Section 5.

2. Methods

Our goal is to simulate the perturbations induced on the orbits of SSOs by a halo of asteroid-mass PBHs. In this section

Table 1
Simulation Parameters, Showing the Adopted PBH Mass and Number, the Size of the Simulation Box, the Total Number of Runs, and the Simulation Time

$M_{\rm PBH}$ (g)	$N_{\rm PBH}$	$R_{\rm box}$ (au)	$N_{\rm runs}$	t (yr)
10^{18}	18525	200	1000	1
10^{19}	6252	300	1000	1
10^{20}	1482	400	3000	1
10^{21}	500	600	9000	1
10^{20}	2110	450	500	20

we briefly describe our simulation methods and relevant quantities.

We use a second-order Leapfrog integrator with a fixed time step to simulate the motions of the Sun, the eight planets, and Earth's Moon. Other SSOs are neglected, as we are only interested in the relative perturbation of planets in the solar system. The goal of this work is not to make accurate predictions on the absolute positions of the bodies of the solar system; rather, we are interested in the relative perturbation of their position $\delta \boldsymbol{r}(t)$. We do not expect the smaller bodies to have a sizable effect on these perturbations. For the same reason, we do not treat finite-size effects or relativistic corrections, as these will only affect the perturbations at second order. We refer to T. X. Tran et al. (2024) for a more detailed discussion on these effects.

The initial conditions for the SSOs are obtained from the Horizons System by JPL, based on the DE441 model (R. S. Park et al. 2021). The solar system is embedded in a halo of PBHs, homogeneously filling a box of size $L_{\rm box}$ with periodic boundary conditions. The halo is populated with $N_{\rm PBH} = L_{\rm box}^3 \rho_{\rm CDM}/M_{\rm PBH}$ PBHs of random positions, thus assuming that PBHs make up the entire DM with a monochromatic mass distribution. During the simulations, the gravitational forces are only computed for PBHs within a sphere of radius $R_{\rm box} = L_{\rm box}/2$. This enables the comparison with the case of a smooth spherical particle DM, where the potential is analytically tractable. The PBHs are given a Maxwellian velocity distribution with a dispersion $\sigma_v = 185\,{\rm km\,s^{-1}}$, as well as an additional component due to the rotation of the galactic disk. The latter has a magnitude of $v_\odot = 230\,{\rm km\,s^{-1}}$, an angle of 60° with respect to the ecliptic plane and a direction such that the relative motion between the PBHs and Earth is maximal on June 1 (K. Freese et al. 2013). These parameters lead to a relative velocity of the PBHs of $v_{\rm rms} \approx 279\,{\rm km\,s^{-1}} \approx 59\ {\rm au\ yr^{-1}}$. Here $\rho_{\rm CDM} = 7 \times 10^{-25}\,{\rm g\,cm^{-3}}$ is assumed to facilitate comparisons with A. Loeb (2024).

To investigate the parameter space of the asteroid-mass window, we choose $M_{\rm PBH} \in [10^{18}, 10^{19}, 10^{20}, 10^{21}]$ g. Note that we discuss how our results can be extrapolated to other PBH masses. For each value of the mass $M_{\rm PBH}$ a large number of simulation runs ($\mathcal{O}(1000)$; see Table 1) are performed, each over a physical time span of 1 yr, to account for the randomness of the encounters with the solar system bodies. These simulations help us to understand the dependence of the perturbation strength on the black hole mass $M_{\rm PBH}$. To answer the question whether PBHs can cause detectable perturbations in the solar system, 500 simulations with $M_{\rm PBH} = 10^{20}$ g are carried out over a time of 20 yr, which is roughly the time span for which the most precise ranging data in the solar system have been available. We checked for each value of $M_{\rm PBH}$ that both the numerical time step and the value of $R_{\rm box}$ do not significantly affect our results. To reduce computational cost, the gravitational force is only calculated for the solar system bodies, whereas the PBHs move on straight trajectories. This is a reasonable approximation owing to the high velocity of the PBHs. We nevertheless performed additional simulations including the gravitational force for the PBHs and found that it only changes our results below the percent level. The exact parameters of our simulation ensemble can be found in Table 1.

The main quantity of interest is the perturbation that the PBHs induce on the distance between Earth and a given SSO,

$$\frac{\delta r}{r}(t) = \frac{|\tilde{\boldsymbol{r}}_{\rm earth}(t) - \tilde{\boldsymbol{r}}_{\rm SSO}(t)| - |\boldsymbol{r}_{\rm earth}(t) - \boldsymbol{r}_{\rm SSO}(t)|}{|\boldsymbol{r}_{\rm earth}(t) - \boldsymbol{r}_{\rm SSO}(t)|}\,, \tag{1}$$

where $\tilde{\boldsymbol{r}}$ indicates the position in a simulation with PBHs and $\boldsymbol{r}$ refers to the comparative simulation with a smooth DM halo. Naively, one might assume that the comparative simulation setup must be a solar system without DM. However, due to our numerical setup with a spherical PBH halo, centered around the barycenter of the solar system, there is a small additional acceleration for each SSO owing to the presence of DM,

$$\ddot{\boldsymbol{r}} = -\frac{4\pi G \rho_{\rm CDM}}{3}\boldsymbol{r}. \tag{2}$$

Adding this term in the comparative simulation is necessary, as we are interested in the perturbations induced by the PBHs and not in the numerical effect of the additional mass within the solar system. We want to mention that in this work we will focus on the perturbation of the magnitude of the vector,

$$\frac{|\delta \boldsymbol{r}|}{r}(t) = \frac{|(\tilde{\boldsymbol{r}}_{\rm earth}(t) - \tilde{\boldsymbol{r}}_{\rm SSO}(t)) - (\boldsymbol{r}_{\rm earth}(t) - \boldsymbol{r}_{\rm SSO}(t))|}{|\boldsymbol{r}_{\rm earth}(t) - \boldsymbol{r}_{\rm SSO}(t)|}\,, \tag{3}$$

which has the advantage of being strictly positive, whereas $\delta r/r$ typically oscillates between $-|\delta \boldsymbol{r}|/r$ and $|\delta \boldsymbol{r}|/r$ within one synodic orbital period of the SSO considered. While the quantity $|\delta \boldsymbol{r}|/r$ is more difficult to observe, it provides a reasonable estimate of the largest observable perturbation $\delta r/r$ per orbital period, as we show in Section 3.

To study the possibility of detecting or constraining PBHs, we compare our simulation results to observational data. We can relate the magnitude of the induced perturbations to the measurement accuracy for solar system bodies. Currently available data for various solar system bodies allow the detection of perturbations as small as $\delta r/r \sim 10^{-11}$. At the moment, the most precise data are obtained for the Moon ($\mathcal{O}$(1 mm)), by lunar laser ranging (J. B. R. Battat et al. 2023; N. R. Colmenares et al. 2023), and for Mercury ($\mathcal{O}$(0.7 m)) and Mars ($\mathcal{O}$(0.7 m)) through various orbiters (R. S. Park et al. 2021). While the SSOs have been monitored for a long time, submeter accuracy for Mars and Mercury has only been achieved in the past two decades. In this work we will focus on the distance between Earth and Mars, as it has been measured with high accuracy and is least susceptible to effects not considered in this work. These include, most notably, finite-size effects for the Moon and relativistic point-mass effects for Mercury (see T. X. Tran et al. 2024 for some estimates).

Finally, let us emphasize that our work does not aim to describe singular encounters with PBHs (for which we refer to B. Bertrand et al. 2023; Y.-L. Li et al. 2023; T. X. Tran et al. 2024) but instead

The Astrophysical Journal, 980:238 (11pp), 2025 February 20

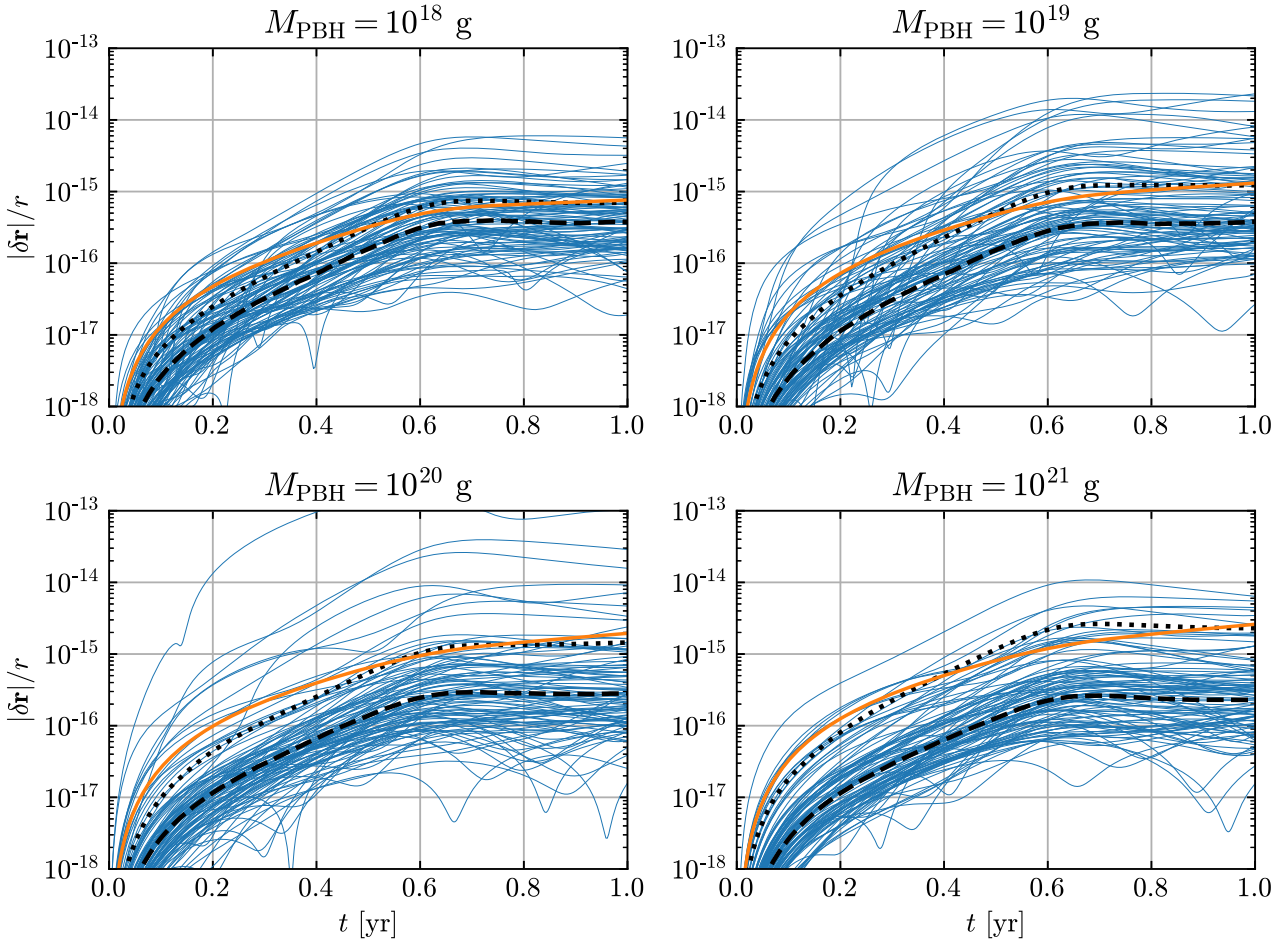

Figure 1. Perturbation of the vector between Earth and Mars, induced by PBHs for different values of their mass $M_{\rm PBH}$. Each blue line corresponds to one simulation run. We only show 100 simulation runs in each case to make comparisons easier and improve readability. The black dashed/dotted line indicates the median/mean value obtained from all simulations. The analytical prediction of the impulse model, given by Equation (8) for $b_{\rm max} = 3b_1$, is shown as an orange line.

focuses on the cumulative effect of a whole halo of PBHs on the dynamics of the solar system.

3. Results

Figure 1 shows the perturbations that are induced on the vector between Earth and Mars over a time span of $t = 1$ yr for $M_{\rm PBH} \in [10^{18}, 10^{19}, 10^{20}, 10^{21}]$ g. Due to the random initial conditions of the PBHs for each run, there is a significant variance in the value of $|\delta \boldsymbol{r}|/r$. The median value of the perturbations induced by a halo of PBHs grows over time and does not show a significant dependence on the black hole mass $M_{\rm PBH}$. The mean value of $|\delta \boldsymbol{r}|/r$ is higher than the median and increases slowly with $M_{\rm PBH}$. The growth of perturbations can be understood using the analytical model derived in Section 4.1 and refined in Section 4.3, which is based on the impulse approximation. The predicted value for the mean perturbation strength is shown in Figure 1 and agrees well with the simulation results.

In general, the model predicts a logarithmic dependence on the black hole mass when the distance b to the nearest PBH is much larger than the distance r to the respective SSO. In contrast, in the limit $b \ll r$ we expect a power-law dependence $|\delta \boldsymbol{r}|/r \sim \sqrt{M_{\rm PBH}}$. To test this, we show the mean perturbation of the vector between Earth and each planet at $t = 1$ yr in the left panel of Figure 2, together with the prediction from the analytical model. Indeed, the perturbation strength depends more strongly on $M_{\rm PBH}$ in the limit $b \ll r$. Overall, the predictions from the analytical model are within a factor of two of the simulation results. It is noticeable that the agreement is better for the inner planets compared to the outer ones. We note that the mean perturbation strength that we obtain from the simulations is subject to some statistical uncertainty because of the finite number of simulations that have been performed. We discuss this in more detail in Section 4.2.

For a subset of all simulations performed we also evaluate the distance of each SSO to the closest PBH. In the right panel of Figure 2 the perturbation strength $|\delta \boldsymbol{r}|/r$ at $t = 1$ yr is plotted against the smallest distance $b_{\rm min}$ of Mars and Earth to a PBH within the simulation run. The dashed lines correspond to an analytical estimate of the perturbation by a single encounter with an impact parameter $b_{\rm min}$, given by Equation (7). The good agreement demonstrates that the perturbation strength is mostly determined by the closest encounter. Note that for $M_{\rm PBH} = 10^{18}$ g the typical distance to the nearest PBH is on the order of $b \sim 1$ au.

A statistical analysis of the perturbations is presented in Figure 3, where we show the probability distribution $p(|\delta \boldsymbol{r}|/r)$ of the perturbations of the Earth–Mars vector at $t = 1$ yr in the left panel. The functions are obtained by a Gaussian kernel

The Astrophysical Journal, 980:238 (11pp), 2025 February 20 Thoss & Burkert

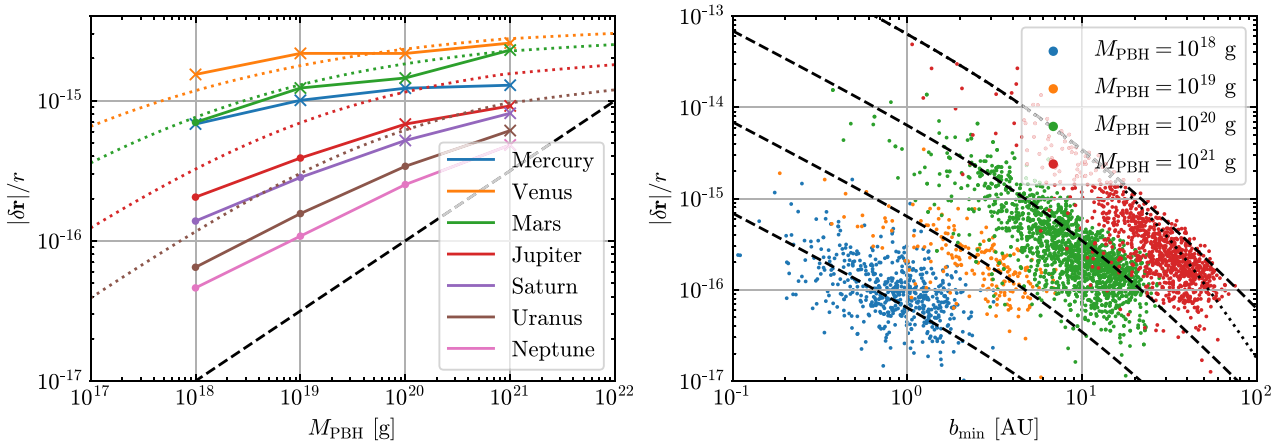

Figure 2. Left: mean perturbation strength $|\delta \boldsymbol{r}|/r$ at $t = 1$ yr as a function of $M_{\rm PBH}$ for the vector between Earth and each planet. The crosses indicate that the distance b to the closest PBH is larger than the distance r between Earth and the respective planet in that case, whereas the points indicate that $b < r$. Colored dotted lines show the analytical prediction from Equation (17) for selected planets. The black dashed line indicates a power-law slope of 0.5. Right: perturbation strength $|\delta \boldsymbol{r}|/r$ of the Earth–Mars vector, evaluated at $t = 1.0$ yr, vs. the minimum impact parameter $b_{\rm min}$ observed within the simulation period. The black dashed lines correspond to Equation (7). The dotted line for $M_{\rm PBH} = 10^{21}$ g takes into account the finite distance traveled by the PBHs within the simulation time and is given by Equation (14).

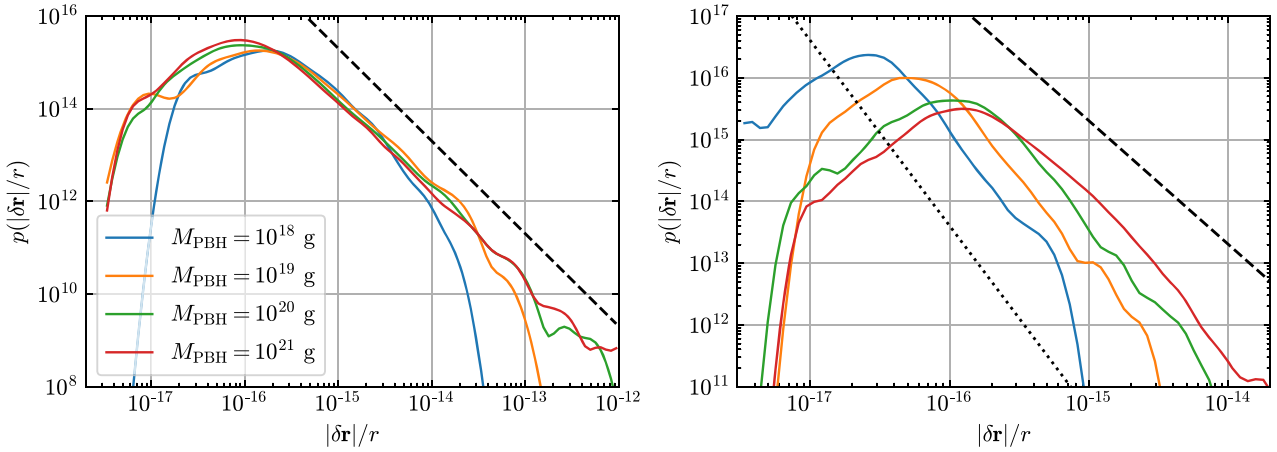

Figure 3. Left: probability distribution function of the perturbation $|\delta \boldsymbol{r}|/r$ of the Earth–Mars vector, evaluated at $t = 1.0$ yr for different values of the PBH mass $M_{\rm PBH}$. The black dashed line indicates a power law with slope of -2. Right: probability distribution function of the perturbation $|\delta \boldsymbol{r}|/r$ of the Earth–Neptune vector, evaluated at $t = 1.0$ yr for different values of the PBH mass $M_{\rm PBH}$. The black dashed and dotted lines indicate a power law with slope of -2 and -3, respectively.

density estimate. Interestingly, there is no strong dependence on the PBH mass, and for $M_{\rm PBH} \geqslant 10^{19}$ g we observe a power-law tail with a slope of -2. As we show in Section 4.2, a power-law slope of -2 is expected if the distance to the nearest PBH b is much larger than the distance r to the respective SSO, here the Earth–Mars distance. This is the case for $M_{\rm PBH} \geqslant 10^{19}$ g (see the right panel of Figure 2). In contrast, if $b \ll r$, in which case there will be many PBHs between Earth and the respective SSO, then our model predicts a slope of -3. To study this limit, we show the probability distribution $p(|\delta \boldsymbol{r}|/r)$ of the perturbations of the Earth–Neptune vector at $t = 1$ yr in the right panel of Figure 3. As the distance between Earth and Neptune is much larger compared to Earth–Mars, a slope of -3 is expected for $M_{\rm PBH} \leqslant 10^{20}$ g (see the right panel of Figure 2), which is indeed what we find. Note that we observe a stronger mass dependence in that case, with an increase in perturbation strength $|\delta \boldsymbol{r}|/r$ toward larger values of $M_{\rm PBH}$. This is consistent with our analytical model, which predicts $|\delta \boldsymbol{r}|/r \sim \sqrt{M_{\rm PBH}}$ in the limit $b \ll r$.

Finally, Figure 4 presents the results from 500 simulations performed over a longer time span of 20 yr for $M_{\rm PBH} = 10^{20}$ g. In the left panel we display the perturbation $|\delta \boldsymbol{r}|/r$ of the vector between Earth and Mars. A notable difference to Figure 1 is that the perturbations oscillate with a period of roughly 2 yr, which corresponds to the synodic orbital period of Mars. We add an estimate for a 3σ detection limit by assuming that $\sigma_r \approx 70$ cm for the Earth–Mars distance (R. S. Park et al. 2021). Out of all 500 simulation runs, only 4 exceed this limit at least once within 20 yr, implying a $\sim$1% chance of detection with a confidence level of 3σ.

In the right panel of Figure 4 we show the mean perturbation strength $|\delta \boldsymbol{r}|/r$ of all simulation runs for the vector between Earth and each planet. Notably, $|\delta \boldsymbol{r}|/r$ is very similar for the inner planets, while it decreases for the outer planets as the distance to Earth grows. Since the smallest typical impact parameter for $M_{\rm PBH} = 10^{20}$ g and $t = 20$ yr is $b_1 \approx 3.4$ au (see Equation (9)), we are in the limit $b > r$ for the inner planets and $b < r$ for the outer planets. The analytical model derived in Section 4.1 predicts a constant value of $|\delta \boldsymbol{r}|/r$ in the case $b > r$ and $|\delta \boldsymbol{r}|/r \sim 1/r$ otherwise. Therefore, the lower perturbation strength for the outer planets is expected.

The Astrophysical Journal, 980:238 (11pp), 2025 February 20

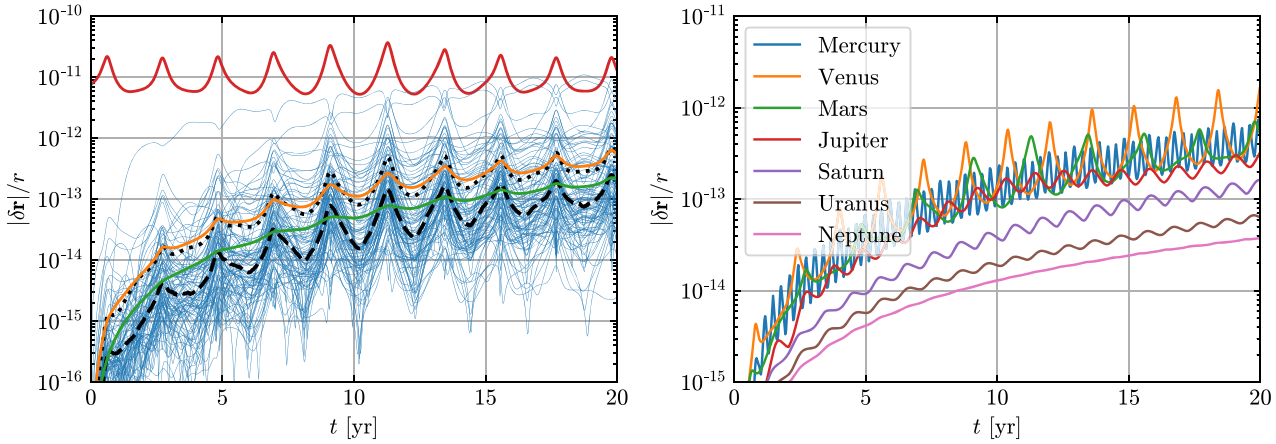

Figure 4. Left: perturbation of the vector between Earth and Mars induced by PBHs for $M_{\rm PBH} = 10^{20}$ g as a function of time. Each blue line corresponds to one simulation run. We only show 100 simulation runs to improve readability. The black dashed/dotted line indicates the median/mean value obtained from all 500 simulations. The analytical prediction of the impulse model, given by Equation (8) for $b_{\rm max} = 3b_1$, is shown as an orange line. The green line shows a model for the median perturbation strength, given by Equation (19). The red line is an estimate of the 3σ observational detection limit. Right: mean perturbation strength $|\delta \mathbf{r}|/r$ as a function of time for the vector between Earth and each planet.

In the results presented in this study, we analyze the perturbation of the vector $|\delta \mathbf{r}|$ between Earth and other SSOs. However, only the perturbation of the distance δr can be observed with high accuracy. We argue that this should not affect our results, as δr typically oscillates between $-|\delta \mathbf{r}|$ and $|\delta \mathbf{r}|$, and thus our results can be regarded as an upper bound of the observable perturbation since $|\delta r| \leqslant |\delta \mathbf{r}|$ by definition. To test this statement, we compare the values of δr and $\delta \mathbf{r}$ for the Earth–Mars pair. The data from the last synodic orbital period from the 500 simulations performed over a time span of $t = 20$ yr are being used. We find that 87% of the simulations reach $|\delta r| > |\delta \mathbf{r}|/2$ at least once and 72% of the simulations reach $|\delta r| > |\delta \mathbf{r}|/2$ during at least 75% of the respective time span. In addition, 50% of the simulations reach $|\delta r| > 0.9|\delta \mathbf{r}|$ at least once within the orbital period. This justifies our approach of studying the perturbation of the vector $\delta \mathbf{r}$ as a reasonable approximation of the largest observable perturbation of the distance δr.

4. Discussion

4.1. Impulse Model

The results obtained from our simulations show that the perturbations induced by a halo of PBHs grow over time, to a median value of $|\delta \mathbf{r}|/r \sim 10^{-13}$ within 20 yr. To provide some analytical understanding of our results, we make use of the impulse approximation (J. Binney & S. Tremaine 2008) to compute the velocity change induced on an SSO by the gravitational pull from a PBH. It is assumed that the black hole moves in a straight line with an impact parameter (distance of closest approach) b. The motion of the SSO itself is neglected, as it is assumed that its orbital period is much longer than the timescale of the flyby. These assumptions are justified owing to the high velocities of the PBHs with $v_{\rm PBH} \sim 280\,{\rm km\,s^{-1}}$. The velocity change induced on an SSO in the direction perpendicular to the motion of the PBH is

$$\Delta v \approx \int_{-\infty}^{\infty} dt \frac{{\rm GM_{PBH}} b}{(b^2 + (v_{\rm PBH} t)^2)^{3/2}} = \frac{2{\rm GM_{PBH}}}{b v_{\rm PBH}}\,. \tag{4}$$

Note that in most cases that we discuss one has $v_{\rm PBH} t \gg b$, and thus the integration boundaries can safely be taken to infinity. This is discussed in more detail in Section 4.3. In the following, we assume that all PBHs move perpendicular to the ecliptic plane, which is a first-order approximation that greatly simplifies our calculations and is also motivated by our initial conditions (see Section 2). This implies that the point of closest approach is identical for all bodies in the solar system and will be reached when the PBH crosses the ecliptic plane.

Let us first discuss the case where the impact parameter b is much larger than the distance r between Earth and another SSO (in our case Mars). Then, Earth and the other SSO will be perturbed by the same amount Δv but in slightly different directions, with an angle between $\Delta \boldsymbol{v}_{\rm earth}$ and $\Delta \boldsymbol{v}_{\rm SSO}$ of $\alpha \approx r/b$. This means

$$|\delta \mathbf{r}| \approx |\Delta \boldsymbol{v}_{\rm earth} - \Delta \boldsymbol{v}_{\rm SSO}| t \approx \frac{\Delta v r t}{b} \approx \frac{2{\rm GM_{PBH}} r t}{b^2 v_{\rm PBH}}\,. \tag{5}$$

If, on the other hand, $b \ll r$, we only need to consider the velocity change of the body closest to the PBH,

$$|\delta \mathbf{r}| \approx |\Delta \boldsymbol{v}_{\rm earth} - \Delta \boldsymbol{v}_{\rm SSO}| t \approx \Delta v t = \frac{2{\rm GM_{PBH}} t}{b v_{\rm PBH}}\,. \tag{6}$$

In the intermediate case, the perturbation strength depends on the specific geometry. Numerically, by averaging over all possible geometries for a fixed b, we find that

$$\frac{|\delta \mathbf{r}|}{r} \approx \frac{2{\rm GM_{PBH}} t}{(br + b^2) v_{\rm PBH}} \tag{7}$$

provides a reasonable fit to the numerical data, with a maximum deviation of a factor of 2.2 at $b = r/2$. For the mean perturbation strength $\langle |\delta \mathbf{r}|/r \rangle$ that we discuss below the difference is at most 20%. The numerical result is discussed further in the Appendix.

So far, we have considered the perturbation from a single encounter with a PBH. For a DM halo composed of PBHs the rate of encounters in the solar system will be $\Gamma = (\sigma/m)\rho v = (\pi b^2/M_{\rm PBH})\rho_{\rm CDM} v_{\rm PBH}$. This means that the number of scattering events per interval of b is $dN/db = (2\pi b/M_{\rm PBH})\rho_{\rm CDM} v_{\rm PBH} t$.

From this we can obtain the perturbation strength,

$$\left\langle \frac{|\delta \boldsymbol{r}|}{r} \right\rangle \approx \int_0^{b_{\max}} db\, \frac{dN}{db} \frac{2GM_{\rm PBH} t}{(br + b^2) v_{\rm PBH}} = 4\pi G \rho_{\rm CDM} t^2 \log(1 + b_{\max}/r)\,. \quad (8)$$

Before we discuss this result in more detail, we have to specify the upper integration bound $b_{\max}$. In principle, the impact parameter b can be as large as the box size $R_{\rm box}$ of our simulation. However, with increasing distance the number of PBH encounters grows until they will no longer cause individual perturbations but rather behave as a spherically symmetric mass distribution. Let us define b_1 as the impact parameter for which we expect one scattering event within the time t:

$$b_1 = \sqrt{\frac{M_{\rm PBH}}{\pi \rho_{\rm CDM} v_{\rm PBH} t}}\,. \quad (9)$$

Accordingly, there are N^2 encounters with an impact parameter $b \leqslant N b_1$ within the same time period. However, as N grows, these perturbations will begin to cancel each other out owing to the random orientation of $\delta \boldsymbol{v}$. As can be seen in Figures 1 and 4 (left panel), the choice $b_{\max} = 3b_1$ provides a good fit to the actual mean perturbation, which suggests that the perturbation strength is well determined by the influence of the closest $N \sim \mathcal{O}(10)$ PBHs. Notably, if we set $b_{\max} = R_{\rm box}$, Equation (8) predicts a mean perturbation strength that is up to an order of magnitude larger than the simulation results and does not recover the correct dependence on $M_{\rm PBH}$. This also demonstrates that our choice of $R_{\rm box}$ has no significant effect on the outcome of the simulation.

The fact that the perturbations are dominated by the closest encounter is also demonstrated in the right panel of Figure 2, where we plot the perturbation strength $|\delta \boldsymbol{r}|/r$ at $t = 1$ yr against the smallest impact parameter within the simulation run. The observed values agree reasonably well with Equation (7), which is displayed as dashed lines. Note that here we have assumed a singular encounter with a PBH that moves perpendicular to the ecliptic plane. Therefore, some deviation from the analytical estimates is expected in the more complex simulation environment. In addition, it is expected that other close encounters will also contribute to the perturbation strength. Note that the approximation of infinite integration boundaries in Equation (4) breaks down for large PBH masses, which explains part of the offset observed for $M_{\rm PBH} = 10^{21}$ g. This will be discussed in more detail in Section 4.3.

Importantly, Equation (8) provides a simple explanation for the observed weak dependence of the perturbation strength $|\delta \boldsymbol{r}|/r$ on the black hole mass, as it predicts only a logarithmic dependence as long as $b_{\max} \gg r$. The underlying reason is that the strength of the gravitational force ($\sim M_{\rm PBH}$) is counteracted by the rate of encounters ($\sim 1/M_{\rm PBH}$). However, if PBHs are sufficiently light (or t sufficiently long), then we are in the limit $b_{\max} \ll r$ (assuming again that $b_{\max} \sim \mathcal{O}(b_1)$ as we argued above) and thus $|\delta \boldsymbol{r}|/r \sim \log(1 + b_{\max}/r) \approx b_{\max}/r \sim \sqrt{M_{\rm PBH}}$. Indeed, the left panel of Figure 2 shows that the mean perturbation strength depends more strongly on $M_{\rm PBH}$ in the limit $b_{\max} \ll r$, in good agreement with our analytical model that is also displayed in the figure. The power-law slope appears to be more shallow than expected, but simulations with $M_{\rm PBH} < 10^{18}$ g are required to investigate this in more detail. Equation (8) also explains the lower values of $|\delta \boldsymbol{r}|/r$ for the outer planets in the right panel of Figure 4, as we have $b_{\max} < r$ and thus $|\delta \boldsymbol{r}|/r \sim 1/r$ there. Finally, we want to emphasize that the decreasing strength of the perturbations at low PBH masses provides consistency, as they should disappear as $M_{\rm PBH} \to 0$ ($\rho_{\rm CDM} = \rho_{\rm PBH} = $ const.) and a smooth DM component is obtained.

4.2. Statistics of the Perturbations

The impulse model derived in the previous section allows us to interpret the results obtained for the probability distribution $p(|\delta \boldsymbol{r}|/r)$. The homogeneous distribution of PBHs implies that the distribution of impact parameters is given by $p(b) \sim b$. In the case where $b \gg r$, Equation (5) can be used to obtain

$$p(|\delta \boldsymbol{r}|/r) = p(b) \left| \frac{db}{d|\delta \boldsymbol{r}|/r} \right| \sim (|\delta \boldsymbol{r}|/r)^{-2}\,. \quad (10)$$

In contrast, for $b \ll r$ it follows from Equation (6) that

$$p(|\delta \boldsymbol{r}|/r) = p(b) \left| \frac{db}{d|\delta \boldsymbol{r}|/r} \right| \sim (|\delta \boldsymbol{r}|/r)^{-3}\,. \quad (11)$$

The predicted power-law slopes of -2 and -3 in the respective limits of $b < r$ and $b > r$ are consistent with the data shown in Figure 3.

The slope of the distribution has notable consequences for the robustness of the mean perturbation strength that we obtain from the simulation data. In the case of Equation (10), the mean perturbation strength is logarithmically divergent, whereas it quickly converges for the case of Equation (11). Indeed, for simulations with $b_1 < r$ we find that the estimated uncertainty of the mean $\sigma/\sqrt{N}$, where N is the number of simulation runs, is very low. In principle, by running enough simulations, the limit $b < r$ can be properly sampled for any value of $M_{\rm PBH}$. However, for large PBH masses this becomes computationally very expensive for the Earth–Mars distance. Nevertheless, we can estimate the uncertainty in the mean perturbation strength by computing the probability distribution $p(|\delta \boldsymbol{r}|/r)$ from Equation (7) using $p(b) \sim b$ and fitting it to the tail of the distributions obtained from simulation data. We can then compute the mean of a combined distribution, where we take the simulation data for the range of $|\delta \boldsymbol{r}|/r$ that are well sampled and the modeled tail for larger perturbations. The mean perturbation strength that we obtain in this way only differs by at most a factor of two from that obtained using only simulation data.

4.3. Extrapolating Our Results

Our simulations help us to investigate perturbations induced by PBHs for a certain range of masses $M_{\rm PBH}$ and timescales t. We find that the dependence on the mass of the PBH is logarithmic as long as $b_{\max} \sim b_1 \gg r$ and that, for the parameters that we studied, the results are well described by the impulse model, discussed in Section 4.1. Therefore, we can use our analytical model to extend the study to longer timescales and to a wider range of PBH masses that we could not investigate so far owing to the computational expense of running a large number of additional simulations. However, it is necessary to make some modifications to the impulse model. The reason is that for large PBH masses or on small timescales

the PBHs will not act as a stream of particles but rather as a cluster with negligible movement. More precisely, the integration boundaries in Equation (4) cannot be taken to infinity if $v_{\rm PBH}t \gg b$ is not valid.

Taking into account the finite travel distance of the PBH, the velocity change induced on an SSO is given by

$$\Delta v(t) \approx \int_{-t/2}^{t/2} dt' \frac{\mathrm{GM_{PBH}} b}{(b^2 + (v_{\rm PBH}t')^2)^{3/2}} = \frac{2\mathrm{GM_{PBH}}}{b v_{\rm PBH}} \frac{\frac{v_{\rm PBH}t}{2b}}{\sqrt{1 + \left(\frac{v_{\rm PBH}t}{2b}\right)^2}}, \quad (12)$$

which reduces to Equation (4) for $v_{\rm PBH}t \gg b$. The displacement of an SSO $\Delta r(t)$ can be computed by integrating Equation (12) with respect to to time:

$$\Delta r(t) \approx \int_0^t dt' \frac{2\mathrm{GM_{PBH}}}{b v_{\rm PBH}} \frac{\frac{v_{\rm PBH}t'}{2b}}{\sqrt{1 + \left(\frac{v_{\rm PBH}t'}{2b}\right)^2}} = \frac{4\mathrm{GM_{PBH}}}{v_{\rm PBH}^2} \left(\sqrt{1 + \left(\frac{v_{\rm PBH}t}{2b}\right)^2} - 1 \right). \quad (13)$$

To obtain an explicit expression for the perturbation strength, we must take into account that for $b \gg r$ one has $|\delta \boldsymbol{r}| \approx r/b\, \Delta r$, as we discussed in Section 4.1. Equivalently to Equation (7), a general expression can be used to good approximation. It then follows that the perturbation strength from a single PBH is given by

$$\frac{|\delta \boldsymbol{r}|}{r} \approx \frac{4GM_{\rm PBH}}{(r+b)v_{\rm PBH}^2} \left(\sqrt{1 + \left(\frac{v_{\rm PBH}t}{2b}\right)^2} - 1 \right). \quad (14)$$

In the limit $v_{\rm PBH}t \gg b$ this expression reduces to Equation (7), as expected. For $v_{\rm PBH}t \ll b$ we have

$$\frac{|\delta \boldsymbol{r}|}{r} \approx \frac{\mathrm{GM_{PBH}}t^2}{2(rb^2 + b^3)}. \quad (15)$$

To demonstrate the effect of this modification, we show this improved model as a dotted line for $M_{\rm PBH} = 10^{21}$ g in the right panel of Figure 2. Taking into account the finite travel distance leads to better agreement with the simulation data and is important in the limit $v_{\rm PBH}t \ll b$.

For $v_{\rm PBH}t \gg b$ the PBHs behave like a stream of particles with $dN/db = (2\pi b/M_{\rm PBH})\rho_{\rm CDM} v_{\rm PBH}t$. On the other hand, if $v_{\rm PBH}t \ll b$, the PBHs behave as a cluster with negligible movement and the distribution of their distances is given by $dN/db = 4\pi b^2 \rho_{\rm CDM}/M_{\rm PBH}$. By studying the numerical distribution dN/db from our simulation data, we found that

$$\frac{dN}{db} \approx \frac{2\pi b \rho_{\rm CDM}}{M_{\rm PBH}} (v_{\rm PBH}t + 2b) \quad (16)$$

provides a good approximation in the general case. Using this, the mean perturbation strength is given by

$$\left\langle \frac{|\delta \boldsymbol{r}|}{r} \right\rangle = \int_0^{b_{\max}} db\, \frac{dN}{db} \frac{|\delta \mathbf{r}|}{r} \approx \int_0^{b_{\max}} db\, \frac{8\pi \rho_{\rm CDM} G b (v_{\rm PBH}t + 2b)}{(r+b)v_{\rm PBH}^2} \left(\sqrt{1 + \left(\frac{v_{\rm PBH}t}{2b}\right)^2} - 1 \right). \quad (17)$$

To include only the closest $\mathcal{O}(10)$ encounters, we set $b_{\max} = 3b_1$ with b_1 now given by

$$b_1 = \min \left\{ \left(\frac{M_{\rm PBH}}{\pi \rho_{\rm CDM} v_{\rm PBH}t} \right)^{1/2}, \left(\frac{3M_{\rm PBH}}{4\pi \rho_{\rm CDM}} \right)^{1/3} \right\}. \quad (18)$$

We display the mean perturbation strength that follows from Equation (17) in the left panel of Figure 2. In the respective mass range, the difference to Equation (8) is insignificant and below the accuracy of the model and the simulation results. This is also the case for Figure 1 and the left panel of Figure 4, where the analytical model is shown as well. Importantly, for $v_{\rm PBH}t \ll b$, Equation (17) converges to $|\delta \boldsymbol{r}|/r = 2\pi G \rho_{\rm CDM} t^2 \log(1 + b_{\max}/r)$, a factor of two smaller than Equation (8). This demonstrates that Equation (8) provides a reasonable estimate of the mean perturbation strength even in the limit $v_{\rm PBH}t \ll b$.

4.4. Prospects for Detecting PBHs

The quantity of interest for detecting PBHs is the ratio between the perturbations $|\delta \boldsymbol{r}|$ that they induce and the observational residual σ_r in the distance between Earth and a given SSO. In Section 4.2 we found that the distribution of perturbations $p(|\delta \boldsymbol{r}|/r)$ is highly skewed. This implies that the mean perturbation strength is not a good measure of detectability, as the likelihood to observe it can be low. Of the 500 simulations that have been performed for $t = 20$ yr, 112 reach a perturbation strength $|\delta \boldsymbol{r}|/r$ that is larger than the mean $\langle |\delta \boldsymbol{r}|/r \rangle$, a fraction of $\sim$27%. Therefore, it is more useful to compare the median perturbation strength to the observational residual. If $|\delta \boldsymbol{r}|_{\rm median} > \alpha \sigma_r$, then there is 50% chance for an observation with a signal-to-noise ratio (SNR) of α. In Sections 4.1 and 4.3 we have derived the impulse model to describe the mean perturbation strength. To a good approximation, the median perturbation strength can be estimated by setting the minimum impact parameter to b_1 Equation (9) when performing the integration over b,

$$\left(\frac{|\delta \boldsymbol{r}|}{r} \right)_{\rm median} \approx \int_{b_1}^{b_{\max}} db\, \frac{8\pi \rho_{\rm CDM} G b (v_{\rm PBH}t + 2b)}{(r+b)v_{\rm PBH}^2} \times \left(\sqrt{1 + \left(\frac{v_{\rm PBH}t}{2b}\right)^2} - 1 \right). \quad (19)$$

The reason is that the median perturbation is dominated by the smallest "typical" impact parameter b_1, whereas the mean takes into account smaller values of b that can occur rarely and is thus skewed to larger values. We demonstrate the validity of this assumption in the left panel of Figure 4, where we show

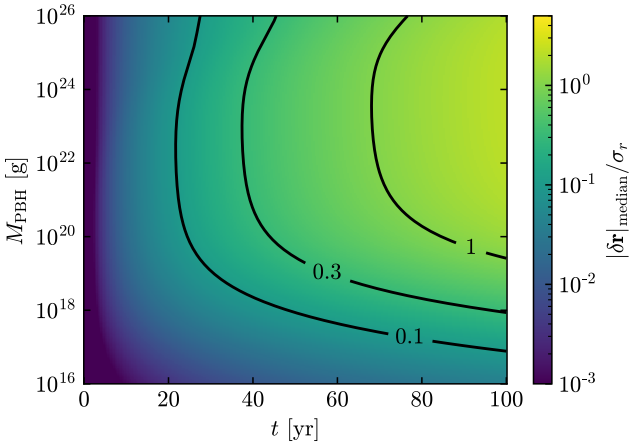

Figure 5. Estimated median SNR $|\delta \boldsymbol{r}|_{\rm median}/\sigma_r$ for the observation of the Earth–Mars distance as a function of the PBH mass and the timescale, assuming $\sigma_r = 70$ cm. Contour levels are drawn for several values of the SNR. The results are obtained using the impulse model, presented in Section 4.1 and refined in Section 4.3.

the result from Equation (19) as the green line, which agrees well with the median from the simulation data (black dashed line).

Figure 5 presents the SNR $|\delta \boldsymbol{r}|_{\rm median}/\sigma_r$ for the Earth–Mars distance using Equation (8) and $b_{\rm max} = 3b_1$, although the results are not very sensitive to the precise value of $b_{\rm max}$ as discussed in Section 4.1. A value of $\sigma_r = 70$ cm is assumed for the residual of the Earth–Mars distance (R. S. Park et al. 2021). Note that the dependence of $|\delta \boldsymbol{r}|_{\rm median}$ on $M_{\rm PBH}$ is weak for $M_{\rm PBH} \gtrsim 10^{20}$ g and the timescales considered here. At lower masses, when $b_{\rm max} \ll r$, one has $|\delta \boldsymbol{r}|_{\rm median} \sim \sqrt{M_{\rm PBH}}$ and the perturbation strength decreases. In the limit $r \ll vt \ll b$ Equation (19) becomes independent of the black hole mass and converges to $|\delta \boldsymbol{r}|_{\rm median}/r = 2\pi G \rho_{\rm CDM} t^2 \log(b_{\rm max}/b_1) \approx 3 \times 10^{-16} (t/1\ {\rm yr})^2$. For $t = 20$ yr this limit is reached for $M_{\rm PBH} \gg 10^{25}$ g, and for $t = 1$ yr the median perturbation strength becomes constant for $M_{\rm PBH} \gg 10^{21}$ g. To test this, we have performed 9000 simulation runs for $M_{\rm PBH} \in [10^{24}, 10^{25}]$ g with $R_{\rm box} \in [4500, 10{,}000]$ au. The median perturbation strength that we obtain in both simulations is almost identical and agrees within a factor of two with the prediction from the model for all planets.

As a conservative estimate, we regard the perturbations induced by the halo of PBHs as a random signal, and thus an SNR greater than 1 is required for detection. We find that a significant detection ($|\delta \boldsymbol{r}|_{\rm median}/\sigma_r \gtrsim 3$) cannot be reached with 100 yr of observational data. If the uncertainty in the distance σ_r decreases by a factor of 30, then only around 20–30 yr of data are required to detect PBHs with a mass $M_{\rm PBH} > 10^{19}$ g with 3σ confidence (this corresponds to the 0.1 contour in Figure 5). Note that $|\delta \boldsymbol{r}| \sim \rho_{\rm CDM}$ and hence the detection window becomes larger if the local DM density is greater than the assumed value of $\rho_{\rm CDM} = 7 \times 10^{-25}$ g cm^{-3}. We want to emphasize that the results presented in Figure 5 are based on the analytical impulse model and for particular parameters one should perform a set of numerical simulations to obtain more accurate results. It would also be interesting to study the probability of detection for a given SNR as a function of $M_{\rm PBH}$ and t. However, this requires a better understanding of $p(|\delta \boldsymbol{r}|/r)$ that is beyond the scope of this work.

So far, we have treated the perturbations as a random signal and thus required an SNR > 1 for detection. However, the perturbations induced by the encounters of PBHs likely have certain characteristics that can be exploited to make predictions of the expected signal $\delta r(t)$. In that case, one can attempt to use template matching techniques in order to detect perturbations with an amplitude well below the noise level σ_r. This was studied by T. X. Tran et al. (2024), who found that there will be a sizable number of detectable encounters if the extraction of signals with an SNR well below 10^{-2} is achieved. A possible caveat regarding the detection of PBHs are potential degeneracies between the perturbations induced by the PBHs and other gravitational effects in the solar system. Accurate models of solar system ephemerides are obtained by iterating over a large number of free parameters, including the physical parameters of all SSOs. To assess the prospects of detecting PBHs, one has to study the degree of degeneracy between the perturbations that they induce and a change in other parameters of these models.

4.5. Poissonian Fluctuations

In our work, we study the cumulative gravitational effect of PBHs on the orbits of SSOs. We find that the perturbations induced by the black holes are dominated by the closest encounter (see Section 4.1). This is in contrast to the work by A. Loeb (2024), which studies the influence of Poissonian fluctuations in the PBH density. If the DM is composed of asteroid-mass black holes, then their number within the solar system can undergo sizable Poisson fluctuations. A. Loeb (2024) considered the rate of change in the total mass of PBHs within a distance R from the Sun, given by

$$\delta \dot{M} = 1.9 \times 10^{-13} \left(\frac{M_{\rm PBH}}{10^{20}\ {\rm g}}\right)^{1/2} \left(\frac{R}{50\ {\rm au}}\right)^{1/2} M_\odot\ {\rm yr}^{-1}. \quad (20)$$

In his work it is then assumed that such fluctuations would induce similar effects to those if a point mass in the center of the solar system were to change its mass with the same rate, effectively changing the solar mass by a small amount. For $R = 50$ au and $M_{\rm PBH} \in [6 \times 10^{18}, 10^{22}]$ g, this would lead to a rate $\delta \dot{M}$ larger than the constraint on $\dot{M}_{\rm sol}$ by E. V. Pitjeva et al. (2021), and thus he concluded that PBHs in this mass range cannot make up the entire DM.

It is important to note that these Poissonian fluctuations can only occur if there is at least one PBH in the volume of interest. For Mars this requires $M_{\rm PBH} \lesssim 3 \times 10^{16}$ g to have at least one PBH inside its orbit. At these low PBH masses the fluctuations that follow from Equation (20) are well below the observational constraint from E. V. Pitjeva et al. (2021) and thus cannot be used to rule out PBHs as DM. For the outer planets, the fluctuations from Equation (20) can exceed the constraint on $\dot{M}_{\rm sol}$, as, e.g., for Neptune this requires $M \lesssim 3 \times 10^{20}$ g, which implies a value of $\delta \dot{M} < 2.5 \times 10^{-13}\ M_\odot\ {\rm yr}^{-1}$. However, it is not justified to apply the constraint by E. V. Pitjeva et al. (2021) for the outer planets in isolation, as it was derived from the entire set of solar system data, assuming no dependence of $\dot{M}_{\rm sol}$ on r, and is dominated by the effect of fluctuations on the inner planets. On the one hand, this is because the observational data of the inner planets currently have the highest accuracy. On the other hand, a change in the solar mass has a much stronger effect on the inner planets compared to the outer ones, as the additional force from the change in the solar mass mass will be proportional to $\delta \dot{M}/r^2$. In essence, an observational constraint on $\dot{M}_{\rm sol}$ at the orbital distance of Neptune

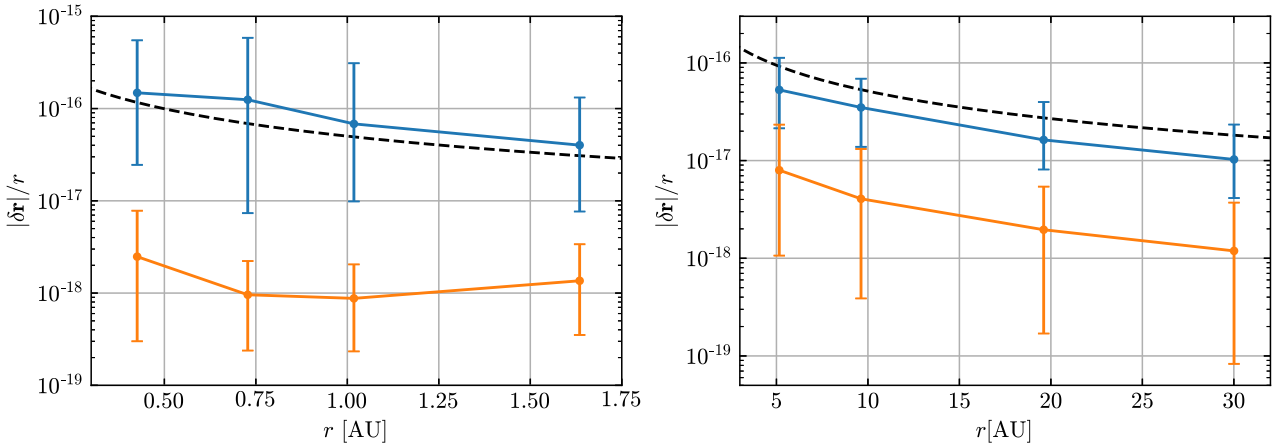

Figure 6. Perturbation of the vector between the Sun and the planets in the solar system. The left panel shows the results for a simulation of the inner solar system with $M_{\rm PBH} = 3 \times 10^{13}$ g at $t = 3$ yr. In the right panel, we present the results for the outer solar system with $M_{\rm PBH} = 10^{17}$ g at $t = 1$ yr. Each data point corresponds to the median perturbation of 100 simulation runs. The error bars indicate the range that includes 90% of the simulation results. The blue points correspond to our usual simulation setup. In orange, we show the results of simulations where the solar mass is changing according to the Poisson fluctuations of PBHs $\delta \dot{M}$, as explained in Section 4.5. The black dashed line is the analytical prediction of the median perturbation strength from the impulse model, according to Equation (19).

would be orders of magnitude weaker than the limit that A. Loeb (2024) is using. Note that similar remarks were already made by J. M. Cline (2024).

For the reasons stated above, one cannot rule out PBHs based on the Poisson fluctuation in their number density. Nevertheless, it remains of interest to compare the effects of these fluctuations to those from individual encounters. To investigate this, we perform a simulation where, at each time step and for each planet, we count the number of PBHs $N_{\rm PBH}(t, r_i)$ within the orbital distance r_i of the planet i to the Sun. We then set the solar mass for each planet to $M_{\rm sol,i}(t) = M_\odot + M_{\rm PBH} N_{\rm PBH}(t, r_i)$. The PBHs do not exert any gravitational force on the solar system bodies in this simulation, acting only through the fluctuations of the solar mass. There needs to be at least one PBH inside the orbit of a planet to observe any fluctuations. For Mercury this implies $M_{\rm PBH} \lesssim 4 \times 10^{14}$ g, which would lead to a computationally infeasible number of PBHs within the entire solar system. We therefore study the inner and outer planets in two separate simulations. For the simulation containing the inner planets and Earth's Moon we choose $M_{\rm PBH} = 3 \times 10^{13}$ g and $L_{\rm box} = 10$ au, whereas we take $M_{\rm PBH} = 10^{17}$ g and $L_{\rm box} = 150$ au for the outer planets. This means that there will be on average $\langle N_{\rm PBH} \rangle \in [13, 120, 347, 858]$ PBHs inside the orbits of Mercury, Venus, Earth, and Mars. For Jupiter, Saturn, Uranus, and Neptune there will be $\langle N_{\rm PBH} \rangle \in [12, 89, 737, 2622]$ PBHs inside their orbits. In Figure 6 we display the perturbations of the vector between the Sun and each planet. The left panel shows the results for the inner solar system at $t = 3$ yr, whereas the simulations for the outer planets are shown in the right panel for $t = 1$ yr. Blue points indicate the median value for simulations where we include the gravity of the PBHs, whereas the orange points show the results for the simulations with a fluctuating solar mass. The perturbations induced by PBHs on the orbit of the planets are roughly an order of magnitude larger compared to the effect of Poisson fluctuations of the solar mass. Based on these results alone, we cannot distinguish whether the disagreement is because the Poisson fluctuations are a small contribution to the total effect of PBHs in the solar system or because one cannot treat the Poisson fluctuations of the PBH number density as a change in the solar mass. However, the analytical model introduced in Section 4.1 suggests that the perturbations induced by PBHs can be predicted with good accuracy by taking into account the closest encounters. We display the model for the median perturbation strength from Equation (19) as a dashed line in Figure 6, and it shows good agreement for $b_{\rm max} = 3b_1$. This suggests that Poisson fluctuations likely play only a minor role in the overall gravitational effect of PBHs on the solar system bodies.

4.6. Limitations of This Work

Our simulations enable us to make general statements about the strength and evolution of perturbations induced by PBHs and to study whether they exceed current detection limits. However, in order to actually detect individual PBHs, one needs a precise model for solar system ephemerides that includes more solar system bodies and treatment of finite-size effects, radiation pressure, relativistic corrections, and other effects that we have neglected. It is crucial to study the possible degeneracy between the mentioned effects and the perturbations induced by the PBHs. A combination of such a model with a sophisticated analysis of solar system *data* could be a viable pathway to the detection of asteroid-mass PBHs.

For the halo of PBHs, we have assumed a monochromatic mass function for simplicity. In reality, PBHs are likely to form with an extended mass distribution. While one can easily expand our analysis for a distribution of PBH masses, it is not straightforward to connect this distribution to the initial PBH mass function at formation in the early Universe. The main reason for this is that one has to deal with migration effects, where the heavier black holes sink toward the center of the halo while the lighter ones move outward. In general, we do not expect that an extended mass function would change the perturbations of PBHs in a drastic way, as we found little mass dependence in our results.

A more sizable impact on our results could be expected if PBHs are clustered (see Section II of B. J. Carr et al. 2024 and references therein). If the size of such a cluster is small compared to the impact parameter, then it will simply act as a

much heavier black hole. However, if the size of such a cluster is comparable to the solar system, then our results could change in a nontrivial way. In addition, the degree of clustering might be dependent on the black hole mass, in which case an extended mass function could have a sizable impact on the result. Therefore, it would be worthwhile to study this aspect in a future work.

5. Summary

In this work, we perform numerical simulations of the solar system, embedded in a DM halo of PBHs. The simulation results are used to quantify the perturbations induced by the PBHs on the distance between Earth and another SSO. First, it is demonstrated that the strength of the perturbations depends only logarithmically on the PBH mass if the nearest PBH is much farther away from Earth than the other SSO. The physical reason for this is the fact that the strength of the gravitational force ($\sim M_{\rm PBH}$) is balanced by the rate of encounters ($\sim 1/M_{\rm PBH}$). We then show for $M_{\rm PBH} = 10^{20}$ g that after a time span of 20 yr the perturbations are still more than an order of magnitude below the current precision of observational data for the Earth–Mars distance, which has been available for a similar time period. Therefore, PBHs cannot be directly constrained based on solar system ephemerides, challenging the results of recent work.

Our findings are interpreted by a simple analytical model that provides an independent test of the accuracy of our simulations. It allows us to show that the perturbations induced by the PBHs are dominated by the closest encounter. We find that the effect of Poissonian fluctuations in the PBH number density studied by A. Loeb (2024) is significantly smaller. In addition, the analytical model enables us to extrapolate our results to longer timescales and to a larger range of PBH masses. We find that the precision of solar system ephemerides has to increase by roughly an order of magnitude for the effect of the PBH halo to become noticeable within a decade of observation. Equivalently, PBHs could be detected using already-existing data if the extraction of signals well below the noise level is achieved. Importantly, in order to reliably detect PBHs, it is necessary to employ accurate models of solar system ephemerides that include finite-size effects, relativistic corrections, and other effects that were neglected in this work.

Acknowledgments

We thank Avi Loeb, whose work has inspired us to pursue this project. We also would like to thank Chris McKee and Florian Kühnel for fruitful discussions and helpful comments. This research was supported by the Excellence Cluster ORIGINS, which is funded by the Deutsche Forschungsgemeinschaft (DFG, German Research Foundation) under Germany's Excellence Strategy – EXC-2094 – 390783311.

Software: Julia (J. Bezanson et al. 2017), Matplotlib (J. D. Hunter 2007).

Appendix
Relation between the Perturbation Strength and the Impact Parameter

In Section 4.1 we derived expressions for the relation between the perturbation strength $|\delta \boldsymbol{r}|/r$ and the impact parameter b in the limit $b \gg r$ Equation (5) and for $b \ll r$ (Equation 6). In the intermediate case $b \sim r$ the result will strongly depend on the precise geometry of the encounter. To investigate this effect, we uniformly sample 10^7 PBH positions in a plane around two SSOs that are separated by distance $r = 1$. For each PBH position we determine the minimum of the distance to both bodies b and the perturbation strength $|\delta \boldsymbol{r}|/r$. Figure 7 shows the range of values obtained for $|\delta \mathbf{r}|$ for each value of b as the shaded area and the mean values as points. We have set $2GM_{\rm PBH}\Delta t/v_{\rm PBH} = r = 1$, as we only care about the functional dependence on b. The analytical relation (Equation (7)) that we use in this work is shown as the orange line and agrees well with the numerical data. The strongest deviation is a factor of 2.2 for $b \approx r/2$. If we integrate over the numerical relation, then we find a deviation of at most 20%. This justifies using Equation (7) to describe the simulation results.

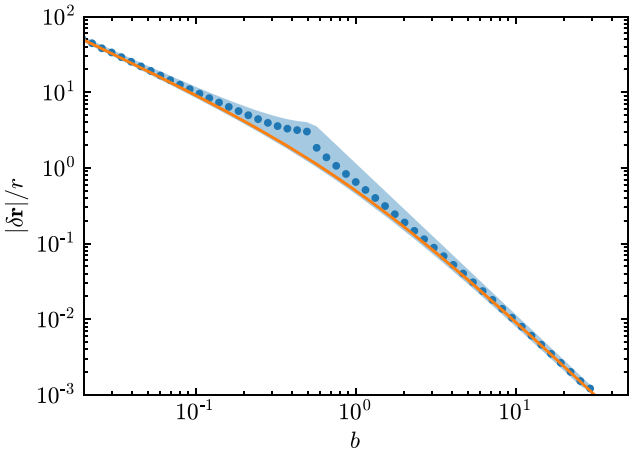

Figure 7. Strength of the perturbation $|\delta \boldsymbol{r}|/r$ induced by a flyby of a PBH as a function of the impact parameter b in units of r. The shaded area displays the range of values for all possible geometries. The blue circles indicate the mean value averaged over all configurations. The analytical relation from Equation (7) is shown as the orange line.

ORCID iDs

Valentin Thoss https://orcid.org/0009-0007-5515-2158
Andreas Burkert https://orcid.org/0000-0001-6879-9822

References

Abbott, B. P., Abbott, R., Abbott, T. D., et al. 2016, PhRvL, 116, 061102
Adams, A. W., & Bloom, J. S. 2004, arXiv:astro-ph/0405266
Alexandre, A., Dvali, G., & Koutsangelas, E. 2024, PhRvD, 110, 036004
Battat, J. B. R., Adelberger, E., Colmenares, N. R., et al. 2023, PASP, 135, 104504
Bertrand, B., Cuadrat-Grzybowski, M., Defraigne, P., Van Camp, M., & Clesse, S. 2023, arXiv:2312.14520
Bezanson, J., Edelman, A., Karpinski, S., & Shah, V. B. 2017, SIAMR, 59, 65
Binney, J., & Tremaine, S. 2008, Galactic Dynamics: Second Edition (Princeton, NJ: Princeton Univ. Press)
Caplan, M. E., Johnston, J., & Santarelli, A. D. 2023, MNRAS, 524, 1927
Carr, B., Kohri, K., Sendouda, Y., & Yokoyama, J. 2021, RPPh, 84, 116902
Carr, B. J., Clesse, S., Garcìa-Bellido, J., Hawkins, M. R. S., & Kühnel, F. 2024, PhR, 1054, 1
Carr, B. J., & Green, A. M. 2024, arXiv:2406.05736
Cline, J. M. 2024, RNAAS, 8, 220
Colmenares, N. R., Battat, J. B. R., Gonzales, D. P., Murphy, T. W., & Sabhlok, S. 2023, PASP, 135, 104503

Freese, K., Lisanti, M., & Savage, C. 2013, RvMP, 85, 1561
Hunter, J. D. 2007, CSE, 9, 90
Li, Y.-L., Huang, G.-Q., Huang, Z.-Q., & Shu, F.-W. 2023, PhRvD, 107, 084019
Loeb, A. 2024, RNAAS, 8, 211
Park, R. S., Folkner, W. M., Williams, J. G., & Boggs, D. H. 2021, AJ, 161, 105
Pitjeva, E. V., Pitjev, N. P., Pavlov, D. A., & Turygin, C. C. 2021, A&A, 647, A141
Seto, N., & Cooray, A. 2004, PhRvD, 70, 063512
Thoss, V., Burkert, A., & Kohri, K. 2024, MNRAS, 532, 451
Tran, T. X., Geller, S. R., Lehmann, B. V., & Kaiser, D. I. 2024, PhRvD, 110, 063533
Yalinewich, A., & Caplan, M. E. 2021, MNRAS, 505, L115

Chapter 8

Conclusions and Outlook

In this thesis, we set out to address the following two main questions:

- What implications does the memory burden effect have for light PBHs, and under what conditions can they make up the dark matter?
- How can we probe PBHs as a dark matter candidate in the newly opened mass window and the asteroid mass window?

In this final chapter, we want to summarise our findings and answers to these questions.

8.1 Memory burden and its implications for primordial black holes

In the past, PBHs lighter than $M_{\rm PBH} \sim 10^{17}\,\mathrm{g}$ had been ruled out as a dark matter candidate due to their strong presumed Hawking evaporation. Recent theoretical studies of the quantum properties of black holes have claimed that the semiclassical description of Hawking radiation breaks down at the latest when a black hole has lost half of its initial mass. Beyond that point, the evaporation rate will be strongly suppressed by the black hole's large entropy, a result which was termed the memory burden effect, as the black hole cannot efficiently lose its information and is burdened by its large information capacity.

Motivated by these intriguing new developments, we studied the implications for light PBHs as a dark matter candidate. In Chapters 3 and 4, we derived constraints on the abundance of light PBHs based on the galactic and extragalactic γ-ray emission and the effect on CMB anisotropies and BBN. As a result, a new mass window emerges where PBHs can make up the entire dark matter. The lower mass limit is a function of the strength of the memory burden effect, parametrized by powers k of the black hole entropy. With increasing k, the range of allowed PBH masses increases. For $k = 2$, the mass window extends down to $M_{\rm PBH} \sim 10^5\,\mathrm{g}$. However, in the conservative case where the memory burden sets in when the black hole has lost half of its initial mass, this requires a very short transition phase to the memory burden phase.

This is demonstrated in Chapter 5, where we extended our model to account for the transition period from the SC regime to the memory burden phase. This can have profound consequences for the available parameter space for light PBHs as a dark matter candidate. We investigated the role of the transition by deriving limits on the abundance of PBHs from galactic γ-ray emission, with the computation of other constraints left for future work. The most conservative scenario, where the memory burden sets in when the black hole has lost half of its initial mass, is strongly constrained based on theoretical models for the transition. However, an early onset of the memory burden, as is motivated by theoretical work, can open up a large mass window for light PBHs as a dark matter candidate. In this case, the lower limit of the mass window is well approximated by the results derived in Chapters 3 and 4.

A natural extension of the work from this thesis would be the incorporation of black hole spin and extended mass functions. Even though neither is expected to radically change the results presented in this work, this would provide a more realistic picture of the allowed parameter space for light PBHs. In addition, mergers of light PBHs can have significant consequences, as the merger product would initially behave according to SC Hawking evaporation. As PBH merger rates have typically been studied in the stellar-mass regime, a careful investigation of the rates for light PBHs would be required to make meaningful predictions.

Important improvements in our understanding of light PBHs and their viability as a dark matter candidate will come from improved theoretical models of the memory burden effect. Precise predictions about the strength of the suppression, the timing of its onset, the nature of the transitional phase, and the evolution of the black hole particle spectrum will enable a clearer picture of the role of PBHs in the early universe. At the same time, it will also be an important step in our understanding of the quantum properties of black holes.

8.2 Dynamical signatures of light primordial black holes

If PBHs of asteroidal or lower masses make up the entire dark matter, then there would be a notable number of them in the Solar System at any given time. Due to their small size and negligible accretion, a direct observation would be very difficult. However, their gravitational attraction could exert tiny perturbations on bodies in the Solar System, which could be probed by high-precision data.

We studied two possible detection mechanisms. One is based on GW experiments, where the fly-by of PBH differentially perturbs the test masses, which would induce a burst-like signal in the detector. Using the sensitivity curves of a number of proposed GW experiments, we investigated their prospects to probe the presence of PBHs or generic dark objects in the Solar System. The results are presented in Chapter 6 of this thesis. We found that the decihertz detector DECIGO is best suited to probe the existence of light PBHs, and that they would induce detectable perturbations if they made up the entire dark matter for $M_{\rm PBH} \in [10^7, 10^{11}]\,\mathrm{g}$. This overlaps with the newly opened mass window based on the memory burden effect, derived in Chapters 3, 4, and 5, representing an opportunity to probe this new parameter space.

The second detection mechanism, presented in Chapter 7, focuses on the gravitational effect that PBHs would have on the extremely well-measured orbits of planets in the Solar System.

Radio ranging between interplanetary spacecraft and ground stations on Earth has achieved measurement accuracies on the order of 1 m for the distance between Earth and Mars or Mercury. By performing N-body simulations of the Solar System, embedded in a halo of PBHs, we investigated the perturbations that they induce on the orbits of the planets. Using the Earth-Mars distance as a representative observational probe, we showed that the induced perturbations are around one order of magnitude below the current measurement accuracy. A future improvement in the observational residuals could enable the search for PBHs in the asteroid mass range around $M_{\mathrm{PBH}} \sim 10^{20}\,\mathrm{g}$.

The dynamical signatures discussed in this work provide an opportunity to probe the nature of dark matter in a previously inaccessible part of the parameter space. There are many questions that should be addressed in future work to further develop these ideas. As we pointed out in Chapter 7, Solar System ephemerides are large models with hundreds of parameters that are fitted based on the observational data. We are currently investigating, using Bayesian inference, whether the presence of a PBH can be reliably inferred from the global fit. This will likely depend on parameters such as the PBH mass, the fly-by distance, and the geometry of the encounter. A crucial aspect in this analysis will be the inclusion of massive asteroids, whose gravitational effect could be degenerate with that from a transiting PBH, potentially masking the signal. The results of such studies could be used to make predictions about the residuals of the observational data that need to be achieved in order to detect PBHs in the Solar System.

In the analysis in Chapter 7 of this thesis, we focused on the Earth-Mars distance as an example for a high-fidelity observable. Detection prospects could be improved by a sophisticated data analysis that cross-correlates data from multiple Solar System bodies. In addition to the meter-level accuracy available from spacecraft ranging, optical astrometry is available for more than a million bodies in the Solar System, with varying accuracy. This number will increase substantially over the next years thanks to the Vera Rubin Observatory. Even though the residuals from astrometric measurements are orders of magnitude larger, the availability of many more bodies that could be perturbed might have interesting implications for the detection prospects.

The distribution of PBHs assumed in Chapter 7 was homogeneous and monochromatic. The former is likely a good assumption, as the dark matter halo is expected to be smooth with little substructure at the position of the Solar System. However, studying a more realistic mass function could be an interesting extension of our work. In addition, even at asteroidal mass, there could be a sizeable fraction of PBHs in binaries which could create a distinct perturbation signal and improve the detection prospects.

The method of detecting dark matter in the form of PBHs can also be extended to probe the substructure of the Milky Way halo, independent of whether the dark matter exists in the form of black holes or elementary particles. The passage of a dark matter subhalo through the Solar System is likely very rare, and the halos are typically not concentrated enough. However, so-called 'prompt cusps', which form from the peaks of the primordial density fields at high redshift, would be much denser and could potentially be probed through their dynamical effects in the Solar System. We are currently exploring this possibility as part of ongoing work.

Finally, the interaction of PBHs with Oort cloud objects is another observational signature that deserves further attention. This has been studied by Siraj and Loeb (2020) for the case

of a captured PBH, but the much larger number density of unbound PBHs passing through the Oort cloud could induce similar flares as they disrupt icy objects. In principle, PBHs of sufficient mass could also contribute to the flux of long-period comets by scattering Oort cloud objects into the inner Solar System.

In 1933, Fritz Zwicky first speculated about the presence of dark matter based on his observations of the Coma cluster (Zwicky, 1933). Nearly a century later, the gravitational evidence for dark matter is overwhelming, yet its fundamental nature remains elusive. Efforts to detect particle dark matter candidates have significantly narrowed the available parameter space, but await any successful detection. In this thesis, we have presented an entirely new possibility to explain the nature of dark matter – light PBHs, enabled by the memory burden effect that suppresses their evaporation. We showed that a potentially large mass range is opened up where they can make up the dark matter. In addition to induced gravitational waves from their formation, we showed that highly sensitive dynamical probes can play a key role in the search for light PBHs. Their gravitational effect on the tightly constrained orbits of planets and on future space-based gravitational wave detectors is a promising way to shed light on the nature of dark matter.

Bibliography

Abac, A. et al. (Einstein Telescope Collaboration)
2025. The Science of the Einstein Telescope. *arXiv e-prints*, P. arXiv:2503.12263.

Abbott, B.P. et al. (LIGO Scientific Collaboration and Virgo Collaboration)
2016. Observation of Gravitational Waves from a Binary Black Hole Merger. *Phys. Rev. Lett.*, 116(6):061102.

Agazie, G. et al. (NANOGrav Collaboration)
2023. The NANOGrav 15-year Data Set: Evidence for a Gravitational-Wave Background. *The Astrophysical Journal Letters*, 951(1):L8.

Alpher, R.A., Bethe, H. and Gamow, G.
1948. The Origin of Chemical Elements. *Physical Review*, 73(7):803–804.

Amaro-Seoane, P. et al. (LISA Collaboration)
2017. Laser Interferometer Space Antenna. *arXiv e-prints*, P. arXiv:1702.00786.

Antoniadis, J. et al. (EPTA Collaboration and InPTA Collaboration)
. The second data release from the European Pulsar Timing Array III. Search for gravitational wave signals. *Astronomy & Astrophysics*, 678.

Auffinger, J.
2023. Primordial black hole constraints with Hawking radiation-A review. *Progress in Particle and Nuclear Physics*, 131:104040.

Bagui, E. et al. (LISA Cosmology Working Group)
2025. Primordial black holes and their gravitational-wave signatures. *Living Rev. Rel.*, 28(1):1.

Bardeen, J.M., Carter, B. and Hawking, S.W.
1973. The four laws of black hole mechanics. *Communications in Mathematical Physics*, 31(2):161–170.

Bardeen, J.M., Bond, J.R., Kaiser, N. and Szalay, A.S.
1986. The Statistics of Peaks of Gaussian Random Fields. *ApJ*, 304:15.

Bartolo, N. et al.
2019. Primordial Black Hole Dark Matter: LISA Serendipity. *Phys. Rev. Lett.*, 122(21):211301.

Bekenstein, J.D.
1972. Black holes and the second law. *Lett. Nuovo Cim.*, 4:737–740.

Bekenstein, J.D.
1973. Black holes and entropy. *Phys. Rev. D*, 7:2333–2346.

Bekenstein, J.D.
1974. Generalized second law of thermodynamics in black hole physics. *Phys. Rev. D*, 9:3292–3300.

Bertone, G. and Hooper, D.
2018. History of dark matter. *Reviews of Modern Physics*, 90(4):045002.

Blaineau, T. et al.
2022. New limits from microlensing on Galactic black holes in the mass range $10\,M_\odot < M < 1000\,M_\odot$. *A&A*, 664:A106.

Boldrini, P. et al.
2020. Cusp-to-core transition in low-mass dwarf galaxies induced by dynamical heating of cold dark matter by primordial black holes. *MNRAS*, 492(4):5218–5225.

Burkert, A.
2020. Fuzzy Dark Matter and Dark Matter Halo Cores. *ApJ*, 904(2):161.

Carr, B. and Hawking, S.
1974. Black holes in the early Universe. *MNRAS*, 168:399–416.

Carr, B., Raidal, M., Tenkanen, T., Vaskonen, V. and Veermäe, H.
2017. Primordial black hole constraints for extended mass functions. *Phys. Rev. D*, 96(2):023514.

Carr, B. and Silk, J.
2018. Primordial black holes as generators of cosmic structures. *MNRAS*, 478(3):3756–3775.

Carr, B., Kohri, K., Sendouda, Y. and Yokoyama, J.
2021a. Constraints on primordial black holes. *Reports on Progress in Physics*, 84(11):116902.

Carr, B., Clesse, S., García-Bellido, J. and Kühnel, F.
2021b. Cosmic conundra explained by thermal history and primordial black holes. *Physics of the Dark Universe*, 31:100755.

Carr, B., Clesse, S., García-Bellido, J., Hawkins, M.R.S. and Kühnel, F.
2024. Observational evidence for primordial black holes: A positivist perspective. *Phys. Rep.*, 1054:1–68.

Carr, B. and Green, A.M.
2025. The History of Primordial Black Holes. In *Primordial Black Holes*, C. Byrnes, G. Franciolini, T. Harada, P. Pani, and M. Sasaki, eds., Pp. 3–33. Singapore: Springer Nature Singapore.

Casanueva-Villarreal, C., Padilla, N., Tissera, P.B., Liu, B. and Bromm, V.
2025. Primordial black holes as dark matter candidates: Multi-frequency constraints from cosmic radiation backgrounds. *A&A*, 699:A49.

Chapline, G.F.
1975. Cosmological effects of primordial black holes. *Nature*, 253(5489):251–252.

Chaudhuri, A., Kohri, K. and Thoss, V.
2025. New bounds on memory burdened primordial black holes from Big Bang nucleosynthesis. *J. Cosmology Astropart. Phys.*, 2025(11):057.

Cirelli, M., Strumia, A. and Zupan, J.
2024. Dark Matter. *arXiv e-prints*, P. arXiv:2406.01705.

Clowe, D., Gonzalez, A. and Markevitch, M.
2004. Weak-Lensing Mass Reconstruction of the Interacting Cluster 1E 0657-558: Direct Evidence for the Existence of Dark Matter. *ApJ*, 604(2):596–603.

Clowe, D. et al.
2006. A Direct Empirical Proof of the Existence of Dark Matter. *ApJ*, 648(2):L109–L113.

Delos, M.S., Rantala, A., Young, S. and Schmidt, F.
2024. Structure formation with primordial black holes: collisional dynamics, binaries, and gravitational waves. *J. Cosmology Astropart. Phys.*, 2024(12):005.

Dewdney, P.E., Hall, P.J., Schilizzi, R.T. and Lazio, T.J.L.W.
2009. The Square Kilometre Array. *IEEE Proceedings*, 97(8):1482–1496.

Domènech, G.
2024. GW Backgrounds associated with PBHs. *arXiv e-prints*, P. arXiv:2402.17388.

Dondarini, A., Marino, G., Panci, P. and Zantedeschi, M.
2025. The fast, the slow and the merging: probes of evaporating memory burdened PBHs. *J. Cosmology Astropart. Phys.*, 2025(11):006.

Drewes, M.
2013. The Phenomenology of Right Handed Neutrinos. *International Journal of Modern Physics E*, 22(8):1330019–593.

Düchting, N.
2004. Supermassive black holes from primordial black hole seeds. *Phys. Rev. D*, 70(6):064015.

Dvali, G. and Panchenko, M.
2015. Black Hole Type Quantum Computing in Critical Bose-Einstein Systems. *arXiv e-prints*, P. arXiv:1507.08952.

Dvali, G.
2018. A Microscopic Model of Holography: Survival by the Burden of Memory. *arXiv e-prints*, P. arXiv:1810.02336.

Dvali, G., Zantedeschi, M. and Zell, S.
2025. Transitioning to Memory Burden: Detectable Small Primordial Black Holes as Dark Matter. *arXiv e-prints*, P. arXiv:2503.21740.

Einasto, J., Kaasik, A. and Saar, E.
1974. Dynamic evidence on massive coronas of galaxies. *Nature*, 250(5464):309–310.

Escrivà, A.
2022. PBH Formation from Spherically Symmetric Hydrodynamical Perturbations: A Review. *Universe*, 8(2):66.

Escrivà, A., Kühnel, F. and Tada, Y.
2024. Primordial black holes. In *Black Holes in the Era of Gravitational-Wave Astronomy*, M. Arca Sedda, E. Bortolas, and M. Spera, eds., Pp. 261–377.

Esser, N. et al.
2025. Constraints on asteroid-mass primordial black holes in dwarf galaxies using Hubble Space Telescope photometry. *A&A*, 698:A290.

Germani, C. and Musco, I.
2019. Abundance of Primordial Black Holes Depends on the Shape of the Inflationary Power Spectrum. *Phys. Rev. Lett.*, 122(14):141302.

Germani, C. and Sheth, R.K.
2023. The Statistics of Primordial Black Holes in a Radiation-Dominated Universe: Recent and New Results. *Universe*, 9(9):421.

Gorton, M. and Green, A.M.
2022. Effect of clustering on primordial black hole microlensing constraints. *J. Cosmology Astropart. Phys.*, 2022(8):035.

Gorton, M. and Green, A.
2024. How open is the asteroid-mass primordial black hole window? *SciPost Physics*, 17(2):032.

Gow, A.D., Byrnes, C.T., Cole, P.S. and Young, S.
2021. The power spectrum on small scales: robust constraints and comparing PBH methodologies. *J. Cosmology Astropart. Phys.*, 2021(2):002.

Griest, K., Cieplak, A.M. and Lehner, M.J.
2013. New Limits on Primordial Black Hole Dark Matter from an Analysis of Kepler Source Microlensing Data. *Phys. Rev. Lett.*, 111(18):181302.

Gunn, J.E., Lee, B.W., Lerche, I., Schramm, D.N. and Steigman, G.
1978. Some astrophysical consequences of the existence of a heavy stable neutral lepton. *ApJ*, 223:1015–1031.

Hawking, S.
1971. Gravitationally collapsed objects of very low mass. *MNRAS*, 152:75.

Hawking, S.
1974. Black hole explosions? *Nature*, 248(5443):30–31.

Hawking, S.
1975. Particle creation by black holes. *Communications in Mathematical Physics*, 43(3):199–220.

Hinshaw, G. et al.
2013. Nine-year Wilkinson Microwave Anisotropy Probe (WMAP) Observations: Cosmological Parameter Results. *ApJS*, 208(2):19.

Inman, D. and Ali-Haïmoud, Y.
2019. Early structure formation in primordial black hole cosmologies. *Phys. Rev. D*, 100(8):083528.

Jungman, G., Kamionkowski, M. and Griest, K.
1996. Supersymmetric dark matter. *Phys. Rep.*, 267:195–373.

Katz, A., Kopp, J., Sibiryakov, S. and Xue, W.
2018. Femtolensing by dark matter revisited. *J. Cosmology Astropart. Phys.*, 2018(12):005.

Kelly, B.C. and Merloni, A.
2012. Mass Functions of Supermassive Black Holes across Cosmic Time. *Advances in Astronomy*, 2012:970858.

Kogut, A. et al.
2025. The Primordial Inflation Explorer (PIXIE): mission design and science goals. *J. Cosmology Astropart. Phys.*, 2025(4):020.

Kohri, K., Nakama, T. and Suyama, T.
2014. Testing scenarios of primordial black holes being the seeds of supermassive black holes by ultracompact minihalos and CMB μ distortions. *Phys. Rev. D*, 90(8):083514.

Kolb, E.W. and Turner, M.S.
1990. *The Early Universe*, volume 69 of *Frontiers in Physics*. Addison-Wesley.

Liu, B. and Bromm, V.
2022. Accelerating Early Massive Galaxy Formation with Primordial Black Holes. *ApJ*, 937(2):L30.

Loeb, A.
2024. Excluding Primordial Black Holes as Dark Matter Based on Solar System Ephemeris. *Research Notes of the American Astronomical Society*, 8(8):211.

MacGibbon, J.H., Carr, B.J. and Page, D.N.
2008. Do evaporating black holes form photospheres? *Phys. Rev. D*, 78(6):064043.

Maiolino, R. et al.
2025. A black hole in a near-pristine galaxy 700 million years after the Big Bang. *arXiv e-prints*, P. arXiv:2505.22567.

Michel, M. and Zell, S.
2023. The Timescales of Quantum Breaking. *Fortsch. Phys.*, 71:2300163.

Milgrom, M.
1983. A modification of the Newtonian dynamics as a possible alternative to the hidden mass hypothesis. *ApJ*, 270:365–370.

Misner, C.W. and Sharp, D.H.
1964. Relativistic Equations for Adiabatic, Spherically Symmetric Gravitational Collapse. *Physical Review*, 136(2B):571–576.

Montefalcone, G. et al.
2025. Does Memory Burden Open a New Mass Window for Primordial Black Holes as Dark Matter? *arXiv e-prints*, P. arXiv:2503.21005.

Montero-Camacho, P., Fang, X., Vasquez, G., Silva, M. and Hirata, C.M.
2019. Revisiting constraints on asteroid-mass primordial black holes as dark matter candidates. *J. Cosmology Astropart. Phys.*, 2019(8):031.

Mróz, P. et al.
2024a. Limits on Planetary-mass Primordial Black Holes from the OGLE High-cadence Survey of the Magellanic Clouds. *The Astrophysical Journal*, 976:L19.

Mróz, P. et al.
2024b. Microlensing Optical Depth and Event Rate toward the Large Magellanic Cloud Based on 20 yr of OGLE Observations. *The Astrophysical Journal Supplement Series*, 273:4.

Mróz, P. et al.
2024c. No massive black holes in the Milky Way halo. *Nature*, 632:749–751.

Mróz, P. et al.
2025. Microlensing Optical Depth, Event Rate, and Limits on Compact Objects in Dark Matter Based on 20 Yr of OGLE Observations of the Small Magellanic Cloud. *The Astrophysical Journal Supplement Series*, 280:49.

Nadezhin, D.K., Novikov, I.D. and Polnarev, A.G.
1978. The hydrodynamics of primordial black hole formation. *Soviet Ast.*, 22:129–138.

Nakama, T., Carr, B. and Silk, J.
2018. Limits on primordial black holes from μ distortions in cosmic microwave background. *Phys. Rev. D*, 97(4):043525.

Niemeyer, J.C. and Jedamzik, K.
1998. Near-Critical Gravitational Collapse and the Initial Mass Function of Primordial Black Holes. *Phys. Rev. Lett.*, 80(25):5481–5484.

Niikura, H., Takada, M., Yokoyama, S., Sumi, T. and Masaki, S.
2019a. Constraints on Earth-mass primordial black holes from OGLE 5-year microlensing events. *Phys. Rev. D*, 99(8):083503.

Niikura, H. et al.
2019b. Microlensing constraints on primordial black holes with Subaru/HSC Andromeda observations. *Nature Astronomy*, 3:524–534.

Nuño Siles, J.F. and García-Bellido, J.
2025. Primordial black hole clusters, phenomenology & implications. *Physics of the Dark Universe*, 47:101789.

Ostriker, J.P., Peebles, P.J.E. and Yahil, A.
1974. The Size and Mass of Galaxies, and the Mass of the Universe. *ApJ*, 193:L1.

Paczynski, B.
1986. Gravitational Microlensing by the Galactic Halo. *ApJ*, 304:1.

Peebles, P.J.E.
1982. Large-scale background temperature and mass fluctuations due to scale-invariant primeval perturbations. *ApJ*, 263:L1–L5.

Penzias, A.A. and Wilson, R.W.
1965. A Measurement of Excess Antenna Temperature at 4080 Mc/s. *ApJ*, 142:419–421.

Planck Collaboration et al.
2020a. Planck 2018 results. V. CMB power spectra and likelihoods. *A&A*, 641:A5.

Planck Collaboration et al.
2020b. Planck 2018 results. VI. Cosmological parameters. *A&A*, 641:A6.

Planck Collaboration et al.
2020c. Planck 2018 results. X. Constraints on inflation. *A&A*, 641:A10.

Press, W.H. and Schechter, P.
1974. Formation of Galaxies and Clusters of Galaxies by Self-Similar Gravitational Condensation. *ApJ*, 187:425–438.

Reardon, D.J. et al.
2023. Search for an isotropic gravitational-wave background with the Parkes Pulsar Timing Array. *The Astrophysical Journal Letters*, 951(1):L6.

Reeves, H., Audouze, J., Fowler, W.A. and Schramm, D.N.
1973. On the Origin of Light Elements. *ApJ*, 179:909–930.

Reitze, D. et al.
2019. Cosmic Explorer: The U.S. Contribution to Gravitational-Wave Astronomy beyond LIGO. In *Bulletin of the American Astronomical Society*, volume 51, P. 35.

Rubin, V.C. and Ford, Jr., W.K.
1970. Rotation of the Andromeda Nebula from a Spectroscopic Survey of Emission Regions. *ApJ*, 159:379.

Shariat, C. et al.
2025. Wide Binaries in an Ultra-faint Dwarf Galaxy: Discovery, Population Modeling, and A Nail in the Coffin of Primordial black hole Dark Matter. *PASP*, 137(10):104103.

Sicilia, A. et al.
2022a. The Black Hole Mass Function across Cosmic Times. I. Stellar Black Holes and Light Seed Distribution. *ApJ*, 924(2):56.

Sicilia, A. et al.
2022b. The Black Hole Mass Function across Cosmic Time. II. Heavy Seeds and (Super)Massive Black Holes. *ApJ*, 934(1):66.

Siraj, A. and Loeb, A.
2020. Searching for Black Holes in the Outer Solar System with LSST. *ApJ*, 898(1):L4.

Smyth, N. et al.
2020. Updated constraints on asteroid-mass primordial black holes as dark matter. *Phys. Rev. D*, 101(6):063005.

Springel, V. et al.
2005. Simulations of the formation, evolution and clustering of galaxies and quasars. *Nature*, 435(7042):629–636.

Thoss, V., Burkert, A. and Kohri, K.
2024. Breakdown of hawking evaporation opens new mass window for primordial black holes as dark matter candidate. *Mon. Not. R. Astron. Soc.*, 532(1):451–459.

Thoss, V. and Loeb, A.
2025. Detecting dark objects in the Solar System with gravitational wave observatories. *Phys. Rev. D*, 112(8):083050.

Thoss, V. and Burkert, A.
2025. Primordial Black Holes in the Solar System. *ApJ*, 980(2):238.

Tisserand, P. et al.
2007. Limits on the Macho content of the Galactic Halo from the EROS-2 Survey of the Magellanic Clouds. *A&A*, 469(2):387–404.

Tremaine, S. and Gunn, J.E.
1979. Dynamical role of light neutral leptons in cosmology. *Phys. Rev. Lett.*, 42(6):407–410.

Ünal, C., Kovetz, E.D. and Patil, S.P.
2021. Multimessenger probes of inflationary fluctuations and primordial black holes. *Phys. Rev. D*, 103(6):063519.

Weinberg, S.
1978. A new light boson? *Phys. Rev. Lett.*, 40(4):223–226.

White, S.D.M., Frenk, C.S. and Davis, M.
1983. Clustering in a neutrino-dominated universe. *ApJ*, 274:L1–L5.

Wilczek, F.
1978. Problem of strong P and T invariance in the presence of instantons. *Phys. Rev. Lett.*, 40(5):279–282.

Wyrzykowski, L. et al.
2011a. The OGLE view of microlensing towards the Magellanic Clouds - III. Ruling out sub-solar MACHOs with the OGLE-III LMC data. *Monthly Notices of the Royal Astronomical Society*, 413:493–508.

Wyrzykowski, L. et al.
2011b. The OGLE view of microlensing towards the Magellanic Clouds - IV. OGLE-III SMC data and final conclusions on MACHOs. *Monthly Notices of the Royal Astronomical Society*, 416:2949–2961.

Xu, H. et al.
2023. Searching for the nano-Hertz stochastic gravitational wave background with the Chinese Pulsar Timing Array Data Release I. *Research in Astronomy and Astrophysics*, 23(7):075024.

Yokoyama, J.
1998. Cosmological constraints on primordial black holes produced in the near-critical gravitational collapse. *Phys. Rev. D*, 58(10):107502.

Young, S. and Musso, M.
2020. Application of peaks theory to the abundance of primordial black holes. *J. Cosmology Astropart. Phys.*, 2020(11):022.

Zel'dovich, Y.B. and Novikov, I.D.
1967. The Hypothesis of Cores Retarded during Expansion and the Hot Cosmological Model. *Soviet Ast.*, 10:602.

Zhang, S. et al.
2025. How do Massive Primordial Black Holes Impact the Formation of the First Stars and Galaxies? *ApJ*, 987(2):185.

Zwicky, F.
1933. Die Rotverschiebung von extragalaktischen Nebeln. *Helvetica Physica Acta*, 6:110–127.

Zwicky, F.
1937. On the Masses of Nebulae and of Clusters of Nebulae. *ApJ*, 86:217.

List of Figures

Acknowledgements

17 years ago, as an 11-year-old student in 6th grade, I joined the astronomy club at my school. It was led by Wolfgang Ober, who taught us about our fascinating universe and the laws that govern it. On clear nights, we set up the school telescope and had the chance to see planets, nebulae, star clusters, and many other wonderful objects with our own eyes. I stayed in the astronomy club until the end of my school time, when I prepared my seminar work, where I measured the orbital parameters of a spectroscopic binary with our telescope. I want to thank Wolfgang Ober for his patience and commitment to sharing his knowledge about astronomy with other students and me. He deeply inspired me and is a major reason why I am here today, writing my dissertation in astrophysics.

In 2018, searching for a topic for my Bachelor's thesis, I first met Andreas Burkert and was immediately caught by his infectious enthusiasm. His inspiration led me to pursue my Master's thesis and my PhD with him. I am extremely grateful to him for giving me these opportunities and for having the chance to learn from him about our amazing universe. His guidance helped me to grow as an independent researcher.

Throughout my studies and my PhD, I was always supported by my parents, Kathrin and Michael Thoss, and my brother Jakob Thoss. They were always there for me when I needed help and continuously pushed me to achieve my goals. I am forever grateful for their loving support.

I am very thankful for the love, support, and patience of my girlfriend, Kristina Lautenschütz. She has been an invaluable source of energy and motivation for me. Without her, I wouldn't have been able to pursue this project.

I want to thank my co-supervisors and members of the thesis committee, Volker Springel, Gia Dvali, and Dieter Lüst, for their valuable feedback and scientific insights that inspired important projects throughout my PhD.

Manuel Behrendt has been my mentor during the PhD and the supervisor of my Master's thesis. I learned a lot from him, both scientifically and personally. I am thankful for having worked with him and for his positive attitude.

My colleagues Leonard Romano, Hans-Christian, and Ming-Yu contributed to a wonderful work environment at the MPE in Garching, and I greatly enjoyed their presence. I want to thank them for countless scientific and non-scientific discussions that have enriched this thesis.

I am very grateful to all the people of the CAST group at the USM for scientific discussions

and valuable feedback throughout my PhD. I also want to thank the secretaries at the USM, Eleni Mallikopoulou, Nicola Auer, Gudrun Niggl, and Ilana Gorayeb-Wald, who provided great assistance with organizational aspects and answered countless questions about travel applications.

I want to acknowledge the work of the ORIGINS staff members Ina Haneburger, Alice Smith-Gicklhorn, and Petra Regenscheit. They supported me with the administrative aspects of my PhD and answered many questions regarding the organization of the 'Black Hole Day(s)' workshops. I also want to thank them for giving me the opportunity to be the manager of the 'Black Holes Connector'.

My PhD project was generously financially supported by the German public through the Deutsche Forschungsgemeinschaft (DFG, German Research Foundation) under Germany's Excellence Strategy – EXC 2094 – 390783311.

Finally, I want to thank all my friends for their love and support over many years, which also provided me with strength throughout this PhD.